Effect of Soiling
on the PV Panel kWh Output

Pramod Nepal

TUDelft
Delft
University of
Technology

Challenge the future

Effect of Soiling

on the PV Panel kWh Output

by

Pramod Nepal

in partial fulfillment of the requirements for the degree of

Master of Science
in Sustainable Energy Technology

at the Delft University of Technology,
to be defended publicly on Wednesday March 28, 2018 at 14:00 PM.

Supervisor:	Prof. Dr. Olindo Isabella,	TU Delft
Thesis committee:	Prof. Dr. Olindo Isabella,	TU Delft
	Prof. Dr. Miro Zeman,	TU Delft
	Dr. A. Rodrigo Mor,	TU Delft
	Dr. Hesan Ziar,	TU Delft
	Dr. Marc Korevaar,	Kipp & Zonen BV

This thesis is confidential and cannot be made public until March 29, 2019.

An electronic version of this thesis is available at http://repository.tudelft.nl/.

TUDelft Delft
University of
Technology

Abstract

Ever since the commercial growth of PV installations, soiling has been a crucial factor to decrease its performance ratio. Environmental factors such as irradiation, wind, rainfall, and back module temperature affect the yield of a system, but, in many environments, soiling of PV modules carries the largest impact. Cost effective soiling measurements within a production area can provide reliable insights into the soiling behavior and allow developing an optimal cleaning schedule.

The deposition of dust, soil, and microfibers resulting from the surroundings as well as the growth of minute pollen like moss and fungi are categorized as PV module soiling. It is a lesser acknowledged factor that significantly reduces the power production by acting as a barrier for effective light photons utilized by a module. The estimated loss in the irradiance and power can be determined with the help of a soiling ratio (SR) parameter, which is the ratio of short-circuit current (I_{sc}) or maximum power produced (P_{max}) by a soiled module to the clean one.

The first step to address this issue was to analyze the different soiling effects on a module. Various outdoor and indoor soiling experiments were carried out in the rooftop PV system to examine the angular dependency, inhomogeneity, optical losses, and color impacts of the dust. Another aspect of this research project was the development of a novel soiling detection system, the DustIQ. The two sensors with the help of on-board mini-PV module measure the soiling ratio of a soiled module. A wide range of dust color test was also carried out for the color calibration of the sensor. This report also introduces an empirical equation based on incident angle modifier (IAM) for soiled and cleaned PV modules. The proposed equation was used to determine SR over the course of the day for three conditions of high, medium, and low daily average irradiance.

The modeled SR, when compared with the measured data resulted in RMS deviation of $\pm0.21\%$ on a high irradiance day. Additionally, analyzed soiling behaviors were used to estimate the annual energy loss due to in Delft, The Netherlands. The average irradiance and power loss was found to be 0.083% and 0.165% per day respectively due to the natural accumulation of soil. This resulted in an annual energy loss of 16.22 kWh for a system of 1.62 kW$_p$, considering rainfall ($\geq$2 mm) as the only source of module cleaning.

Acknowledgements

This thesis report on "Effect of Soiling on the PV Panel kWh Output" has been written in fulfillment of the graduation requirements of Master of Science in Sustainable Energy Technology at Delft University of Technology. The topic of this research was offered by Kipp & Zonen BV to PVMD group and later to me. I would like to express my sincere gratitude to everybody who has directly or indirectly helped and supported me in this journey.

First of all, I would like to thank Dr Olindo Isabella for introducing me to this interesting project and guiding me throughout the whole thesis process. I would also like to thank Dr Marc Korevaar, my daily supervisor, for his enduring support, comprehension, and contribution towards the project. I really appreciate all the suggestions that were discussed during our progress meetings, they really helped me moving forward. I am very grateful to all the employees of Kipp & Zonen for their constant motivation and providing me with the best environment to learn and grow professionally. Next, I am also thankful to Dr Hesan Ziar for patiently answering all my questions and helping with the report.

To all my friends who were always there for me especially, Sandeep, Rakshit, Gijs, Matthias, Bibek, Ranganath, and Sharad. Your direct/indirect support really helped me during the tough times.

Finally, I express my profound gratitude to my parents and sisters for their unconditional love, encouragement and support all my life. This achievement would not have been possible without them.

I believe you will enjoy reading this report.

Pramod Nepal
Delft, The Netherlands
March 2018

Contents

List of Figures

List of Tables

1

Introduction

1.1. Background

Solar energy in the form of photons is converted to usable electricity with the help of semiconductor materials. In the recent past, the technological advancement in this field has provided PV technology as one of the leading and affordable renewable energy source currently available. The compound annual growth of PV installations was 40% from 2010 to 2016 [1]. This means, the global cumulative installed PV was at least 303.1 GWp, which accounted for annual electricity production of 375 TWh during the year 2016 [2]. With the recent introduction of a competitive call for tenders to allow power purchase agreements (PPA), Dubai and Abu Dhabi had the bid as low as 0.03USD/kWh [2]. These low costs are attracting many countries to invest in the field to tackle growing energy demand. The modularity, low maintenance cost, and longer lifetime of PV systems are becoming apparent reasons to invest more in this field.

In 2016, around 48% of the total installed PV capacity was represented by Asian countries, Middle East regions had 2%, whereas north and south American countries had a share of 16% [2]. The numbers are increasing every year due to abundant solar radiation near the equatorial regions. These tropical areas are mostly arid with high ambient temperature and low rain frequency, which promotes dust settlement termed as "Soiling" of the PV modules. When incoming solar irradiation is blocked due to the presence of any foreign elements on the surface, it reduces the transmittance of photons resulting in lower power output. Module soiling is considered to be the third major environmental factor after irradiation and module temperature that directly accounts for lower performance statistics of a PV system [3]. The irradiance and module temperature are well understood and are already taken into account while designing the PV system, but for soiling, there is still limited understanding and only basic measurements are carried out.

An exponential increase in PV installations in the Sun Belt regions has put soiling as the major factor for a lower performance ratio (PR) of PV systems. In Figure 1.1, regions like Asia Pacific, Middle East, the African continent, and South America shows the higher dust concentration in the atmosphere. The higher amount of atmospheric dust in an urban area is a result of an incomplete combustion process, smog, and due to construction work as well as the chemical reactions in the atmosphere, where for rural areas atmospheric dust is mainly composed of minute sand particles. In addition to PM10[1] and PM2.5[2] concentration of dust particles in the aerosols, dust storm frequency also significantly contributes towards soiling [4]. Dust storm frequently occurs in Middle East region, the northern part of Africa, South American countries as well as in the eastern part of China. Thus, the major part of the world with a high prospect of PV generated electricity suffers from the detrimental effects of soiling.

---

[1]Particulate matter with a diameter of 10 micrometers or less
[2]Particulate matter with a diameter of 2.5 micrometers or less
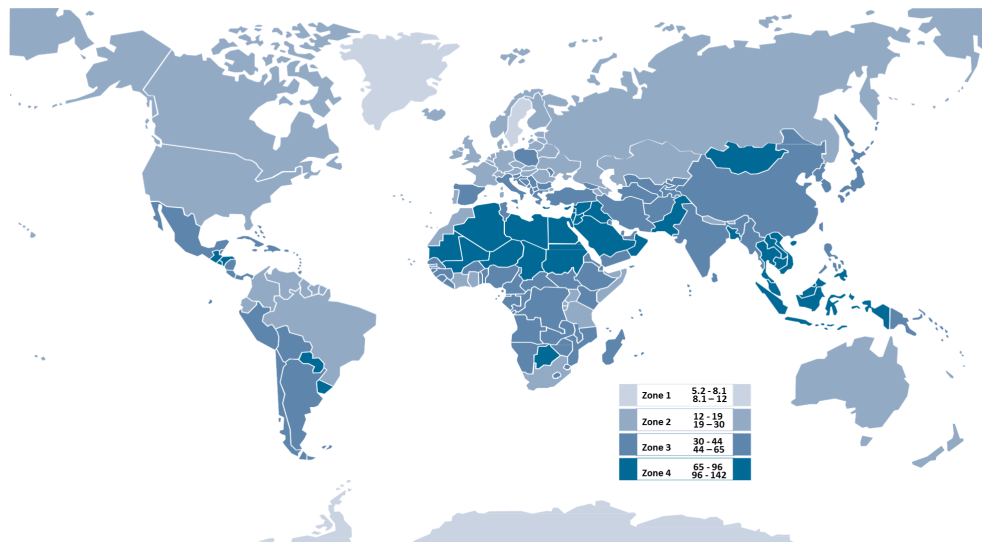
Figure 1.1: Dust concentration around the world based on PM10. The values shown in the figure are in µg/m³ [5].

The soiling majorly depends on two factors: i. Location of the PV plant ii. Local environmental conditions like relative humidity (RH), wind, and rainfall [6]. Six major types of dust to have a high degree of influence are identified as ash, calcium, limestone, soil, sand and silica [5]. Thus, based on the location and dust types the soiling losses might vary. An average daily energy loss due to soiling was found to be around 4.5% in Malaga, Spain, whereas for longer dry periods, the daily energy loss can be much higher than 20% [7]. In another experiment, carried out on a module tilted at an optimum angle of 35°in northern Belgium, resulted in an annual power loss of 3-4% [8]. Similarly, an average increase in soiling loss for rural and suburban locations of USA was measured to be around 0.1%/day but for desert regions, the losses were as high as 0.3%/day [9]. Furthermore, several experiments suggested that the soiling loss in the Middle East regions were more severe than other parts. In Egypt, an experiment was done on 100 different glass samples installed at different tilt angles and azimuth for 8 months resulted in monthly power reduction of 17.4% in cells at an angle of 45°facing south [10]. Rainfall event acts as a cleaning agent for soiled modules. Around 5 mm of rainfall was noticed to completely clean a soiled module in Arizona [11]. However, for Northern California rainfall of 5 mm was not sufficient and more than 20 mm of rain was noticed to regain its normal efficiency [9]. Moreover, in the month of August, an average irradiance and power loss for Delft, The Netherlands were found to be 0.083%/day and 1.32%/day respectively, discussed in chapter 5.

As the soiling process is an environment-dependent parameter, it can greatly affect the yield of a system [6]. Generally, the total energy yield of a system is used as a measure to compare its performance. The yield is a function of location, PV technology used, module tilt and orientation, and balance of systems (BOS). Dust accumulation on the modules is generally not considered or assigned an arbitrary value (3%) during the design phase [12]. Any erratic assumption might associate with huge financial uncertainty for the larger project of several hundreds of megawatt (MW). The main challenge for the designers and installers would be the determination of soiling loss and module cleaning frequency. Thus, the deployment of a project can be hindered due to the difficulty to estimate the exact soiling loss. Module soiling drives up the levelized cost of electricity (LCOE) by reducing total energy generated. The cleaning frequency is associated with a trade-off between energy saved (kWh) by cleaning process and the cost of cleaning (€/kWh). Therefore, sometimes it might be financially beneficial not to clean a module to avoid the extra cleaning cost.

It is therefore very important to realize the soiling behavior on a module. The upcoming sections of this chapter discuss the different soiling mechanisms, module characteristics and environmental factors influencing the soiling process, soiling measurement technique, and cleaning products commercially available in the market.

1.2. Soiling of the Photovoltaic Module

Despite the outstanding growth of PV systems, the performance ratio (PR) has been greatly compromised due to various environmental factors like non-uniform irradiance, wind, rain, module temperature, and soiling [13]. The accumulation of dust, sand, biological deposits like the growth of algae, moss or bird droppings (most severe), and air pollution results are categorized as module soiling. It directly obstructs the irradiation falling on a module by forming a thin layer of dust usually lesser than 10 μm, which depends on the environmental conditions including wind intensity, a probability of volcanic eruptions or frequent vehicular movements [5]. Any particulate matter below 500 μm is termed as dust and is estimated to be about the size of an optical fibre used for communication purposes or a size 10 times a human hair [14].

1.2.1. Sources of Dust

The location of installed PV systems could be residential, rural and industrial, that directly relates to the deposition of atmospheric particles (aerosols). Dust aerosols are mainly classified as primary dust and secondary dust. Primary dust is the particles as they formed, whereas secondary dust particles are the result of complex chemical reactions of primary gases in atmosphere [15]. The primary emission is mainly resulted of the various anthropogenic activities [16] like;

a. Combustion Process

These include the emission of pollutants from coal or gas-fired thermal power plant as well as by the use of heater and boilers at commercial, industrial, and residential levels.

b. Industrial Process

The production of different chemicals, food, oil refining, and metal forming also contributes to a major amount of suspended particles in the atmosphere.

c. Vehicular Movement

The movement of cars, trucks, and motorbikes result in smog entrainment and lifting up dust from the road.

d. Agricultural and Other Activities

Construction of buildings, farms, lawnmowers, nearby wildfires, and controlled burning by the farmers contributes largely to the pollution and generation of dust in the aerosols. Similarly, dust source in a desert location is due to the natural weathering process and the wind movements.

These activities also serve as grinding and milling of coarser particles that again facilitates in light dust re-suspension. Major activities and their relative contribution source in atmosphere can be seen from table 1.1.

Table 1.1: Dust contribution from different activities [17].

Source	Range ($\mu g/m^3$)
Secondary PM	11-22 (mostly NO_3^-,SO_4^{2-},NH_4^+)
Traffic	5-17 (mostly diesel engines)
Soil dust	1-23
Industry (heaters,boilers)	4-6
Wood burning	1-4
Cooking	2-3

Additionally, according to NASA's Earth Observatory map, hundreds of million tons of dust are lifted from the African deserts and deposited in the Atlantic ocean as well as in coastal regions of North America [18]. Location more prone to dust storms results in higher particulate concentration than during normal. Normally, a rural location has a dust concentration of around 30 μg/m^3, whereas for polluted urban areas it's 170 μg/m^3. After a dust storm, the concentration can reach as high as 100,000 μg/m^3 [19]. This process severely affects the total PV power production in those areas.

1.2.2. Composition of Dust

The composition of dust is a result of various anthropogenic and natural activities. The emission of ions like sulphates, nitrates, carbon, ammonia, lead, and organics are associated with human activities, whereas entrainment of coarser particles like sea-salt, soil, dust, and bio-aerosols are the result of wind or birds. Schwela et al. have summarized the different sources and its corresponding elemental composition recreated in the table 1.2.

Table 1.2: Elemental emissions from various sources [17].

Source	Identified elements
Industry	
Oil fired power plants	V,Ni
Coal combustion	Se, As, Cr, Co, Cu Al, S, P, Ga
Nonferrous metal smelters	V
Petroleum refineries	As, In, Cu, Zn
Iron mills	Pb
Manganese production	Mn
Copper refinery	Cu
Road transport	
Vehicle emissions	Br, Pb, Ba, Mn, Cl, Zn, V, Ni, Se, Sb, As
Wearing of engines	Fe, Al
Wearing of tyres	Zn
Roadside dust	EC, Al, Si, K, Ca, Ti, Fe, Zn
Catalytic converters	Rare earth metals
Small-scale combustion	
Refuse incineration	Zn, Sb, Cu, Cd, Hg, K, Pb
Coal combustion	Se, As, Cr, Co, Cu Al, S, P, Ga
Wood smoke	Ca, Na, K, Fe, Br, Cl, Cu, Zn
Emissions from meat grill	Na, Al, K, Sr, Ba, Cl
mineral and material processing	Mg, Al, K, Sc and Fe, Mn
Seaspray	Na, Cl, S, K
Re-suspended soil	Si, V, Cr, Ca, Ti, Sr, Al, Mn, Sc

An XRD analysis of dust samples collected from Kuwait were mainly composed of Quartz (SiO_2), Calcite ($CaCO_3$), Ordered Albite, Calcian ($(Na,Ca)Al(Si,Al)_3O_8$), Dolomite ($CaMg(CO_3)_2$), Muscovite ($KAl_3Si_3O_{10}(OH)_2$), Palygorskite ($Mg_5(Si,Al)_8O_{20}8H_2O$), and Kaolinite ($Al_2Si_2O_5(OH)_4$) [20]. The dominant minerals in arid regions were found to be Chloride, Calcium, Silicon, Oxygen, Aluminum, Potassium, Sodium, and Sulphur was mainly due to the nearby sea source [21]. In contrast, for Europe, the major constituents of dust were mainly ammonium (NH_4^+), Nitrate (NO_3^-) and Sulphate (SO_4^{2-}) as a result of oil, coal-fired boiler, incinerator, and animal farming [17].

1.2.3. Particle Size Distribution

The atmospheric dust particles can be mainly characterized into four classes according to their sizes. Particles higher than 1 mm are classified as pebbles, whereas sand ranges from 0.02 mm to 1 mm. Particle size up to 1000 microns are called dust and smaller than dust are commonly characterized as thin smoke or haze [22]. In a study done in Kuwait, dust collected from a module after one year of exposure resulted in following sediment sizes.

Table 1.3: Grain-size distribution and sediment types of dust [20].

Grain-size (µm)	% in the sample	Sediment type
1000-500	0.00	Coarse
500-250	0.00	Medium
250-125	0.82	Fine
125-63	4.78	Very fine
63-31	8.16	Coarse silt
31-16	16.47	Medium silt
16-8	23.82	Fine silt
8-4	20.19	Very fine silt
<4	25.75	Clay

When a particle's diameter is larger than the wavelength of the light, the extinction coefficient is directly related to the exposed surface area of the particle [23]. Therefore, finer particles are found to have a more deteriorating effect on the surface due to the large exposed specific surface area per g and results in larger light scattering compared to the coarser particles. The size of dust particle deposited also depends on the local wind conditions. At lower wind speed (<24 m/s) smaller dust particles (30 µm) have a more influencing impact than the larger particles (75 µm) [23]. The surface chemistry of dust particles plays an important role in its adhesion on the surface. Dust grains consisting of secondary salts and organics possess higher degree of adhesion force (>400 nN) for removal, whereas particles rich in quartz requires lower adhesion force (<100 nN) [21].

1.2.4. Soiling Mechanism

The soil deposition is a complex collective process of different stages. The interdependent interactions in between are vital to understand the mechanics involved in dust settlement as well as its removal. The soiling process involves include following major steps.

Figure 1.2: Different processes involved for dust deposition on a PV module.

a. Dust Transportation

Transportation of atmospheric dust minerals from one place to other is mainly due to the wind or sandstorm for arid regions. This process is commonly known as Aeolian or alluvial process. If the wind speed surpasses a "threshold velocity", it results in dust re-suspension and transfer [22]. The movement also strongly depends on its surface texture and dust wetness. As discussed in 1.2.3, smaller particles have high adhesion force thus, the threshold velocity of a fine particle is higher. Based on the particle size, the Aeolian process can be divided into three modes.
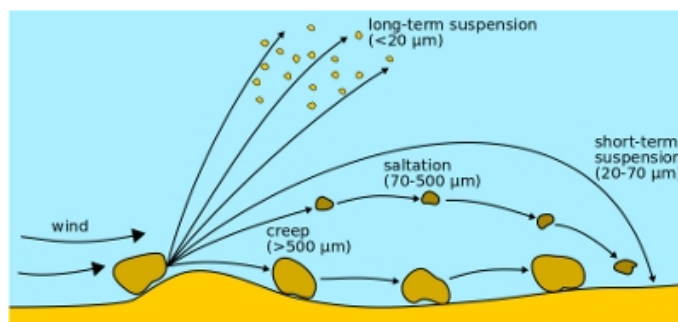
Figure 1.3: Three modes of Aeolian process [22].

A short-term or long-term aerodynamic entrainment of smaller particles (<20 μm) is known as suspension. Medium size particles (70-500 μm) that do not stay in the air for a longer time and hop to a shorter distance by saltation process. The rolling of larger particles (>500 μm) is termed as creep motion, which again forms fine particles by disintegration process [22]. Dust particles suspension and saltation are deposited by sedimentation process due to gravity.

b. Primary Adhesion Process
The adherence of the atmospheric dust depends on the its composition, surface reactions at front cover, particles size, module tilt angle and orientation, and surface electrostatic charge. Dust settlement is followed by activities mainly based on its size [21].

i. Gravitational Settling: Particles are mainly settled by the gravitational forces, which is more dominant in coarser particles than smaller ones.

ii. Brownian Motion: This movement is mainly seen for smaller particles due to the imbalance in the applied force.

iii. Eddy Diffusion: Dust particles are deposited either by turbulent or laminar flow near a module surface. A laminar wind flow near the surface provide enough force for the deposition.

iv. Electrostatic Charge: During the transportation process, dust particles are electrostatically charged after its interaction with other surfaces. Depending on the opposite charge, dust particle gets attached to the surface.

v. Coalescence: A random movement of the particles in atmosphere results in its coalescence to form a larger and heavier particles. After some time, the particles are settled due to gravity.

c. Adhesion Modification
A particle adhesion tends to change with wind speed, relative humidity, rainfall event, and presence of the dew. With time, the deposited particle gets modified as a result of following mechanics [24].

i. Dust Cementation: As mentioned in section 1.2.2, dust particles contain both organic and inorganic salts soluble in water. After light rainfall and dew events, the outer layer of particles tend to dissolve and form salt scaling on the surface driven by Sun's heat. Few repetition cycles, result in a cemented layer formation, which can develop as a hard soiling. It has larger detrimental effects compared to soft soiling (thin soiling). The cementation process is shown by the Figure 1.4.
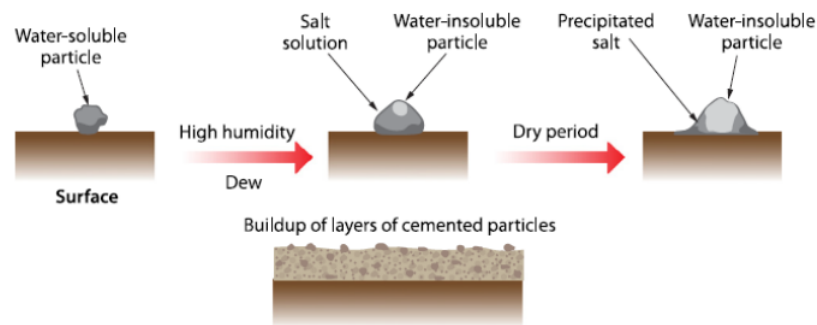
Figure 1.4: Dust cementation process [21].

Dust sample collected from a module in Qatar showed the presence of Palygorskite (clay mineral), which forms a nanoscopic needle structure to promote adhesion on the surface. Similarly, dust sample from Chile was rich in phyllosilicates (kaolinite), that has a morphological structure of platelets resulting in adhesion through increased contact area known as caking [25].

ii. Deposition of Organics: Sometimes prior to the cementation process, a thin layer of organic compounds gets deposited on the surface. This layer favors a high degree of cementation leading into difficult cleaning process.

iii. Surface Tension: When the surface force increases, the coalescence of droplets become more prominent to form larger dust spot on a module.

iv. Particle Energy: The interaction between particles as well as its energy increases for smaller particles (<10 μm). This makes it very difficult for particle removal even at higher wind speeds (>150 m/s).

d. Surface Alterations

The above discussed adhesion mechanisms can alter the surface characteristics of a module by salt scaling or weathering. This might promote more dust deposition.

e. Restorative Process

The cleaning procedure of a soiled module can be natural (rainfall) or artificial (manual and automatic). Light amount of rain could attenuate the module performance by forming non-uniform patches on the surface. Rainfall of more than 20mm was found to be sufficient for a cleaning process [10]. Similarly, dry cleaning of a module might electrostatically charge its surface resulting into more accumulation, whereas a wet surface might as well attract more dust particles to get deposited.

1.2.5. Factors Influencing Soiling Process

Various interdependent factors responsible for soiling are broadly divided into two sections; module characteristics and the environmental parameters.

a. Module Characteristics

Different types of PV technology are available in the market that utilizes Sun's irradiation to produce an equivalent power. Once a module is installed, it's characteristics are fixed and it is highly influenced by the soiling occurring at a different rate throughout the year. In this section, some of these characteristics that aid towards soiling have been discussed.

i. Module Tilt: A module can be installed either on a fixed tilt or with Sun tracking mechanism. An optimum module tilt for a location is determined by performing maximum annual energy yield calculation over a range of tilt angles. However, according to a rule of thumb, the tilt angle should be almost equal to the latitude of a location. Sun tracking system is cost intensive, therefore most of the PV systems are installed at a fixed tilt. When a module is completely facing upwards (tilt = 0°), the gravitational settling rate is dominant and results in high deposition of dust [26], whereas for higher tilt angles (>0° up to 90°), dust diffusion is the major soiling mechanism. The gravitational settling velocity is directly proportional to the square of the diameter of the particle ($\propto d^2$), therefore the larger the particle, higher the deposition at low tilt. In contrast, diffusion process is inversely proportional to the diameter of the particle ($\propto d$), thus fine particles gets deposited on modules with higher tilt angles [26]. A systematic study done for three months on the 9 different modules at 5°, 10°, 15°, 20°, 23°, 30°, 33° and 40° tilt angles in Arizona, dust deposition and irradiance loss for 0° was found to be the highest at 2.02%. Furthermore, the losses decreased with tilt angle and reached lowest at 0.69% for 40° [27]. In another experiment, the soiling non-uniformity was noticed to be highest for 30° compared with 0° and 15° due to dew formation and partly cleaning [20]. Therefore, modules installed in dry climates and near the Sunbelt will highly suffer from soiling due to higher dust settlement at lower tilt.

ii. Sun Tracking: Diurnal and seasonal tracking facilities could assist in cleaning by stowing module facing down during night and sandstorms. A year-long experimental test performed in Saudi Arabia, resulted in a monthly average energy gain of 18% for single-axis tracking system and 20% for double axis tracking system compared to the fixed tilt module [28]. The reflection losses in a module increases with angle of incidence of the light source [29], therefore, for a fixed tilt system, the reflection losses (hence angular losses) are larger in the mornings and evenings. In addition, the presence of dust

on a module increases its angular loss thus , Sun tracking system might as well help reducing these reflection losses by keeping an angle of incidence (AOI) low at all the time.

iii. PV Technology: A module's transmittance reduces with soiling in a spectral dependent manner. The spectral loss at same mass loading (g/m^2) was found to be highest at lower wavelength range (350-500 nm) [20]. Therefore, spectral photo-current loss in lower bandgap material (a-Si and CdTe) was larger than for larger bandgap technology (c-Si and CIGS). At 14 mg/cm^2, the loss was around 66% for a-Si modules, whereas for c-Si it was almost 59%.

iv. Module Surface: Module's surface is textured to utilize the incoming radiation in a best possible method by reducing reflection losses [30]. However, textured surface tend to increase the soiling loss by trapping dust particles into its voids or trap sites. This deposition might also lead to non-uniform soiling condition imposing larger effect for power generation [31]. If there's no bypass diode, the current generated by a non-uniformly soiled cell will determine the overall current from a module. At this condition, natural or manual cleaning is rarely complete due to the difficulty in removing dust from the trap sites.

v. Module Mounting: In a c-Si module, 60 or 72 cells are connected in series mostly in three strings (each string with one bypass diode), whereas CIGS module have 100-120 cells connected in series with each cell stretching from top to bottom in a portrait mode. When dust gets deposited on the larger edge of a c-Si module, a bypass diode is activated due to partial shading and a module will perform at two-thirds of its capacity, this could be better than all strings being shaded in a portrait mode. For a thin film module, a portrait mode might result in the shading of all the cells partly resulting in lower power losses than for a landscape mode. Hence, thin film modules are generally installed with smaller edge facing ground to avoid the shading of an entire cell as presented in 1.5.

(a)   (b)
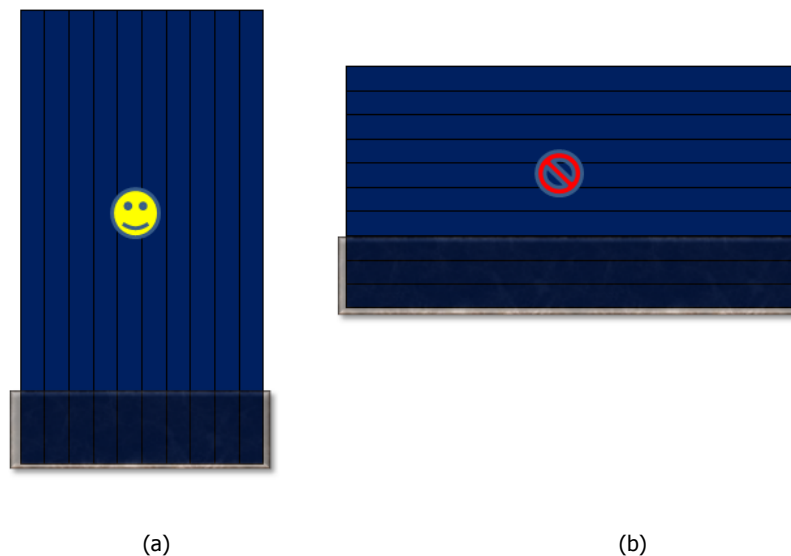
Figure 1.5: Thin film module on a portrait (a) and landscape mode (b).

b. Environmental Factors

Different environmental parameters play an important role for a soil accumulation. Some of these factors depends on the time as well as on the geographical location that can change over a day or with seasons. Some major environmental factors highly influencing dust collected on a module are discussed in the following.

i. Wind Speed: Wind Velocity is one of the major carrier of dust. It acts as a cooling medium as well as facilitates soiling of the module. Dust accumulation is a result of the rate of deposition and

rate of removal by the wind event [26]. High wind improves dust removal rate at higher module angle but at lower tilt the limitation of air boundary layer at module's surface inhibit the cleaning action. As mentioned in section 1.2.5, tilt angle also relates with the size of dust deposited. It has been also found, that dust removal rate is proportional to the diameter of dust ($\propto d$) but adhesion force is proportional to the square of the diameter ($\propto d^2$) [26]. Thus, fine grains becomes very difficult to remove even at 50 m/s.

ii. Altitude: The vertical concentration of PM2.5 and PM10 showed that the concentration up to the height of 5 metres was highest at 125 µg/m^3 but after 100 metres the concentration decreased to around 95 µg/m^3 [32]. Therefore, PV systems at higher altitude will have low the atmospheric dust concentration so lower soiling losses but systems at high altitude are less safe in case of wind storm.

iii. Nearby Dust Sources: For a ground mounted PV modules, the vehicular movement, construction works, and natural vegetation are the sources of soiling. In an experiment, the concentration of elemental and black carbon deposited on the modules kept 10 to 300 metres from a highway showed lowest concentration of 6 µg/m^2 at the largest distance. The deposition increased with the decrease in its distance [33].

iv. Relative Humidity (RH):   Desert locations with minimum rainfall suffers from a high relative humidity. These high humid conditions, promotes dust adhesion by forming a sticky layer of dust and reduces direct normal irradiance (DNI) incident on a module [26]. The overall performance of a module declined sharply if the relative humidity increases. Although high wind speed decreases the relative humidity of the air, a thorough cleaning need to be done to increase a module's performance after a humid day.

v. Rainfall: Rainfall is the most efficient natural cleaning factor for a module. Light rainfall aids in the formation of undesirable dust spots at a lower tilt. A minimum of 3.5 mm of rainfall is needed to recover soiling losses by 50% whereas light rain (<20 mm) affected the cleaning process as it facilitated the formation of hard soiling on a module [5]. For a prolonged dry days in a PV park, a sufficient rainfall can re-establish the plant capacity at its maximum. Timely rainfall would also avoid the cost of manual cleaning, which is one of the major O&M cost in a power plant. In Sun tracking system, changing a stowage position to an optimum tilt will fully utilize the cleaning effects of the rain and minimize non-uniform or hard soiling.

vi. Dew Frequency: Sufficient amount of dew formation could act as a cleaning agent. Dew formation in arid and semi-arid areas could also facilitate in forming a sticky layer because a wet module relatively attracts more dust particles to its surface [26]. A study carried out to measure dew frequency around the globe showed that places like Australia, South-East Asia, Middle East and North African regions account for extremely low amount of dew frequency for an entire year [34]. These places are very prone to have soiling losses due to high RH and low dew formation. In Figure 1.6, the blue part represents high dew formation, whereas the red part signifies lower dew frequency. Acronym DJF stands for December, January and February, MAM (March, April, May), JJA (June, July, August), SON (September, October, November). Lower dew frequency is mostly due to insufficient night cooling of Earth's surface, high cloud fraction, and high RH.
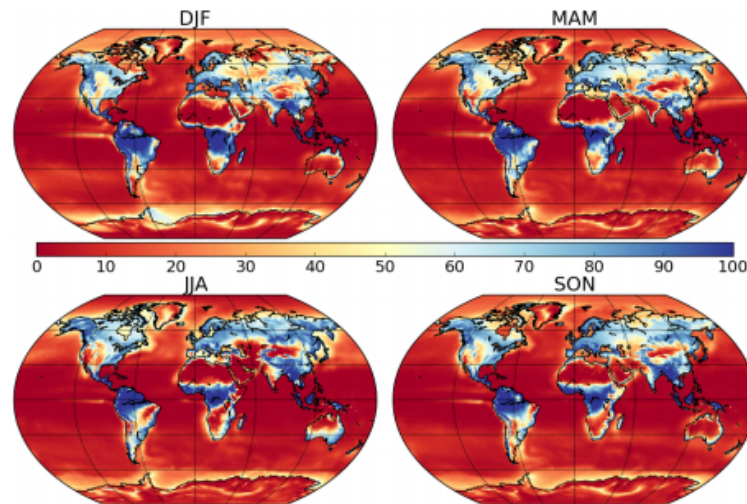
Figure 1.6: Seasonal dew frequency as a fraction of days (%) with minimum of 0.1 mm/day [34].

vii. Dust Storm: Dust events are frequently experienced in Middle East and North African countries as well as for central Asian regions. Dust storms could be several kilometers high and wide [12]. A yearly average of seven dust storms are experienced in Abu Dhabi, UAE [35]. Similarly, North African country, Egypt experiences frequent sandstorms during the month of April and May [36] and Kuwait possess higher sandstorms probabilities during the month of June and July and least during last three months of the year [37]. Frequent dust events escalate deposition rate and blocks all the irradiation leading a module to be completely non-functional. Figure 1.7 represents a PV park in Qatar before and after a dust storm.

(a)   (b)

Figure 1.7: Module soiling due to the sandstorm event observed in Qatar, Doha [38].

1.3. Soiling Measurement

Soiling refers to everything that is deposited on a module either naturally or artificially that bars the incident light photons. There are different terminologies normally used during soiling measurements. Some of these are defined as:

i. Soiling Level: The average percentage reduction on the incident irradiance due to the presence of dust or dirt on a module [3]. If a module has 20% soiling level this relates same amount of irradiance reduction falling on a module.

ii. Transmission Loss (TL):   The percentage reduction in the transmission of the light photons due to the presence of any blocking objects (soil, snow, clouds or any other foreign elements) is known as

transmission loss of a PV module [7]. This can be calculated as a complement of the irradiation from temperature corrected short-circuit current of cleaned and soiled modules as given by a equation 1.1,

$$T_{loss} = 1 - \frac{G_s}{G_c} \times 100\% = 1 - \frac{I_{sc,s}}{I_{sc,c}} \times 100\% \tag{1.1}$$

In equation 1.1, G_s and G_c represent the irradiation utilized by a module at soiled and clean conditions respectively whereas, $I_{sc,s}$ and $I_{sc,c}$ are the temperature corrected short-circuit current produced by respective modules.

iii. Soiling Power Loss: It is the percentage reduction in power output caused by soiling [39]. This is estimated as a complement to the unity of equation 1.3.

iv. Rain-free Period (RF$_p$): A number of dry days in between rainfall events.

v. Soft Shading or Uniform Soiling: Occurs when a thin layer of dust is deposited on a module uniformly, which reduces an overall irradiance to a module [5]. At this condition, only short-circuit current is affected but not V_{oc}. The effect of uniform soiling on the I-V/P-V curves is represented by Figures 1.8 and 1.9.
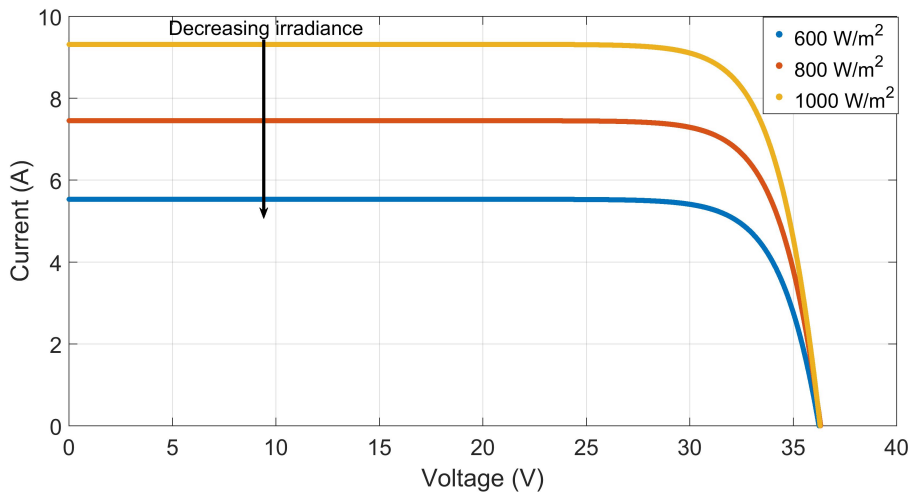
Figure 1.8: The effect of soft or uniform soiling on the I-V curve of a standard 60-cells polycrystalline module.
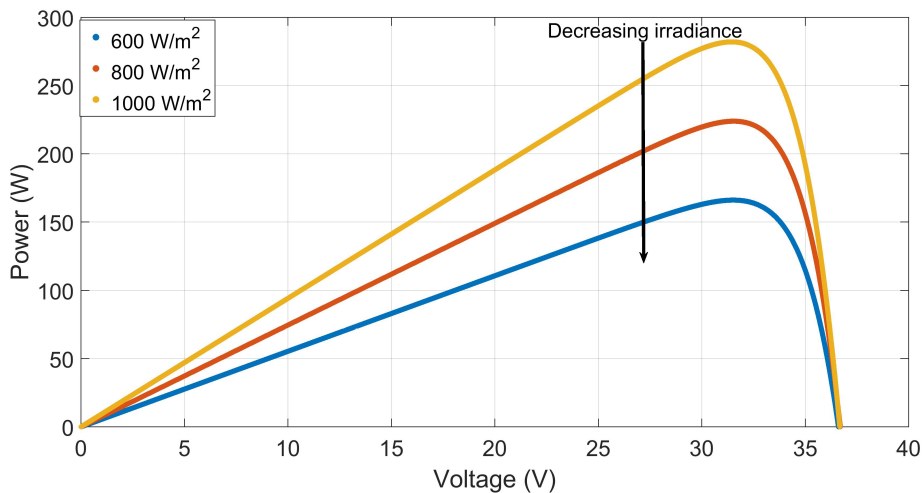
Figure 1.9: The effect of soft or uniform soiling on the P-V curve of a standard 60-cells polycrystalline module.

vi. Hard Shading or Non-uniform Soiling: Occurs after a cementation process and when patches of dust or any foreign objects block the light in a definite shape similar to partial shading. Therefore, when a module is partially shaded, the activation of bypass diode might facilitate to keep the short-circuit current constant, but decreasing the voltage produced by the shaded cells [5]. A detailed experiment has been carried out in section 2.20 from chapter 2. The effect of hard or non-uniform soiling on the I-V/P-V curves is represented by Figures 1.10 and 1.11.
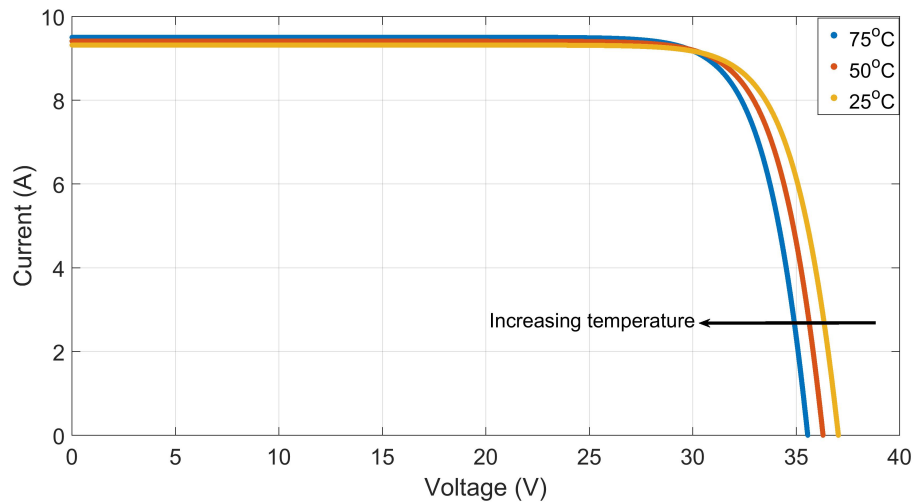
Figure 1.10: The effect of hard or non-uniform soiling on the I-V curve of a standard 60-cells polycrystalline module.
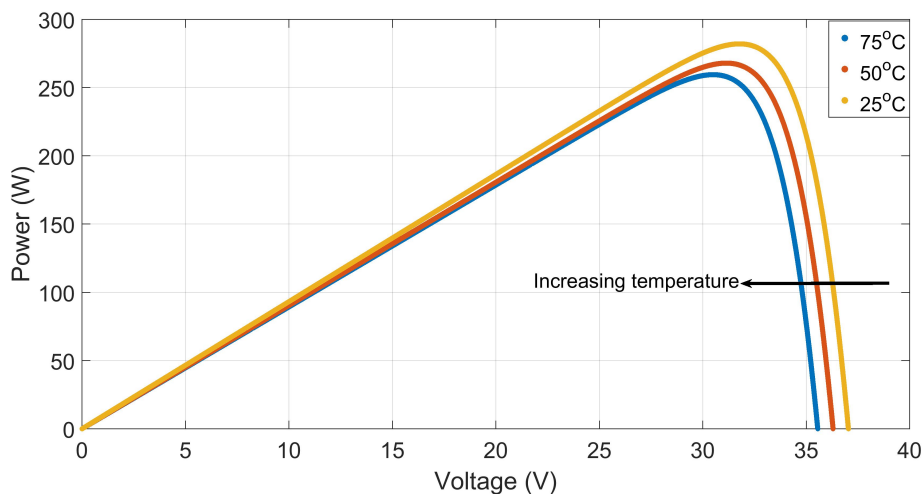
Figure 1.11: The effect of hard or non-uniform soiling on the P-V curve of a standard 60-cells polycrystalline module.

vii. Soiling Ratio (SR):   Soiling ratio (SR) is defined as the ratio of irradiance utilized by a soiled compared to a cleaned in order to produce corresponding short-circuit current or power [40]. This parameter will be further studied in detail in section 1.3.1.

1.3.1. Measurement techniques

The quantification of a module soiling at a field level is carried out in various ways. The severity of soil on the PV performance can be determined by characterizing and measuring the amount of dust deposited on a module, measuring the relative transmission loss at particular soiling level, and comparing the external parameters to calculate the output of a module. Next, some of the methods will be summarized, which is generally used to determine and quantify the soiling loss of a module.

a. Amount of Dust

This is a straightforward estimation of a module soiling. Dust collected from a module allows determining its physical and chemical properties. This analysis can then be translated to determine an equivalent output power or transmission loss. [41]. This method is a labor-intensive process, where a timely collection of dust is required. A piece of glass coupon or a mini PV module can be used for dust collection. The collected dust particles are analyzed by their amount, sizes, color, and composition. The determined properties are approximated to the transmission or power loss from a module. This is not the perfect measurement approach as the characteristics of different PV technologies have varying influence on the same conditions.

b. Transmission of the Light Photons

Generally, soiling is identified as attenuation and scattering of the light from a module's perspective. The transmission loss can be readily measured by a pyranometer or spectrometer installed in the proximity of a module [42] [14]. Moreover, silicon pyranometers with photo-diode detection installed at the plane of array (POA) can measure the irradiance loss due to the soil. However, the relative transmission loss given by a pyranometer might not be exact to that of a PV module due to spectral differences. Commonly, a glass coupon is used alongside a PV module and left for dust accumulation, later, with the help of a spectrometer transmission loss of the glass is estimated [36]. The equation to calculate the transmission loss follows the same principle as presented in 1.1.

c. Module Performance

Soiling measurements using PV modules gives the exact losses rather than above methods. As discussed in section 1.3, a module might suffer from uniform and/or non-uniform soiling conditions, therefore, the actual PV output will accurately estimate the real-time losses. The estimated soiling irradiance or power loss can be determined with the help of a soiling ratio (SR) parameter. According to *International Electrotechnical Commission* (IEC), "The soiling ratio is the ratio of the actual power output of the PV array under given soiling conditions to the power that would be expected if the PV array were clean and free of soiling". Referring to IEC 61724-1, soiling ratio can be measured by comparing two identical calibrated PV modules, one of which is left for the natural dust accumulation whilst other is frequently cleaned. The short circuit current (I_{sc}) and the maximum power produced (P_{max}) by these modules are measured and compared using equations 1.2 and 1.3 [40].

$$SR^{Isc} = \frac{G_s}{G_c} = \frac{I_{sc,s}(1 - \alpha(T_{m,s} - T_{ref}))}{I_{sc,c}(1 - \alpha(T_{m,c} - T_{ref}))} \times \frac{C_{Isc,s}}{C_{Isc,c}} \tag{1.2}$$

$$SR^{Pmax} = \frac{P_{max,s}(1 - \gamma(T_{m,s} - T_{ref}))}{P_{max,s}(1 - \gamma(T_{m,s} - T_{ref}))} \times \frac{C_{Pmax,s}}{C_{Pmax,c}} \tag{1.3}$$

In equation 1.2, the irradiance received by a soiled module (G_2) to the clean (G_1) or short circuit current generated from the soiled module ($I_{sc,s}$) to the clean module ($I_{sc,c}$) are measured to calculate soiling ratio from short-circuit method (SR^{Isc}), whereas, the maximum power point of a soiled module ($P_{max,s}$) to the clean module ($P_{max,s}$) is measured to estimate soiling ratio from maximum power point method (SR^{Pmax}) from equation 1.3. α and γ in above equations represent temperature coefficients for short-circuit current and maximum power point respectively. In equation 1.2, $C_{Isc,c}$ and $C_{Isc,s}$ are the short-circuit calibration values for clean and soiled module respectively. Similarly, $C_{Pmax,c}$ and $C_{Pmax,s}$ are for the maximum power point of a clean and soiled module. Two co-planar modules are generally normalized with a help of calibration factors calculated by comparing clean I_{sc} or P_{max} produced at the same irradiance and temperature level. These calibration factors account for manufacturing defects, differences in cable resistance or any other abnormal behavior, which might lead to variable current and power production at an identical conditions [3]. $T_{m,s}$ and $T_{m,c}$ in equations 1.2 and 1.3 are measured module temperature of soiled and cleaned modules respectively. Finally, T_{ref} is the temperature for the module when the ambient temperature is 25°C.

The measured current and power are subjected to a temperature correction to account for net irradiance loss only due to soiling. SR computed from short-circuit current method quantifies the loss in irradiance, while the actual power reduction in a module is accurately measured by soiling ratio from maximum power point method [40]. This dependency can be explained with the help of equations

The short-circuit current, open-circuit voltage and maximum power of a module at Standard Test Conditions (STC) are given by [43]:

$$I_{sc}(25°C, G_m) = I_{sc}(STC)\frac{G_m}{G_{STC}} \tag{1.4}$$

$$V_{oc}(25°C, G_m) = V_{oc}(STC) + \frac{nk_bT}{q}\ln(\frac{G_m}{G_{STC}}) \tag{1.5}$$

$$P_{max}(25°C, G_m) = \eta \times G_m \times A_m = V_{oc}(25°C, G_m) \times I_{sc}(25°C, G_m) \times FF \tag{1.6}$$

G_m and G_{STC} are the irradiance at instantaneous and at STC respectively, n is the ideality factor, k_b is the Boltzmann's constant and T is module temperature. I_{sc}(STC) and V_{oc}(STC) are the short-circuit current and open-circuit voltage at STC. The temperature of soiled module is higher due to the current limited in the cells. Therefore, when temperature rises, I_{sc} slightly increases due to the thermal generation of carriers (increase in I_o) in p-n junction given by its positive temperature coefficient value (α = 0.053%/°C). In contrast, open-circuit voltage inversely related with saturation current (I_o) decreases given by its negative temperature coefficient (α = -0.31%/°C) [44]. The V_{oc} decreases with higher magnitude than the increase in I_{sc}, therefore overall performance of a system falls at higher module temperature. η and A_m are respectively module's STC efficiency (%) and module's active area (m^2). Equation 1.4, represents a linear relation between current and the POA irradiance. Therefore, a temperature corrected I_{sc} is sufficient to estimate the loss in irradiance from soiling. On the other hand, equation 1.5 shows a logarithmic dependency of V_{oc} with irradiance so during low light conditions, the V_{oc} is less influenced and reduction in power output is majorly due to lower current generated.

For a larger system like a PV park, the energy yield (kWh/kW$_p$) and performance ratio can be used as an estimate of soiling losses [45]. Plant performance can be calculated by comparing the actual and estimated production:

$$\text{Performance Ratio (PR)} = \frac{\text{Actual plant production (kWh per annum)}}{\text{Nominal or estimated production (kWh per annum)}} \tag{1.7}$$

In the work of [39], soiling rate was studied by analyzing the power plant's performance in southwest desert of USA, Western Australia, and Arabian Peninsula. The soiling rate was found to vary spatially resulting into different PR over the production area (minimum PR of 89% and the maximum was 95%).

Dust on a PV module also increases its angular losses (AL), thus decreasing the transmittance of irradiance at the same angle of incidence (AOI) compared with the clean module [29]. Therefore, soiling loss varies with the angle of the Sun's ray on a module. The least angular losses are noticed during the mid of the day when AOI of the Sun is minimum. A detailed study of module angular losses has been done in chapter 4.

d. Photography, Satellite Data and Microscopy
Photography and image processing technique is an emerging technology to estimate soiling losses by the means of captured images and videos [42]. An experiment was performed in northern Australia, where the researchers analyzed different images taken with the help of a drone and compared it with the photographic database of known soiling [46]. In another study, an outdoor soiling microscope was developed and deployed to study the soiling rate based on the environmental parameters of aerosol concentration, wind speed and relative humidity (RH). The microscope was able to measure deposition and re-suspension of particles larger than 10 µm^2 in a matter of seconds [42]. Moreover, a Dutch company (Sobolt energy intelligence) uses satellite images to determine dust accumulation on the modules [47]. Similarly, some solar O&M companies also compare infrared (IR) image of a soiled module with a normal image to determine the soiling level as well as the electrical defects in a module.

1.3.2. Commercial Products
Cost effective soiling measurements within a solar plant can give a reliable insight into the soiling behavior, which will allow for an optimal cleaning schedule. Different research institutes and companies

are concentrating to develop a product that can precisely measure a soiling loss. Some of the major instruments that are commercially available in the market will be next discussed. Lastly, all the products are compared in table 1.4 based on their measuring parameters and precision.

a. DustIQ (Kipp & Zonen)

A Dutch company based in Delft, The Netherlands has developed a soiling detection sensor called the DustIQ. It utilizes the optical soiling measurement principle (OSM) avoiding daily manual cleaning, moving parts or water for measurements [48]. DustIQ measures the transmission loss from a module with the help two measurement sensors after local dust calibration with an onboard mini PV module. A detailed explanation has been done in chapter 3.

b. SMP100 and CR-PVS-1 (Campbell Scientific)

Campbell Scientific are the manufactures of data loggers, data acquisition systems for measurement and control based in Canada. There are two different products available for soiling loss measurements, SMP100 and CR-PVS-1. SMP100 was originally designed to track the maximum power point of modules without an inverter. Later, it has been modified to estimate soiling that consists of two co-planar PV modules on the vertical support. One of the reference modules is kept clean and the test module is left for soil accumulation. The instrument estimates the soiling rate by measuring short-circuit current, open-circuit voltage, temperature, the irradiance of clean and soiled modules [49].

CR-PVS-1 is a Modbus connected data logger system, which records the daily average or real-time soiling index implying data filtering technique. The short-circuit current and module temperature of a 20 W_p reference mini-modules are measured [50]. The measured parameters are compared with one of the test module (can be up to 300 W) in the field. The collected raw data can be stored for further analysis [50]. Both the instruments are shown in Figure 1.3.2.

(a)   (b)
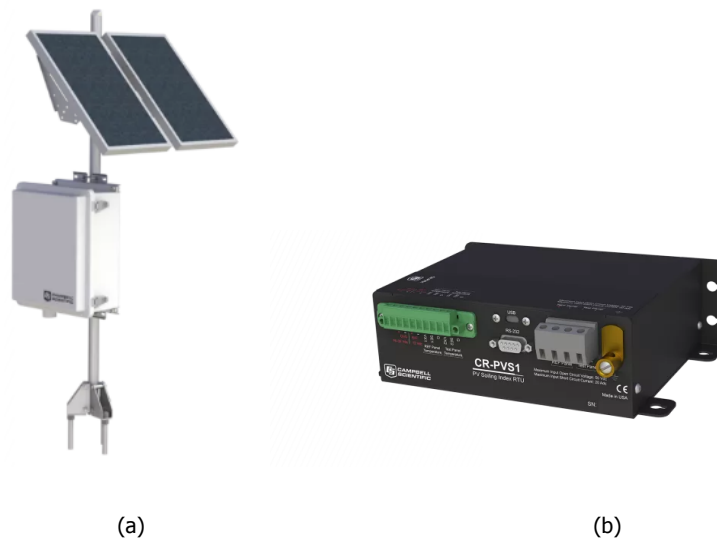
Figure 1.12: SMP100 and CR-PVS-1 from Campbell Scientific [49] [50].

c. PVSOIL (Groundwork)

Groundwork is a US-based company specializing in solar resource management. PVSOIL is a soiling measurement instrument, which consists of a data logger and two reference solar modules of 20 W_p each. One of the modules is timely cleaned while other is left for soil accumulation. The short-circuit current, module temperature and irradiance are measured to calculate the real-time soiling ratio (SR) [51]. The data can be stored and monitored via their SCADA interface. The working principle of PVSOIL is similar to SMP100 by Campbell Scientific.

d. Ammonit Soiling Measurement Systems (Ammonit)

Ammonit is a Germany-based company, which offers various measurement instruments for solar and wind field. The Ammonit soiling measurement systems consist of two co-planar PV modules connected to a meteo-40 data logger powered by onboard PV. The short-circuit current and module temperature from both the modules are recorded to determine the soiling losses. The system also considers the pollution level and other environmental parameters at the site [52]. The working principle and instrument setup is similar to that of SMP100 as discussed above.

e. Soiling Measurement System for PV power Plants (Atonometrics)

Atonometrics is a US-based company that makes equipment for PV module reliability testing in a high volume manufacturing scenario or different measuring services aiding for manufacturers to scale up their production. The soiling measurement system consists of a small reference PV cell, a large size PV module and two boxes, one with I-V sweep, which measures the instantaneous irradiance and temperature measurement for data analysis and other is fitted with pump and water reservoir as shown in Figure 1.13 [53]. The reference cell is used to measure the irradiance that is automatically cleaned every day by a flow/level sensor. The large PV module measures the soiling power loss by comparing soiled I-V curve of a clean reference cell. Since it employs I-V curve tracing, it easily identifies both uniform and non-uniform soiling.
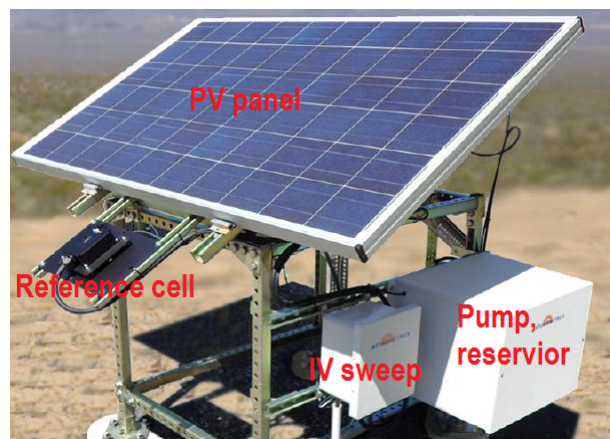
Figure 1.13: Soiling measurement system by Atonometrics [53].

f. Dust Detection System (DDS) (UKC Holdings Corporation)

UKC holdings is a Japan-based company, which mainly manufactures semiconductor components (PV module) and inverters. The company manufactures four different soiling monitoring solutions namely DDS-Ground, DDS-mini, DDS-lite and DDS-Analyzer [54]. The DDS-Ground is suitable for power plants with more than 10 MW_p capacity, whereas DDS-mini is designed for a small system of few hundred kW_p to 1 MW_p and DDS-lite is for rooftop systems. DDS-Analyzer is a portable setup, consists of PV modules with different technologies mainly used for performance analysis. All these instruments are based on the comparison of two co-planar modules, one of which is naturally soiled and other is cleaned with the help of adjustable nozzles installed at the top [54]. A number of DDS systems in a PV park can be connected with a central display solution for further monitoring process.
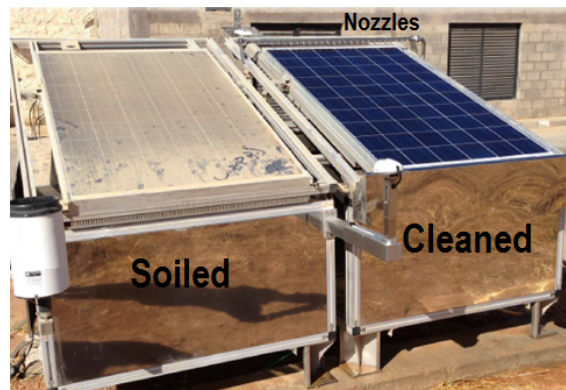
Figure 1.14: DDS-Ground installed in the desert of Amman, Jordan [54].

g. Soiling Measurement Kit (NRGSystems)

NRGSystems is a US-based company majorly manufactures instruments for solar and wind measurements. The soiling measurement kit is a three module (15 W_p each) setup, two of them compare short-circuit current of a soiled module to clean. The Third module is to power the data logger (SymphoniePRO) attached to the system [55].

A comparison of different soiling measurement devices is done in the table 1.4. A detailed study about the DustIQ has been studied in Chapter 3 thus, it excluded from the table.

Table 1.4: Product overview for soiling measurement [49][50][51][52][53][54][55].

Company	Campbell Scientific	Groundwork	Ammonit	Atonometrics	UKC	NRGSystems
I_{sc} or P_{max}	Both	I_{sc}	I_{sc}	Both	Both	I_{sc}
module temp.	Yes	Yes	Yes	Yes	Yes	Yes
Temp. range (°C)	-40 to +135	-73 to +260	NA	NA	NA	-40 to +85
Accuracy (%)	≈1	>0.29	NA	3-5	NA	<1
Cleaning method	Manual	Manual	Manual	Automatic	Automatic	Manual
Data storage	Yes	Yes	Yes	Yes	Yes	Yes
Warranty	1 year	NA	NA	NA	NA	2 years

1.4. Cleaning of the Soiled Module

Cleaning cycles is a trade-off between energy that would have been saved if a module was clean (€/kWh) and the cleaning cost (€/KW_p). Soiling rate has been identified by its installed location as well as a module characteristics. For a high cleaning cost and lack of availability of water, minimizing cleaning frequency would be an optimal solution. In a tropical region at 15-25°latitude range, weekly cleaning schedule has been recommended [6], whereas for a dry arid region like Riyadh, Saudi Arabia, thrice a week cleaning is needed [26]. After a rainfall or manual cleaning (labor or robots), the soiling loss is eliminated and power generation is restored to 100%. For an artificially soiled modules at an average transmission loss of 13.2% from section 2.2.3, a total rainfall of 27.5 mm was required to clean the module completely. Different models has been developed to optimize the manual cleaning cycles. One such model determines an average optimum time between washing (T (days)), cost of washing (W ($)) and the rate of revenue loss due to soiling (r ($/day²)) [56].

$$T = \sqrt{\frac{2W}{r}} \tag{1.8}$$

Different cleaning methods that remove dust from a module are discussed in a chart 1.16.
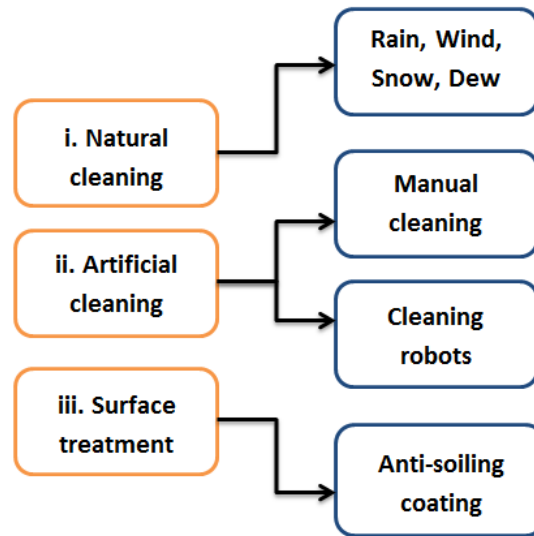
Figure 1.15: Different cleaning methods for dust removal.

a. Natural Cleaning

A cost-free natural cleaning process involves heavy rainfall, frequent dew occurrence, high wind, and melting of the snow. As mentioned in section 1.2.5, light rain could have a deteriorating effect on a module and most of the arid/semi-arid regions experience lesser annual rainfall. This makes natural cleaning of a module as a non-reliable cleaning method.

b. Artificial Cleaning

If the rainfall is not effective, artificial cleaning is done at most of the times. For a MW_p plant, approximately 7000-20000 litres of water is required and the cleaning cost could be anywhere from 100 to 800 USD [57]. For a water-based cleaning, the applied pressure should be less than 1000 Pa, water pH should be in the range of 6 to 9, the temperature difference of the water and module should not be more than 10°C, and salt concentration in the water should not exceed 2% [57]. These requirements need to be followed to avoid rapid PV module aging. Depending on the size of the plant, availability of water, and the cost involved, artificial cleaning can be broadly divided into two categories.

i. Manual Cleaning: Small-scale PV systems, ranging from few kW_p to 1 MW_p can be cleaned manually by employing labor. The application of normal or distilled water often with a cleansing agent (detergent) and soft fabric or a brush is best for manual cleaning. However, a support vehicle is used to carry a large amount of water, it tends to increase the overall cleaning cost. Although a labor employed cleaning cost is as high as 2 $/kW_p$, most of the times it is insufficient and incomplete [58]. Applying high-pressure water jets along with the scrubber has been found to clean the module completely but excessive brushing could also degrade the module output by forming scratches on the surface. The atmospheric content of urban location is rich in carbon, therefore a mixture of anionic and cationic cleaning mixture is generally recommended for sufficient cleaning [59].

ii. Cleaning Robots: For plants larger than 1 MW_p, the manual cleaning cost, water usage and cleaning efficiency are greatly compromised. Therefore, it is cost-effective to use automatic cleaning robots. Today, a number of cleaning robots are commercially available in the market that uses the minimal amount of water and completely restores modules' performance. Similarly, a computer controlled mechanical devices consisting of a microcontroller is also available that applies an optimum method (with or without water) based on the type of dust. A gearbox and stepper motor rotate at high speed and allow the user to select between wet and dry cleaning [26]. This cleaning technology is still at a developmental stage, therefore a team of technicians is always needed at the site for supervision. One

more drawback is the total power consumed by these robots might not be a cost-effective option for some of the systems. Some commercially available cleaning robots have been compared in 1.5.

Table 1.5: Commercially available automatic cleaning devices [57][60][61].

Company	Solar ACM	SUNPOWER	Eccopia	ExoSun	Energy Guru	Wylton	NOMADD
Water or dry	Dry	Minimal Water	Dry	Dry	Dry	Dry	Dry
Automatic	Yes	Yes	Yes	Yes	Yes	Yes	Yes
Power supply	External	Solar	External	Solar	External	External	External
Array transfer	No	Yes	No	Yes	Yes	Yes	No
Cleaning rate (m^2/min)	30	30	11.55	36	12.8	15-20	30
Weight (kg)	60	NA	86	35	30	NA	20
Device width (m)	2,3,4	2.67	2,3,4	1.8-2	1,2,3,4	NA	2,3

c. Surface Treatment

The outer cover of a module is a glass type material, that provides a window for incoming radiation and protects against thermal and mechanical stress. Applying an appropriate anti-soiling coating to the surface can increase the module performance by becoming more resilient against deposition of foreign bodies (dust, dirt). The treatment can be either water repellent or water attracting commonly known as hydrophobic or hydrophilic [62]. Hydrophobic coatings have a large contact angle (α) leading to a low contact area, which aids in cleaning by keeping off the dirt and avoiding dust coalescence. Hydrophilic coatings have large contact area and small contact angle (α) forming a film of water washing away the dirt from the surface. The principle of the hydrophobic and hydrophilic coating has been shown in a Figure 1.16

(a)   (b)
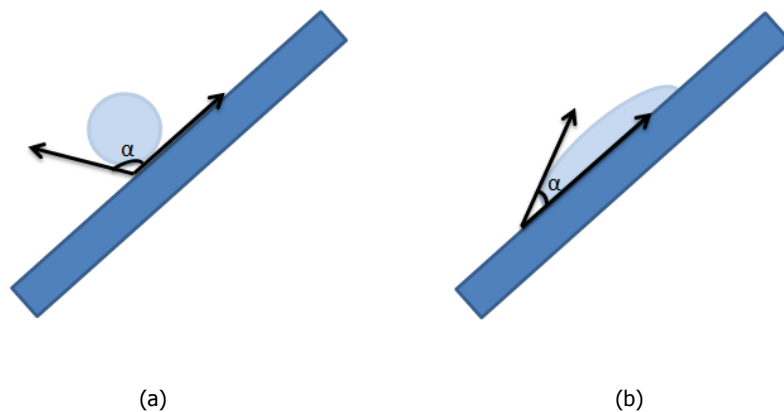
Figure 1.16: Different contact angles of a water droplet in a hydrophobic and hydrophilic coating.

A comparison between these two types of coating showed that hydrophilic coating has slightly better performance [26]. Anti-soiling coating presented by DSM (Dutch company) is claimed to keep optical losses less than 0.5% even after 15000 cleaning events [63]. Similarly, CSD nano coating (nanostructured silica) of the modules results in an energy gain of 3-6% by avoiding dust settlement [64]. An electrodynamic screen (EDS) technique is emerging as one of the innovative cleaning methods. It generates single, multiphase, standing or travelling waves to repel and transport particles away from the surface [26]. This technique is generally used for solar module cleaning in space applications.

1.5. Motivation and Research Objectives

With the increased installation of PV systems around the world, soiling has one of the largest impacts on its performance ratio that is often ignored. The work in this thesis is motivated to address soiling effects on the PV modules and development of a new soiling senor, the DustIQ. After analyzing the physical and chemical nature of dust, different factors, and its deposition mechanisms, the next question is how to experimentally measure and quantify the soiling loss. Measuring the relative transmission and power loss gives a good indication but how does this vary in real life conditions.

For a location like Delft, the natural soiling is low compared to other regions. Therefore, to conduct soiling research experiments, PV module is simulated with artificial soiling. The process of artificial soiling involves preparation of the soiling mixture and suitable outdoor/indoor conditions. So, a standard procedure for artificial soiling could assist in analyzing the various soiling effect despite the location. A module performs best at high solar insolation normally at solar noon but soiling attenuates the light photons incident on the module and decreases the generated electrical energy. Therefore, it is important to know how the performance of a PV module is related to the angle of incidence (AOI) of the light source.

Soiling is a result of various natural and anthropogenic activities varying with season and time. These external activities could result in uniform and non-uniform dust distribution on the module surface. The performance differences during these cases are extremely important to know as well as their effect on corresponding I-V/P-V curves. Dust composition and color varies with the geographical location, hence characterizing module performance based on dust color could give reliable insights about losses prevailing in different parts of the world. Dust size in a PV module is largely composed of finer particles (<30 μm), which is a function activity nearby, thus grain-size influence in the power output will be very crucial to understand.

Cost-effective soiling measurements might help to understand the soiling behavior and allow for an optimal cleaning schedule. Another interesting aspect of this research project is working towards the development of a soiling detection system, the DustIQ. The indoor and outdoor calibration and testing of the sensor will be done to decide an appropriate PV module to integrate into the sensor. The results will be compared with a full-scale module to validate its performance deviation. The sensor is for an outdoor application so it is crucial to understand the impact of different dust grain-sizes. Finally, after understanding the soiling behavior and its effect, an actual energy loss due to natural soiling in Delft is interesting to know.

To summarize, the main research questions have been mentioned below:

- What are the characteristic differences between soiling measurement methods (Short-circuit current and Power)?
- What are the methods to create good outdoor/indoor soiling conditions for soiling experiments?
- How a soiled module is dependent on the position of a light source?
- How can dust inhomogeneity and grain-size be taken into account?
- What are the principle features and first calibration test results of the new soiling sensor, the DustIQ?
- By knowing the irradiance loss due to soiling, how can the energy loss of a module be determined?

1.6. Thesis Structure

This report consists of six chapters. The proposed research objectives will be addressed in these chapters. A brief introduction to each chapter has been presented next.

Chapter 2 - PV Module Soiling: In this chapter, rooftop PV modules are soiled with an artificial soiling procedure to measure the daily soiling ratio. The outdoor results were then validated with indoor experiments at different dust color. Further, the impact of soiling homogeneity or inhomogeneity has been addressed by experimental and circuit simulation method.

Chapter 3 - Soiling Sensor-The DustIQ: In this chapter, a novel soil detection sensor called the DustIQ is introduced. The working principle along with its measurement procedure has been discussed. The results from its outdoor and Indoor testing of the sensor have been discussed.

Chapter 4 - Soiling Ratio Determination with IAM: Here, the measured soiling ratio over a whole day will serve as a reference to model soiling ratio curve based on one mid-day SR value and angular losses in the modules for three average daily irradiances of high, medium and low conditions. To do so, an empirical equation has been introduced based on incident angle modifier (IAM) for soiled and cleaned PV modules.

Chapter 5 - Natural Soiling: The natural soiling of PV modules in Delft was measured and analyzed. The annual energy loss and the optimum cleaning frequency has been estimated. The obtained transmission loss also served as a reference soiling rate to predict energy yield in the Dutch PV portal 2.0.

Chapter 6 - Conclusions and Recommendation: The answers obtained for proposed research objectives has been addressed. Finally, future works in the field have been suggested.

2

PV Module Soiling

In the previous chapter, the significance of considering PV soiling based on module characteristics and environmental conditions were analyzed. The chemistry and time-based modifications as a result of human activities and natural events were explained. After having a thorough understanding of these processes, it is important to realize the effect of soiling on a module and its estimation method. Module soiling at the outdoor and indoor level was carried out to estimate the losses. Next, an influence of dust inhomogeneity on a module performance was studied experimentally and then supported by a circuit simulation. Similarly, dust on a module is believed to have a three-dimensional shading effect that was examined by an indoor setup. Likewise, module's optical degradation is an important aspect that was analyzed with the determination of its relative optical response at different soiling level.

2.1. Soiling Ratio Estimation and Deviation

A yearly loss from a soiled module might be very significant compared to the clean module. As noticed in section 1.3.1, soiling ratio from short-circuit current (SR^{Isc}) and maximum power point (SR^{Pmax}) can be measured to estimate the prevailing soiling loss on the module [40]. This method compares the soiled module to clean by calculating the ratio of their current or power. The loss estimation by each of the method might vary as the former considers the only current generated and later takes into account both current and voltage to calculate the total power output. Equation 1.4 and 1.6, showed the dependency of current and power on the irradiance. The current was seen to linearly correspond while power is a function of both I_{sc} and V_{oc}. The measured soiling loss can be represented as a loss of both irradiance and power, therefore its value might vary depending on the chosen method.

In this section, the difference in SR at the same uniform soiling level will be quantified with few assumptions. An initial and final condition have considered being STC (1000 W/m^2, 25°C and 0% soiling) and NOCT (800 W/m^2, 45°C and 20% soiling) respectively. Referring to the provided data sheet for the polycrystalline module of 270 W$_p$ provided by Canadian Solar, a module was simulated from its STC to NOCT conditions at an interval of 1% of soiling level up to 20%. The estimated irradiance loss at each soiling level increased by 10 W/m^2, while the temperature was raised by 1°C in case of a soiled module and 0.5°C for the cleaned. The temperature corrected SR^{Isc} and SR^{Pmax} at each soiling level using equations 1.2 and 1.3.
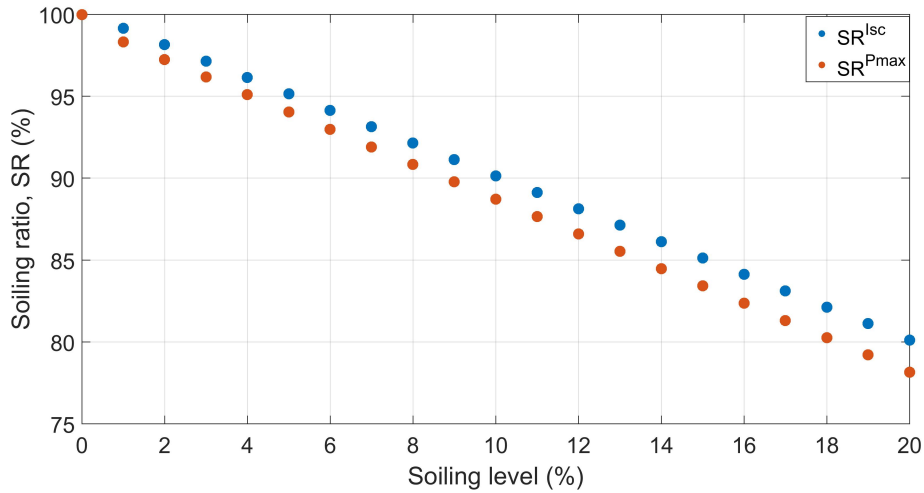
Figure 2.1: Estimated SR from two methods at increasing soiling level.
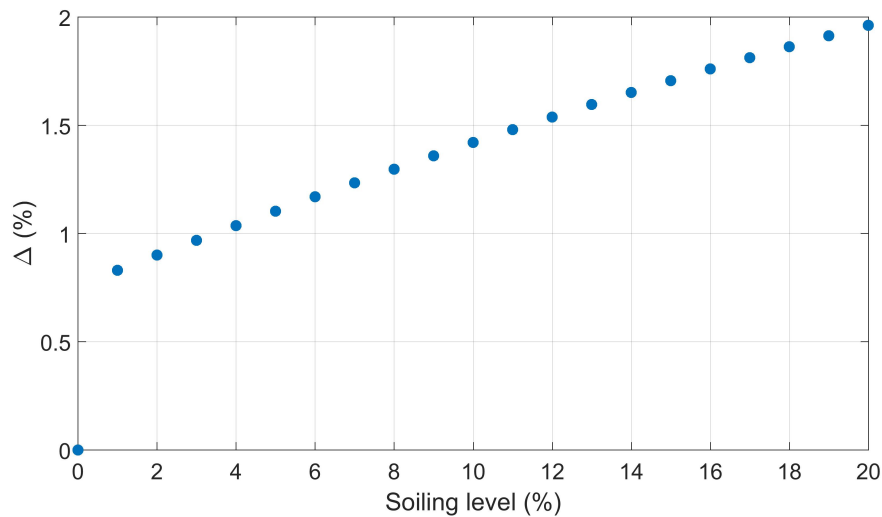
Figure 2.2: Absolute SR deviation at each soiling level.

The first graph in the Figure 2.1 and 2.2, shows the differences in loss estimation by each method. At 15% of soiling level, SR from short-circuit current was seen to be 86.14% while maximum power estimated a lower value of 84.48%. Furthermore, the graph on right represents the absolute deviation between two methods. Initially, the divergence can be seen to be low but, as soon as soiling level was 20%, the deviation was as high as at around 2%. The result signified the increase in variance with the amount of soil on a module because of the rise in temperature as well as the irradiance loss. SR^{Pmax} should be considered as a measure of actual performance of a module whereas SR^{Isc} to estimate the net irradiance lost from a module [40]. Similar results have also been reported in the work of [3]. However, the deviation presented were solely based on the simulation of module's electrical data, an experimental study has been performed in section 2.2.3.

2.2. Artificial Soiling-Outdoor

From the Figure 1.1, the average atmospheric dust concentration for the northwestern part of Europe (experiments' location) is around 12-19 (µg/m^3). This average value is relatively low compared to the MENA and Asian Pacific regions. Such dust concentration, when deposited on the modules, resulted into a transmission loss (TL) of just 0.083%/day (estimated in chapter 5), this value is not sufficient

to conduct proposed experiments for this research project. Therefore, modules were soiled with the help of an artificial dust solution prepared by mixing dust with deionized water as explained in section 2.2.1. The experimental results will follow thereafter.

2.2.1. Experimental Setup and Procedure

In this research project, PV performance under soiling conditions has been evaluated by calculating soiling ratio (SR). The transmission loss associated was then quantified at every soiling ratio conditions referring to the IEC 61724-1 norms. The outdoor experiments were carried out on 11th August 2017 from 11:00 to 17:00 and next for a period of 8 days between rainfall from 22nd to 30th August 2017 from around 10:40 to 17:15 each day at the rooftop PV setup of Kipp & Zonen BV in Delft, The Netherlands. The first experiment was to estimate SR measurement uncertainty while other was to analyze angular dependency of dust on the light source. The location is within 100 meters from N470 highway at the height of 16 meters from the ground. The system consists of 12 identical polycrystalline modules, CS6K-270P by Canadian Solar, six of which are connected to a central inverter (Sunny boy-1.5kW) and rest six are connected to the grid via micro-inverters (Enphase215 and Enphase250). The rooftop PV system can be seen in the Figure 2.3.

Figure 2.3: Rooftop PV setup for soiling experiment.

Four polycrystalline modules form the last two rows were chosen for both the experiments. A detailed specification of the module has been presented in Appendix A.1. The orientation of the modules is 180°due South at a tilt angle of 30°from a horizontal surface. Each module was mounted on an identical mounting mechanism to avoid angular misalignment. One of the modules was uniformly soiled while other was kept clean by frequently wiping with a soft fabric. An instantaneous short-circuit current (I_{sc}) from both the modules was recorded by measuring its voltage drop (V_{drop}) over a 10-meter long TUV solar cable with a resistance (R_{cable}) of 63 mΩ ± 0.126 mΩ (0.2% of reading ±1 reading) [65] given by equation 2.1.

$$I_{sc,i} = \frac{V_{drop,i}}{R_{cable}} \tag{2.1}$$

The voltage drop from both the modules was logged into CR6 data logger from Campbell Scientific with an average of 5-second samples every minute. Short-circuiting of the modules with the help of a low shunt resistor is schematically represented by a circuit diagram in Figure 2.4.
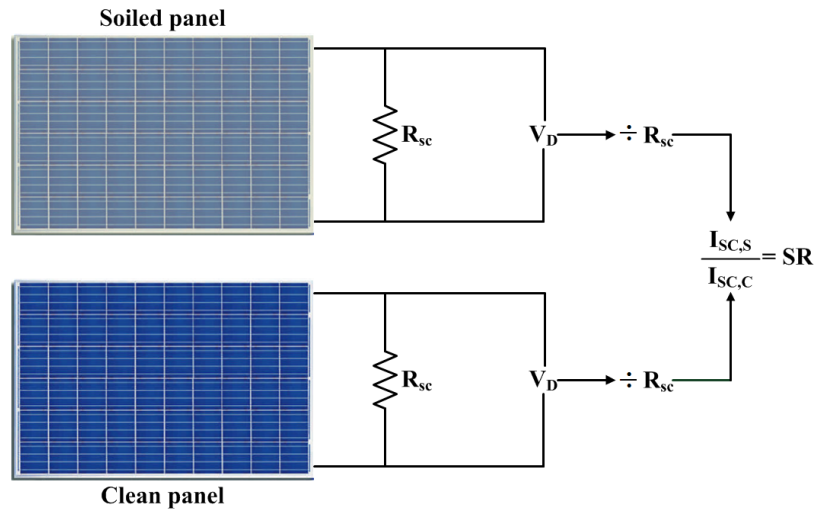
Figure 2.4: Short-circuiting of soiled and clean modules.

The general outlay of the experiment has been presented with the help of the flowchart 2.5. Each block in the chart has been explained in upcoming sections.
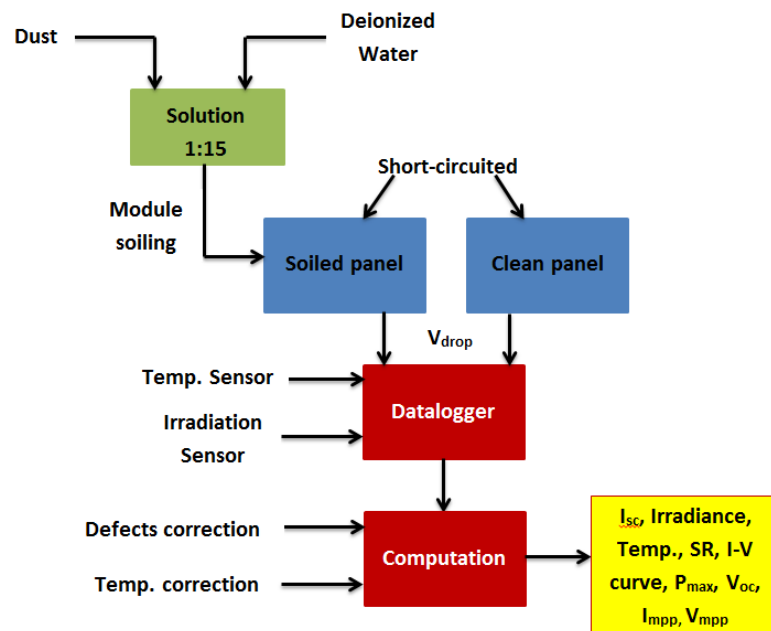
Figure 2.5: Flowchart for artificial soiling experiments.

An instantaneous irradiance every minute was recorded with the help of CMP-21 pyranometer by Kipp & Zonen installed at the plane of array (POA). The module temperature of both modules was also measured using two temperature measuring sensors (negative temperature coefficient (NTC) Thermistor of 10 kΩ) applied at the rear side of each module. To facilitate a homogeneous soiling by reducing the wind effect, a wooden-aluminum chamber was also built. The chamber was carefully placed on the top of the module to be soiled.

(a) (b)
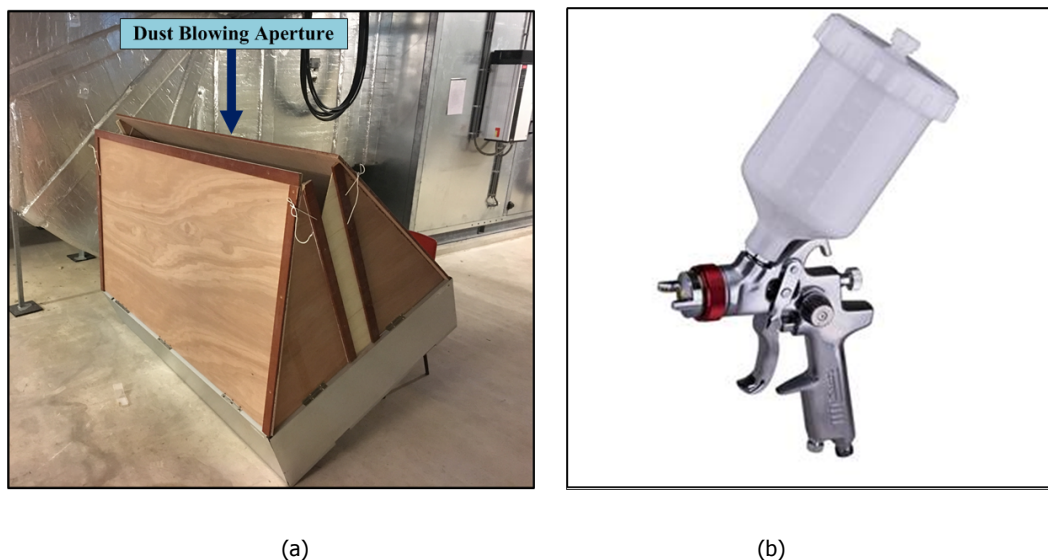
Figure 2.6: A wooden-aluminum chamber and a paint gun used for soiling.

A soiling mixture was prepared by dissolving grand canyon dust (Eisenoxid-Fe2O3, KSL-312 in Figure 2.24) with deionized water at 1:15 ratio. A smart weather sensor WS601-UMB by Lufft has also been installed at the proximity of the array to record the environment parameters like Temperature, relative humidity, precipitation, air pressure, wind direction and wind speed. Finally, module soiling was carried out with the help of a paint gun at 1.5 bars of air pressure from a 1-meter distance (pointed vertically). The experimental setup after soiling can be seen from the Figure 2.7.
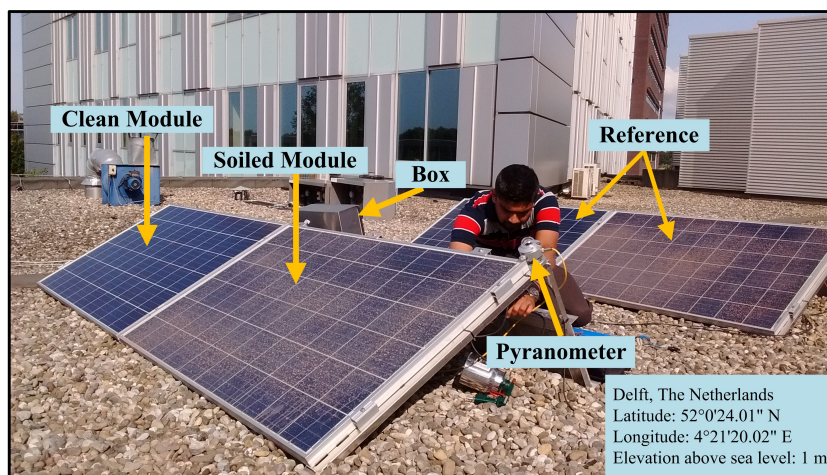
Figure 2.7: Experimental setup for soiling ratio (SR) measurement.

2.2.2. SR Uncertainty

Like any other measurements, SR also has a certain amount of associated uncertainty due to the limitation of measurement sensitivity of different instruments. For determining real soiling loss, it is very important to estimate the accuracy of the whole measurement procedure. The calculations were carried out referring to the BSRN uncertainty report, which is a brief version of Guide to the Expression of Uncertainty in Measurement (ISO GUM method) [66]. Following this model, every minute average short-circuit currents (I_{sc}), as well as module temperatures (T_m) of both the module at experimental and calibration level were considered as error contributing variables. Temperature coefficient (α) of the modules only at the experimental condition was taken as the calibration of modules were already temperature corrected. The soiling procedure has been explained in the section 2.2.1. All the measured instantaneous values were curve fitted for a straightforward analysis using "cftool" in MATLAB software.

The results of the uncertainty calculation have been shown in a graph 2.8, however, Appendix A.2 can be referred for a detailed explanation of the procedure.
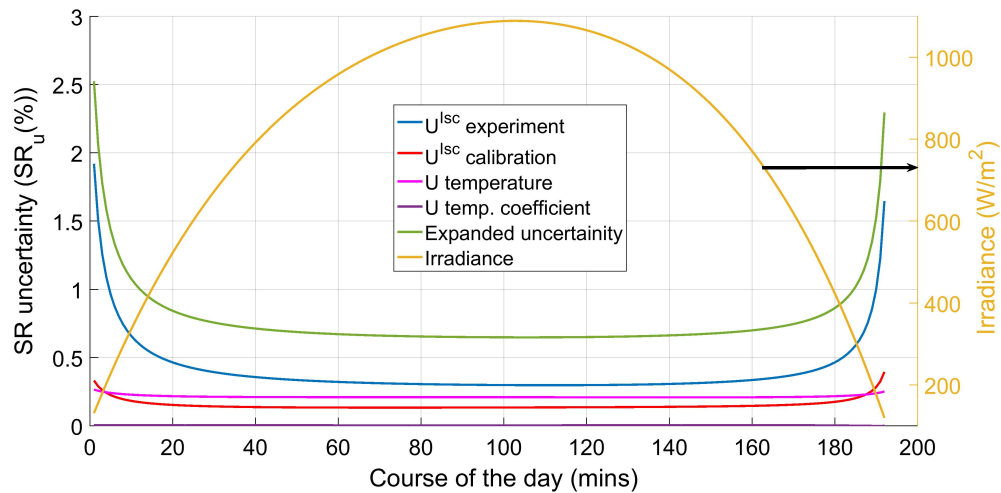
Figure 2.8: Expanded uncertainty during SR measurement. The minimum uncertainty of 0.65% was noticed at mid of the day (13:45 PM) at 1089.4 W/m^2.

Considering the sufficient irradiance of >400W/m^2, the expanded uncertainty in SR measurement varied between 0.65% to 0.926%. It can be noticed that the expanded uncertainty gets minimum at the noon while it goes up for low irradiance conditions. The minimum uncertainty of 0.65% was noticed at the highest irradiance value of 1089.4 W/m^2. The uncertainty during SR measurement is represented by a green curve, whereas blue and red curve is for short-circuit current at experimental and calibration level respectively. Finally, error due to module temperature and its coefficient was represented by magenta and violet curve respectively. Angular misalignment in tilt/orientation between two co-planer modules becomes very crucial if the difference is more than 0.5°[3]. If one module is tilted more than the other it might receive a larger amount of direct normal irradiance (DNI), which could significantly affect the results. The effect becomes more prominent for a soiled module as different altitude or azimuth might result in larger/smaller scattering of the incident ray. In Arizona, the effect of <0.5°angular misalignment resulted in <0.25% of uncertainty in 2 hours [67]. Therefore, considering the angular misalignment of 0.5°, the total expanded uncertainty in SR measurement was around $\pm$ 0.9% at solar noon and increases further at other times.

2.2.3. SR Measurement
After estimating the associated uncertainty with SR measurement, it is interesting to look at the soiling loss behavior for a longer period of time. The two sets of four polycrystalline modules as represented in 2.7 were soiled following the same procedure as explained in section 2.2.1 for two individual analysis. The last row was soiled to study an angular dependency of dust over the course of the day, whereas other two were to experimentally verify the SR deviation calculated by I_{sc} and P_{max} methods.

a. Module Set-1
This experiment was performed for 8 days between rainfall events. As mentioned in section 2.2.1, a smart weather transmitter was installed to measure the weather parameters. One of the modules was homogeneously soiled with grand canyon dust solution. The voltage drop over both the modules was logged into data logger from 22nd to 29th of Aug 2017. Minute average data (voltage drop and module temperature) were taken to calculate the SR from short-circuit method using equation 1.2. Thus, calculated SR^{Isc} along with the measured irradiance and both module temperatures were plotted to check their relationship with each other. Figure 2.9, showed the behavior of soiled module during the course of the day for 7 rain-free days. The last red curve was after the rainfall events where the SR values has been represented on secondary vertical axis. On the first day, the average SR during mid of the day was around 89% but slightly decreased for later days due to the additional accumulation

of soiling also discussed in the chapter 5. An average SR for the day before the rainfall was found to be around 87%. Therefore, using equation 1.1, the overall transmission loss (T_{loss}) in a module was estimated to be around 13%. Furthermore, each day's SR curve has a parabolic shape before rainfall but afterwards the shape was no longer same but concentrated.
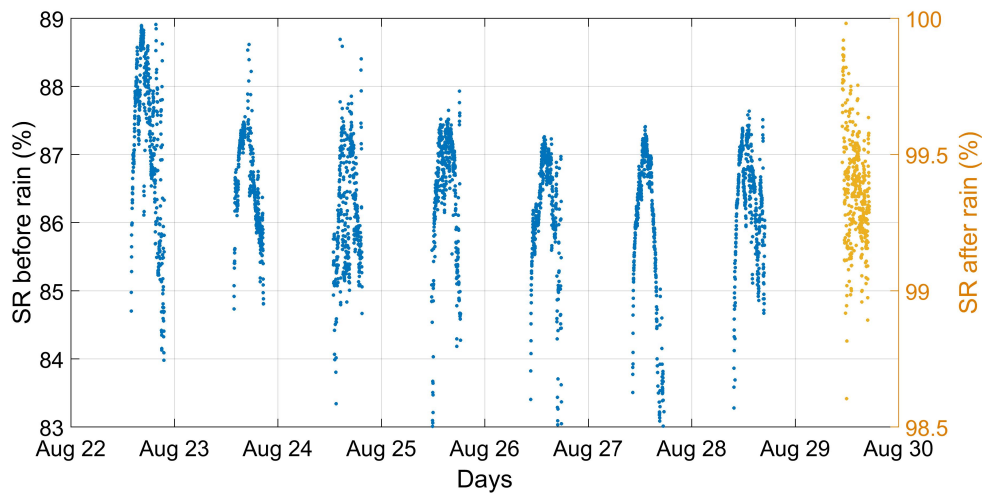
Figure 2.9: Measured SR due to artificial soiling of PV module for 8 days.
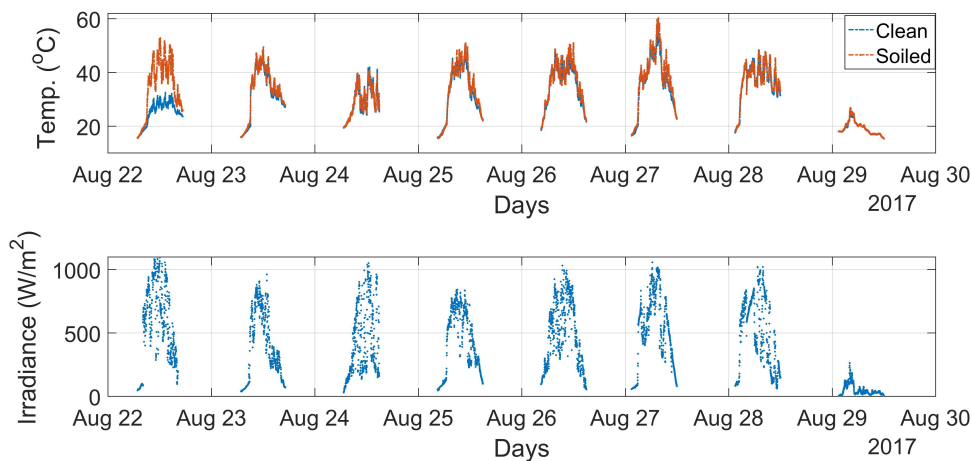
Figure 2.10: Measured soiled/clean module temperature and Irradiance.

Figure 2.10 shows the corresponding irradiance and module temperatures at two conditions (soiled and clean). Irradiance values were quite high and well above >400 W/m² for 7 dry days but was very low for a rainy day. The temperature plot signified that the soiled module generally had a higher temperature compared to the clean. On 22nd August, due to the accidentally removal of the thermistor off the clean module, the temperature difference were as high as 20°C but that was not the actual case. The similarity between SR and Irradiance can be also seen in the above figures, for a high irradiance day SR curve was found to fluctuate lesser than the other days. Soiling limits the current generated in the cells leading into higher module temperature thus, the open-circuit voltage (V_{oc}) of soiled module's might be reduced largely than during clean. This can result in varying module performance measured by SR^{Isc} and SR^{Pmax} even at uniform soiling case, which has been studied in the next section.

Now, SR curve will be analyzed more closely by plotting them individually before and after the rainfall for a shade free window of 6 hours from 10:57 to 17:07 to avoid partial shading on the PV

modules caused by nearby objects. Figure 2.11, represents SR plot for high irradiance day, which showed that soiling ratio (SR) was not constant throughout the day but changed with AOI of the Sun. Soiling ratio was seen to be highest during mid of the day ($\pm$ 1 hours) fluctuating between 86.5 and 87%. Therefore, the transmission loss at this point can be estimated to be around 13-13.5%. During the morning and evening time, it reached a lower value due to larger AOI of the Sun. The increase transmission loss (decreasing SR) can be speculated because of higher angular losses and scattering of light at larger angles. A detailed experiment related to the angular losses has been done in chapter 4. SR was noticed to vary even during the mid-day time by around $\pm$1%, probably because of the passing of the clouds and its dynamic shading on a module. The change in irradiance resulted into changing SR as seen in Figure 2.9 and 2.10. Figure 2.11 shows the result of SR measurements on a high irradiance day on 27th August 2017.
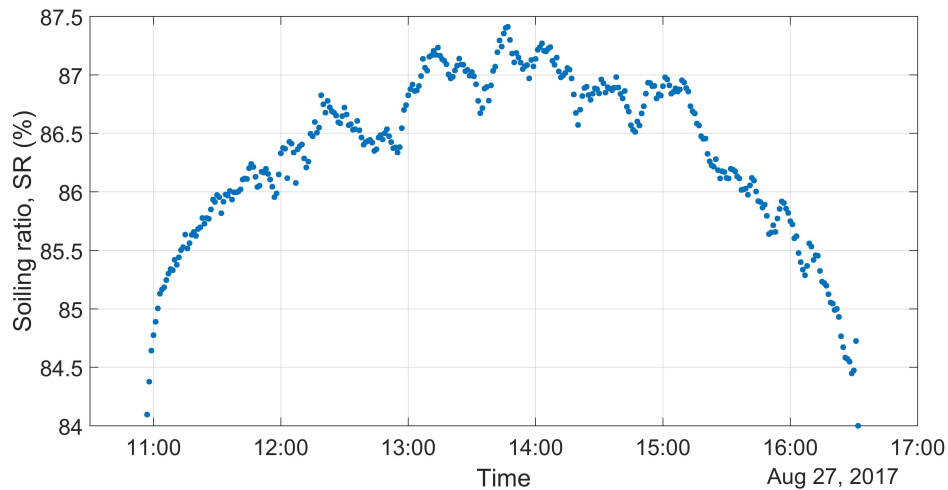
Figure 2.11: Soiling ratio (SR^{Isc}) on 27th August 2017 at the rooftop PV setup.

Furthermore, the rainfall events were observed after a day on 29th of August 2017. Figure 2.12 can be referred to notice the cleaning action of rain events on the soiled module as SR reached to all the way to 99.5-100% most of the time. The angular dependency was completely eliminated when both modules were cleaned. A total of around 27.5 mm of rainfall was needed to completely clean the module, measured with the help of the smart weather sensor by Lufft.
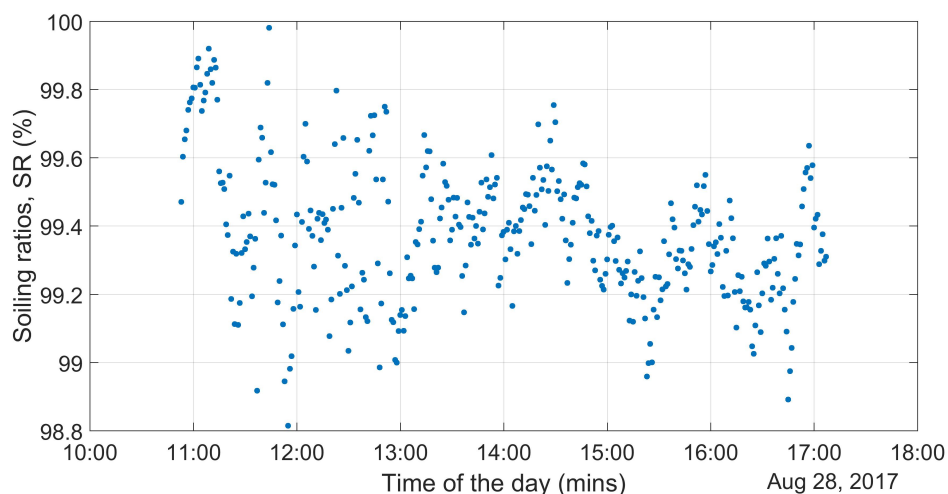
Figure 2.12: Soiling ratio (SR^{Isc}) on 29th August 2017 after the rainfall events at the rooftop PV setup.

The SR as a function of time for 23rd (medium irradiance) and 24th (low irradiance) August 2017

can also be followed from the Appendix B.1.

b. Module Set-2

Another set of modules were experimented to validate the deviation between soiling ratio from two methods (i.e. I_{sc} and P_{max}). Again, homogeneous soiling was done on one of the modules as represented in Figure 2.7. These modules were connected to an I-V curve tracer, MP-11 by EKO instruments. It is a portable instrument with a pyranometer and temperature sensor that can be connected separately. As mentioned in equation 1.2 and 1.3, current and power were temperatures corrected to calculate soiling ratios only due to soiling. All the external parameters from the module were measured by the I-V curve tracer. Soiling ratio from short-circuit current and maximum power point was calculated and represented for 9 different measurements.
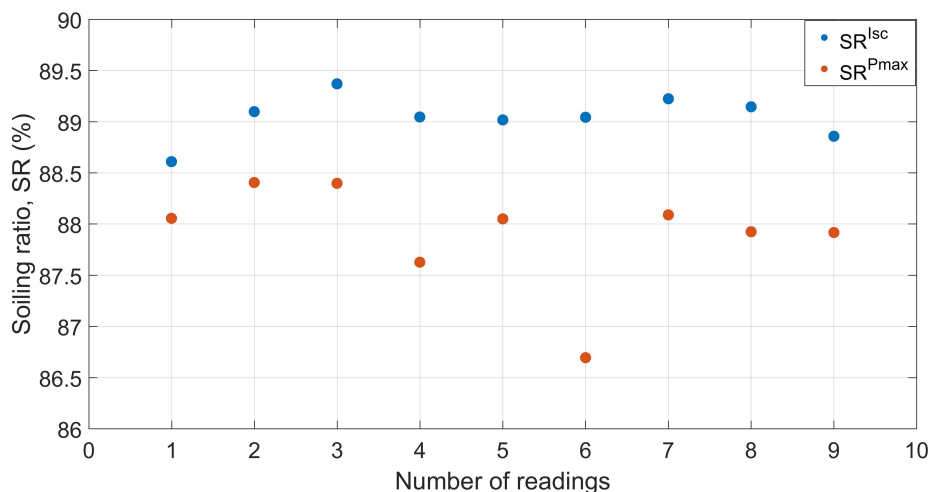
Figure 2.13: Measured SR^{Isc} and SR^{Pmax} from I-V curve tracer.

The average loss estimate by SR^{Isc} and SR^{Pmax} were 89.04% and 87.91% respectively that translates into average irradiance loss of 10.96% and actual module loss of 12.09%. For every measurement, SR^{Pmax} method has indicated higher losses than SR^{Isc}. A higher module temperature resulted in larger V_{oc} loss in case of SR^{Pmax}. These results prove the speculation made during SR deviation with soiling level in section 2.1. Therefore, module performance under soiling should be measured with SR^{Pmax} rather than SR^{Isc}. Similarly, the same amount of rainfall was needed to clean the module completely to regain its full capacity.

2.2.4. Soiling Non-uniformity

Uniform and non-uniform soiling lead to different soiling ratio value as discussed in section 1.3. The difference between two methods for a uniform soiling was explained in the above sections from a simulation and experimental approach. Now, an additional effect of non-uniform soiling was examined by calculating SR^{Isc} and SR^{Pmax}. Non-uniform soiling is more severe compared to the same amount of dust spread uniformly on a module. Insufficient rain, wind, dew occurrence and module position on a tracking mechanism might result in accumulation of soil near the frames or on patches. Apart from equatorial regions, modules are tilted at a certain angle, which carries dust particles to the bottom edge after dew or light rain events. The gravitational force acts on dust and results in dust directed towards the lower edge of a module in a vertical fashion.

The same setup was used to examine the effect of homogeneous and inhomogenous soiling. The module consists of 60 series connected cells (each cell 152.4×152.4 mm) with three bypass diode every 20 cells. Two types of fabric were used to simulate the soiling effect (as shown in Figure 2.16). The experiment was conducted on the mid of the bright sunny day and at each case, I-V curve tracer was used to measure the external parameters of the module to calculate SR^{Isc} and SR^{Pmax}. A SPICE circuit simulation was also performed to validate the experimental results. First, the development of a

SPICE module design will be explained followed by the experimental results.

a. PV Module Model-LTspiceXVII

A PV cell was designed in LTspiceXVII simulator software using a single-diode model as shown in Figure 2.14. A single cell circuit consists of a p-n junction diode, current source, and two resistances; one in parallel and other in series. The main purpose of developing a spice module model was to validate if soiling results were only due the experimental conditions, as well as to interpret the data and check main governing factors for the difference in soiling ratio (SR) during uniform and non-uniform soiling conditions. The input for each cell is the irradiance (V_i) and module temperature ($^{\circ}$C), which is defined globally by changing variables V_i and T in Figure 2.14. Therefore, by changing these input parameters instantaneous outdoor conditions can be reproduced for the simulation.
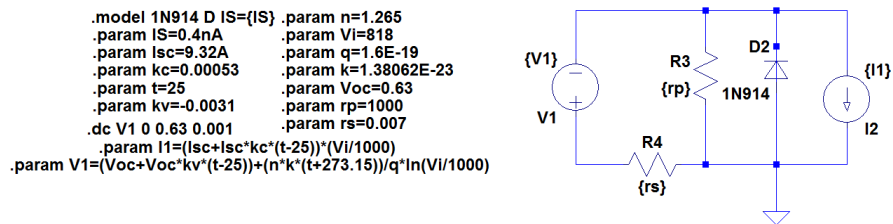
Figure 2.14: LTspiceXVII- PV cell model.

The next step was to construct a full 60-cell polycrystalline module from a cell model. Therefore, 60 single-diode model were connected in series and a suitable bypass diode in was chosen with the rated cell current connected for one-third of the solar cell array.
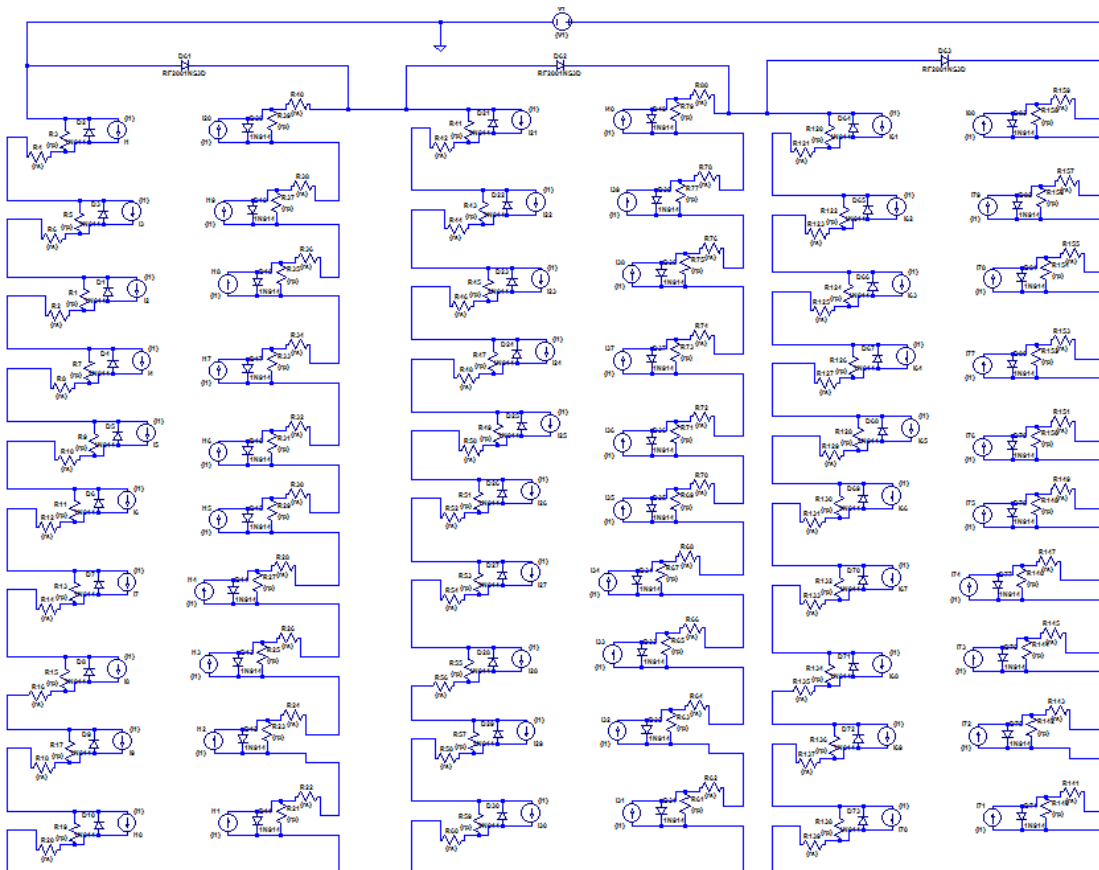
Figure 2.15: LTspiceXVII- PV module model.

The current, voltage and their coefficients were taken from the Appendix A.1. The series (r_s) and parallel resistances (r_p) along with ideality factor (n) for this module were estimated by comparing the external parameters; (V_{oc},I_{sc} and P_{max}) of unshaded module measured by I-V curve tracer. After a series of trial and error analysis for the adjustment of r_s, r_p and n, following results were obtained.

Table 2.1: Comparison between actual and SPICE module.

Set	I_{sc} (A)	V_{oc} (V)	P_{max} (W)	% difference
From experiment	7.62	37.37	213.4	-
r_s= 0.001Ω, r_p= 1000Ω, n= 1.5	7.62	36.1	225	5.43
r_s= 0.001Ω, r_p= 500Ω, n= 1.26	7.62	36.73	229	7.3
r_s= 0.007Ω, r_p= 1000Ω, n= 1	7.62	37.66	217	1.7
r_s= 0.007Ω, r_p= 1000Ω, n= 1.26	7.618	37.5	214	0.28

The maximum power point (P_{max}) in the last set well matches with the experimental measurement with 0.28% of the relative difference. Thus, r_s, r_p and n were kept constant at this value for further SPICE simulations.

b. Uniform Soiling

As discussed above, uniform soiling is a deposition of thin layers of dust evenly distributed over a module area. Therefore, to simulate uniform soiling, fabrics were placed to cover all the cells on the short-edge. First, a white fabric having a T_{loss} of 30% was chosen followed by the black fabric of 47% T_{loss} placed in a similar pattern as shown in Figure 2.16.

Figure 2.16: Placing of white fabric to simulate uniform soiling of 30% T_{loss}.

The result of this was measured with the I-V curve tracer represented by dotted lines, whereas solid lines represent curve constructed from SPICE simulation. Both I-V and P-V curve has been constructed to show the effect of uniform soiling on the module. The modeled curves with above parameters are seen to agree with the experimental curves quite well.
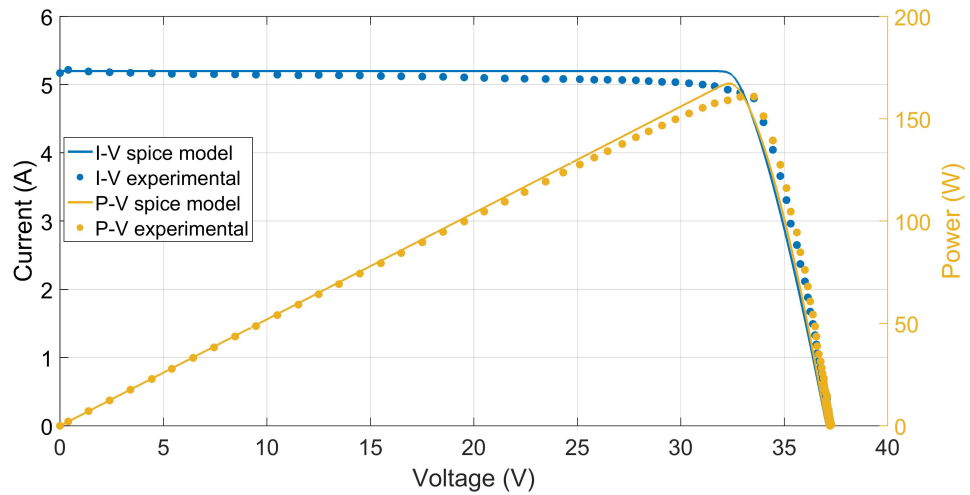
Figure 2.17: I-V and P-V curve from the measured and modeled PV module at uniform soiling at T$_{loss}$ of 30% (white fabric).

Due to the homogeneous spreading of the white fabric, the same amount of maximum current (5.17 A) was generated in each string. At this point, the maximum power point was measured to be around 163 W. Similarly, for a lesser transparent black fabric, maximum current and power production reduced to 3.65 A and 120 W at STC conditions. For a uniform soiling, there was variable current produced in the module.
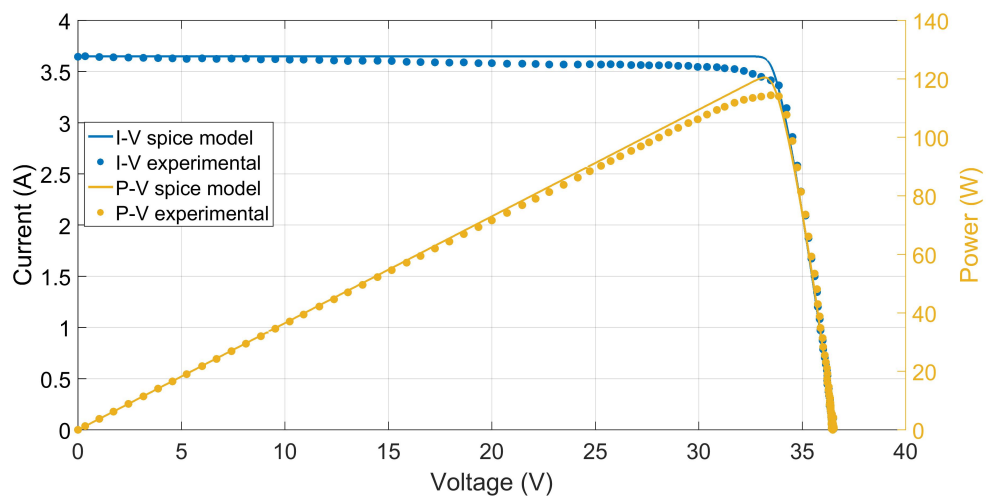
Figure 2.18: I-V/P-V curve from the measured and modeled PV module at uniform soiling at T$_{loss}$ of 47% (black fabric).

c. Non-uniform Soiling

Non-uniform soiling has been identified as an unevenly distributed dust in the form of patches or hot spots. Both the fabrics were now placed in such a manner that it shaded bottom-most 10 cells of one string on the larger edge of a module as shown in Figure 2.19. This affects one cell more than other, which might trigger one or more bypass diodes to kick in.

Figure 2.19: Placing of white fabric to simulate non-uniform soiling at T_{loss} of 30%.

The measurements were taken again with the I-V curve tracer. Both the curves seem to match well with a presence of small offset at the notch of local MPPs.
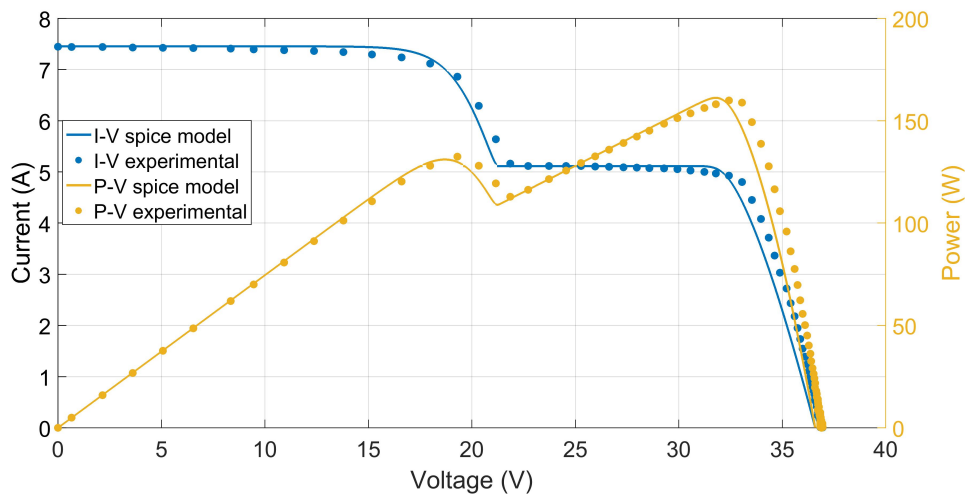
Figure 2.20: I-V/P-V curve from the measured and modeled PV module at uniform soiling at T_{loss} of 30% (white fabric).

The non-homogeneous placing of the fabric covering only the longer edged cells lead to a generation of variable current seen by the presence of a step changing current. The shaded string generated just 5.1 A, whereas two unshaded strings were producing 7.45 A. This lead to a formation of local and global maximum power points. The local maxima was 128 W but the actual power point was at 158 W.
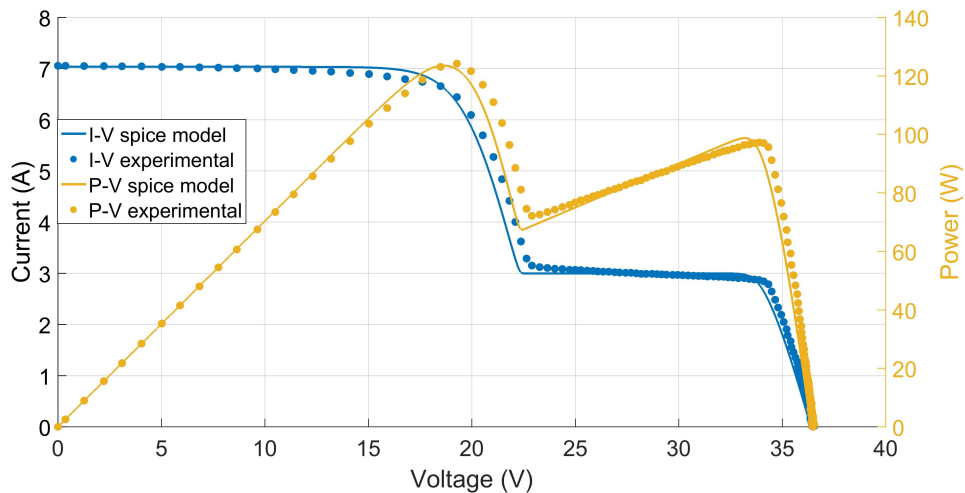
Figure 2.21: I-V/P-V curve from the measured and modeled PV module at uniform soiling at T_{loss} of 47% (black fabric).

Similar activation of a bypass diode was seen for black fabric. The local maxima was 97 W, whereas global maxima was 123 W. For non-uniform soiling with white fabric, current generated by shaded string determined the module output current, but for black fabric, it was noticed to be another way around.

d. SR^{Isc} and SR^{Pmax}

Soiling effect during uniform and non-uniform shading was studied with the help of I-V/P-V curves. Considering that a module can be mounted with longer or shorter edge facing bottom, SR^{Isc} and SR^{Pmax} has been calculated to evaluate module performance at changing homogeneity conditions. Referring to the equation 1.2 and 1.3, the generated current and power were temperature corrected and translated to STC. Figure 2.22 has been constructed to present the results.
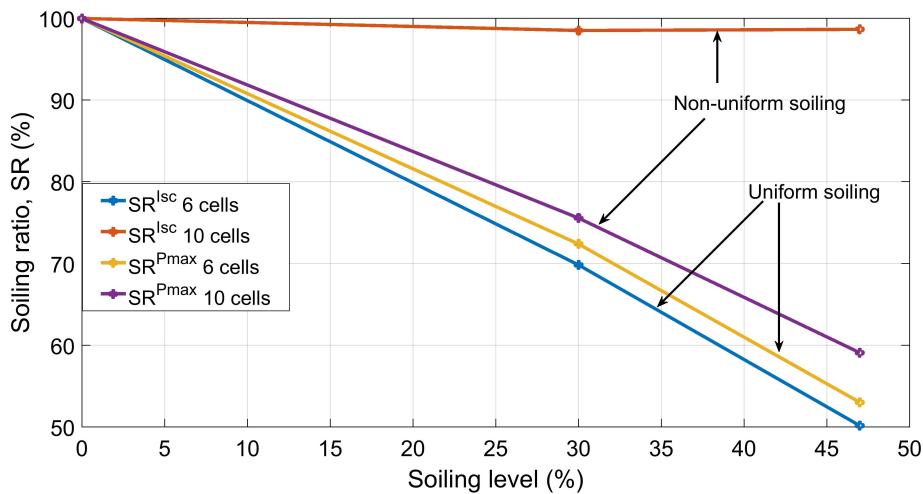
Figure 2.22: Calculated SR^{Isc} and SR^{Pmax} for uniform and non-uniform soiling of 30% and 47% T_{loss}.

The top red line was constructed by simulating shading on longer side (10 cells) and calculating the SR^{Isc}. This line showed virtually no loss as the soiling ratio was almost constant at 100%. Similarly, violet line represents SR^{Pmax} due to non-uniform soiling on a larger edge. The module's performance represented by SR^{Isc} was much higher in contrast to SR^{Pmax} due to the fact that only I_{sc} of a module was considered (ref. 2.20 and 2.21). But for uniform soiling of 6 cells, SR^{Isc} method indicated slightly larger losses than by SR^{Pmax} method. Therefore, depending on the side of a SR^{Isc} either over-estimates or under-estimated the losses. In case of SR^{Pmax}, despite of the shading type, the indicated losses were fairly constant representing the actual module's performance. Therefore, it can be concluded that SR^{Pmax} method is an exact way to characterize a module's performance for any soiling condition, whereas SR^{Isc} is only beneficial to quantify the irradiance loss at uniform shading conditions.

2.3. Artificial Soiling-Indoor

After measuring the SR at outdoor conditions, PV module was subjected to indoor experiments to validate if dust also has similar effects. Outdoor condition vary with the time and some other factors contribute towards soiling and its modifications. Moreover, module at outside condition passes through varying irradiation and temperature conditions, which was seen to be associated with fluctuating data sets. Therefore, a mini PV module was utilized in a controlled space at various soiling conditions. Some dust majorly characterized by their color were used with indoor experimental set up. The angle of incidence (AOI) effect of the light source on the dusty module was examined in each experiment. The impact of soiling on the relative optical response of a module was investigated at different dust densities. Finally, the physical effect of dust was studied with the help of spherical balls and flat patches placed on the module.

2.3.1. Experimental Setup and Procedure

An incandescent light of 2000 watts (Arrilite 2000) from Arri group was used as a constant light source. A CMP 10 pyranometer (S.No. -4) from Kipp & Zonen was used to determine a distance, where the irradiance of the light source was 1000 W/m². A mini-monocrystalline module of $2W_p$ was kept at a distance of 1.5 meters from the light source. The module was supported on a flexible arrangement to allow its movement in two axis, i.e. 360°horizontally and 0-60°vertically. The light source and module were kept at the same height measured with a level meter provided by Sola and the entire setup was supported by an aluminum bar. The experiments were carried out in a dark room to avoid the influence of other lights in the proximity. Module was rotated carefully from -90°to 90°with 10°interval measured with a 360°circular scale attached at the bottom of the module. An instantaneous module temperature of soiled and clean module was measured by a 10 KΩ temperature measuring sensor (thermistor, Negative temperature coefficient (NTC)), applied at the back of the module. The entire experimental setup has been shown in Figure 2.23.
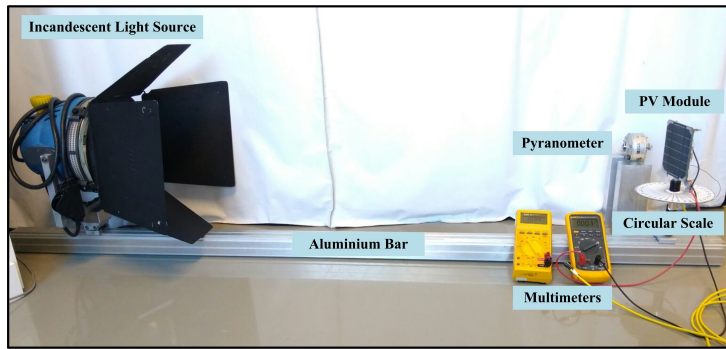
Figure 2.23: The experimental setup for indoor experiments.

Three multimeters namely voltmeter, ammeter and ohmmeter were used to measure the open circuit voltage (V_{oc}), short-circuit current (I_{sc}) and resistance in thermistor respectively at each AOI interval. Measured resistance at each angle of incidence (AOI) was subjected to Steinhart–Hart's equation to calculate the module temperature. Each V_{oc} and I_{sc} were subjected to temperature correction before calculating the transmission and power loss. A soiling mixture was prepared by dissolving 1.5 grams of dust with 20 ml of deionized water. An equal amount of 8 ml (0.0029 gm/cm²) of soiling mixture was applied on the module with the help of a air gun at 1 bar from a distance of 25 cm pointing horizontally. After each spraying, the hot air blower was used to dry the soiling on the module. Again SR^{Isc} and SR^{Pmax} was calculated in each case to measure module performance. Temperature corrected SR^{Isc} was calculated using equation 1.2 and SR^{Pmax} was estimated with the help of equation 2.2.

$$SR^{Pmax} = \frac{[I_{sc,s}(1 - \alpha(T_{m,s} - T_{ref}))] \times [V_{oc,s}(1 - \beta(T_{m,s} - T_{ref}))] \times FF}{[I_{sc,c}(1 - \alpha(T_{m,s} - T_{ref}))] \times [V_{oc,c}(1 - \beta(T_{m,c} - T_{ref}))] \times FF} \quad (2.2)$$

The maximum power produced by a module (P_{max}) can be represented as a product of maximum point of voltage and current at which a module is operating. Such maximum power point can be determined with the help of V_{oc}, I_{sc} and Fill factor (FF). n is the ideality factor, which represents the quality of the cell used. $V_{oc,s}$ and $V_{oc,c}$ are the open circuit voltage of soiled and clean module respectively. α and β represent the temperature coefficients for current and voltage from the datasheet A.2. The fill factor (FF) of a module can be calculated as [68],

$$FF = \frac{v_{oc} - ln(20)}{v_{oc} + \frac{v_{oc}}{20}} \quad (2.3)$$

$$v_{oc} = V_{oc} \frac{q}{nK_B T} \quad (2.4)$$

In equation 2.3, K_B is the Boltzmann's constant (8.617×10⁻⁵ eV K⁻¹), q is the elementary charge (1.60×10⁻¹⁹ coulombs) and T is the room temperature in Kelvin. For this experiment, temperature effect on FF was assumed to be constant hence, they are normalized for soiled and cleaned condition.

2.3.2. Different Dust Colors

Different types soil were used to characterize the soiling behavior with respect to its color and AOI of the light source. Four different dust were used; i. Prufstaub P-030KS16 (black), ii. Grand Canyon KSL 312 (red), iii. Quarz KSL 314 (white), iv. Arizona-Staub ARIZ-TD (brown). At each AOI interval, I_{sc} and V_{oc} of the clean module were first noted as a reference value. The homogeneity of the different dust can be seen from the Figure 2.24.
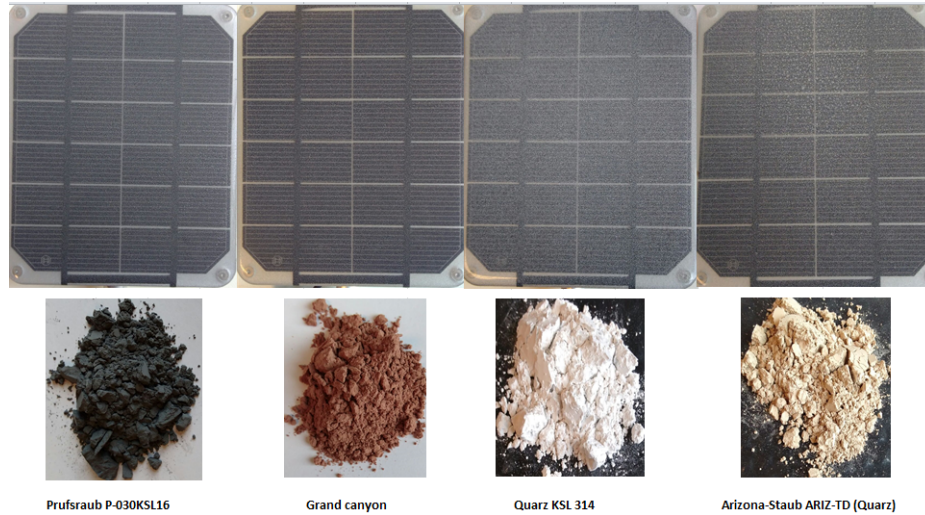
Figure 2.24: Indoor soiling of PV module with different dust.

All the parameters of the experiment were noted to calculate and compare SR^{Isc} and SR^{Pmax} at each soiling condition. Figure 2.25 can be referred to study the SR due to AOI of the light for four soiling condition at the same gravimetric density (g/m^2).
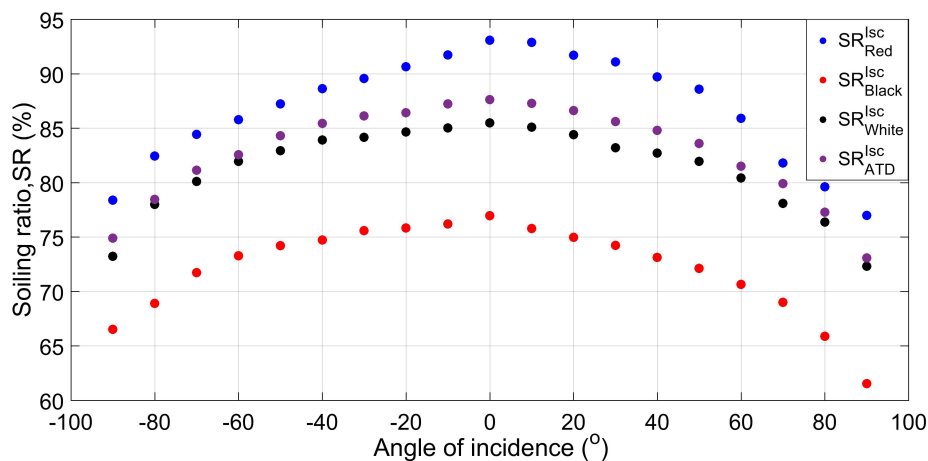
Figure 2.25: Comparison of transmission loss at different soiling condition.

The presence of angular dependency of the soiled module has been also noticed in the indoor setup. For the larger AOI, SR is very small while it increased and reached the maximum as the light source was more perpendicular to the module's surface. At the same mass loading, the maximum amount of transmission loss was resulted by black soil followed by the white, while least amount of losses was seen in case of the red soil. Black color absorbs the larger amount of light radiation, therefore it had higher transmission losses, but in contrast, white color reflects the major portion of the light. The white quartz might also have facilitated in transmittance due to its crystal-like semi-transparent nature.

These results suggest black/brown dust deposition due to smog or petroleum burning could result in higher losses, than for a desert location for the same amount.

After analyzing the losses due to the different dust color, the attenuation of angular response for the two dust color at the same T_{loss} value was compared. To do this, ATD was deposited twice than previous(5 mg/cm^2) to reach same SR (76.5%) as it was given by the black dust in Figure 2.25.
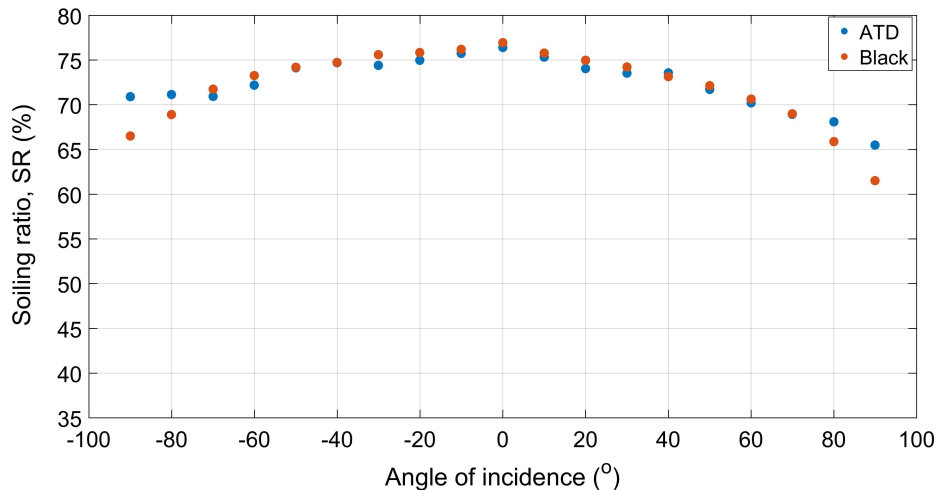
Figure 2.26: Comparison of transmission loss for black and ATD dust.

Apart from the outliers at very large AOI, no significant difference in SR value was noticed between black and 2×ATD dust 2.26. The results suggested, when two different types of dust having the same SR at the noon, they will always have similar angular losses for all AOI of the light source. The results will again be examined by calculating an optical response of the module.

2.3.3. Optical Response of a Module

A PV module is subjected to two AOI influences, namely mechanical and optical [12]. The mechanical response is associated with its tilt and orientation and light source. The solar radiation is reduced by a cosine of an angle between Sun's altitude when normal and at time t commonly known as "cosine effect" [69]. The optical effect is due to the surface properties of a module. For a module with a surface coating like anti-reflective coating (ARC), it would be more resilient against the effect of AOI than without [12]. A larger AOI relates with higher reflectance losses by reducing the total amount of solar beam available for producing current. Here, "The Sandia module performance model" was used to see the influence on the optical response of a module. The relative optical response $f_2(AOI)$ can be expressed as [70],

$$f_2(AOI) = \frac{G_M - (G_{poa} - G_{dni} \times cos(AOI))}{G_{dni} \times cos(AOI)} \qquad (2.5)$$

The maximum value of $f_2(AOI)$ is 1 when AOI is 0°. G_{poa} and G_{dni} are the irradiance at the plane of the array and direct irradiance on a module in W/m^2. G_M is the irradiance utilized by a module to produce corresponding short-circuit current, which is given by equation 1.4. Equation 2.5 was used to calculate the relative optical response at each AOI interval by considering POA irradiance and cosine corrected DNI was same for indoor conditions. Figure 2.27 represents the relative optical response of four different types of soil. The results were used to determine the dust "critical AOI" above which the losses are 3% or above compared with normal incidence of 0°[12].
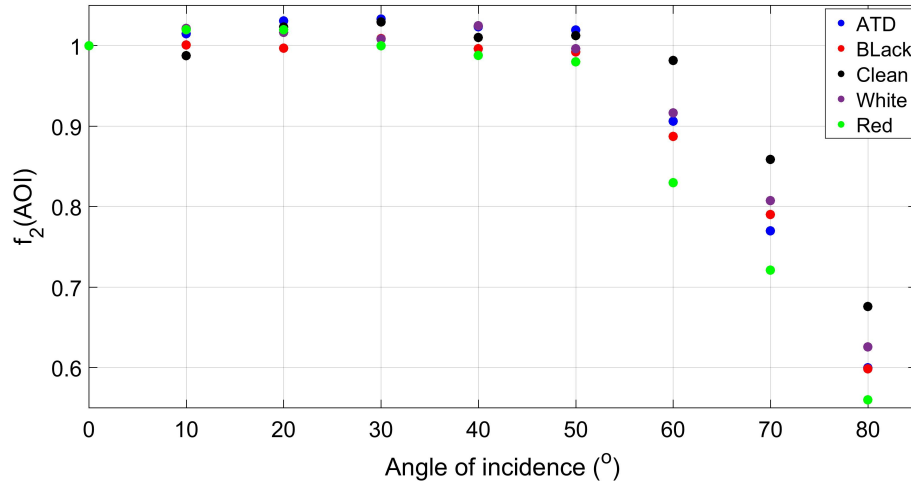
Figure 2.27: Relative optical response of clean and soiled module.

However, an optical response for every dust was found to decrease drastically after around 50°, this model results in optical response greater than 1 at lower angles (20-40°). This is a major drawback of this model [71]. The critical AOI for clean module was found to be 65°, whereas once the module was soiled at a density of 0.0029 gm/cm^2, the critical AOI decreased by almost 8°for each dust. Furthermore, when a module was heavily soiled with 0.005 gm/cm^2, the critical AOI further reduced to around 46°. This can be seen in the Figure 2.28.
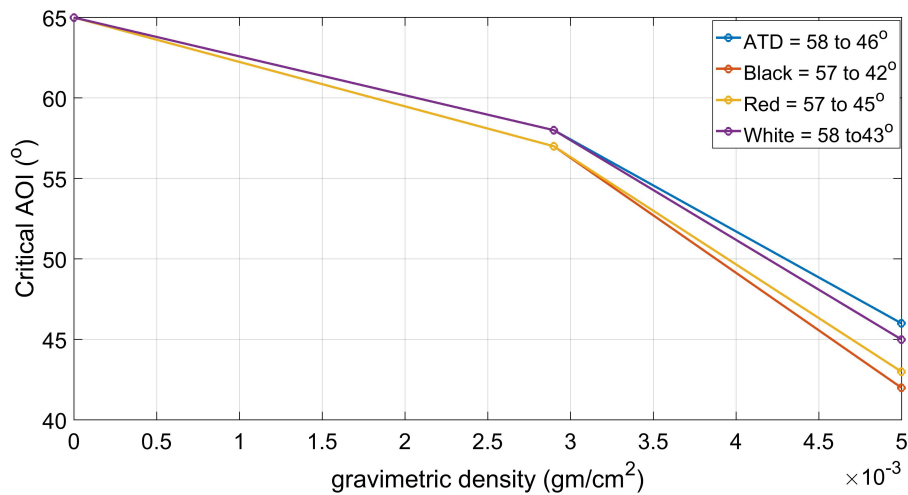
Figure 2.28: Relative optical response of clean and soiled module. Dots represent the measurement points and lines represents the interpolation between measured critical AOI

This result suggests that critical AOI was independent of soil color but only dependent only the mass loading. Larger gravimetric density (gm/cm^2) decreased the critical AOI resulting into higher angular losses at the same AOI. The Sandia model also defines a generic polynomial equation of fifth order to represent the relative optical response of a module at a particular density. The equations were generation with the help of a polynomial fitting in the MATLAB software. Table 2.2 provides a summary of the results found for each case.

Table 2.2: Optical response for soil samples.

Dust color	Critical AOI (°)	Difference compared to 0°	Empirical equation
Clean	65	3%	$-9E\text{-}10(AOI)^5 + 2E\text{-}07(AOI)^4 -1E\text{-}05(AOI)^3 + 0.0004(AOI)^2 -0.003(AOI) + 0.9983$
Black soil	57	11%	$4E\text{-}10(AOI)^5 - 8E\text{-}08(AOI)^4 +3E\text{-}06(AOI)^3 - 3E\text{-}05(AOI)^2 -0.0003(AOI) + 1.0007$
Red soil	57	17%	$2E\text{-}09(AOI)^5 - 4E\text{-}07(AOI)^4 +2E\text{-}05(AOI)^3 - 0.0006(AOI)^2 +0.0064(AOI) + 0.9999$
Quartz	58	9%	$1E\text{-}09(AOI)^5 - 2E\text{-}07(AOI)^4 +2E\text{-}05(AOI)^3 - 0.0004(AOI)^2 +0.0048(AOI) + 1.0007$
Arizona test dust (ATD)	58	9%	$2E\text{-}09(AOI)^5 - 3E\text{-}07(AOI)^4 +2E\text{-}05(AOI)^3 - 0.0004(AOI)^2 +0.0047(AOI) + 0.9991$
2×ATD	46	10%	$-4E\text{-}10(AOI)^5 + 7E\text{-}08(AOI)^4 -7E\text{-}06(AOI)^3 + 0.0003(AOI)^2 -0.0038(AOI) + 1.0104$

2.3.4. SR due to 3D Effect

Scattering, absorption, and the reflection of light takes place due to the presence of dust. Soil is believed to have a three-dimensional shading effect on a module, which shall be examined by placing a number of spherical polystyrene balls of approximately 3.5 mm in diameter. The balls act as a larger shading objects on a module. Following the experimental procedure SR^{Isc} and SR^{Pmax} were calculated from -90° to +90°. The spherical balls were applied in an ordered pattern to avoid the shading differences. The module after soiling with spherical balls has been shown along with the SR calculation in Figure 2.29.

(a)　　　　　　　　　　　　　　　　(b)
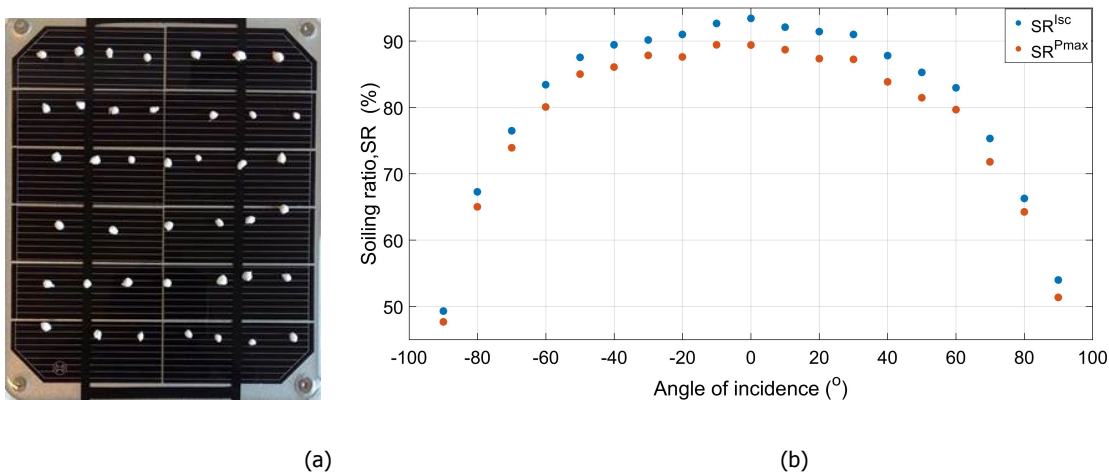
Figure 2.29: Measured SR by placing 3.5 mm spherical balls as a blocking object for the light source at different AOI.

As speculated, the effect of spherical balls on the module was found to be in a similar fashion as it was with the soil. SR reached minimum value for large AOI corresponding to morning and evening time, when the shadow of balls were larger. In contrast, it was found to be maximum at the mid of

the day when balls cast least shadow on a module, which also proves upon the cosine effect due to spherical balls.

2.3.5. SR due to 2D Effect

Lastly, the results obtained in 2.3.4, was further validated by placing several flat patches on a module to simulate the 2D effect. Spherical balls were replaced with 5.6 mm flat and circular patches placed in each cell as shown in Figure 2.30.

(a)   (b)
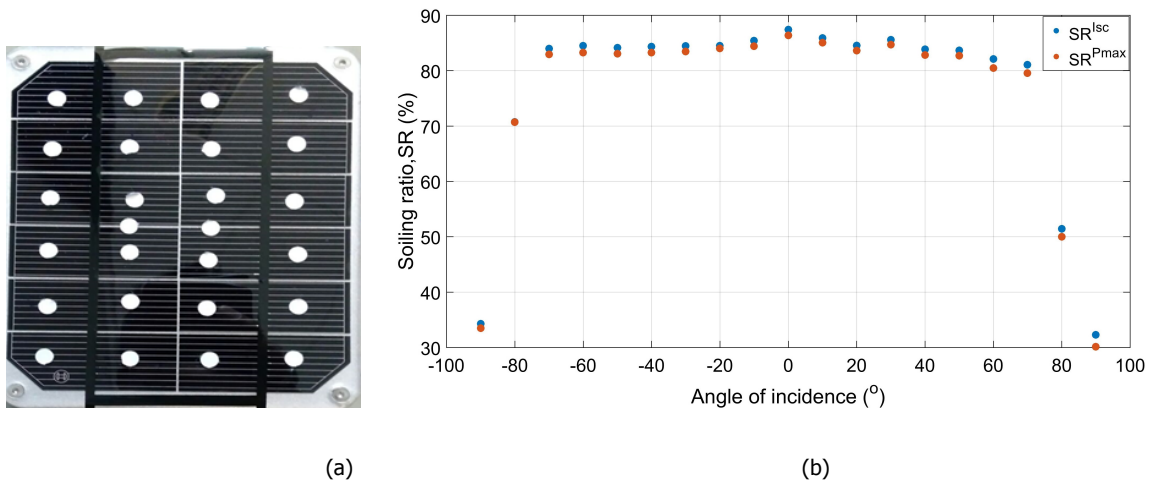
Figure 2.30: Measured SR by placing 5.6 mm flat and circular patch in each cell as a blocking object for light source at different AOI.

Calculated SR for angles in between -70° to 70° were fairly constant by varying by just 5%. This minimal dependency of SR on the AOI for flat objects further confirms the 3D role of soil on a module.

3

Soiling Sensor-The DustIQ

The deposition of thin sheets of dust, soil, and microfibers resulting from the surroundings reduce the total electricity generated from a PV module. Modules installed outside are subjected to a variable environment and weather conditions thus, can become dirty with time. Some of the modules at higher tilt angle need not be cleaned for a long time due to hydrophilic/hydrophobic anti-soiling coatings facilitating a self-cleaning mechanism. In a PV park, even small increase in module level soiling losses can get very significant affecting the performance ratio (PR) of an entire system. An accurate estimation of soiling behavior and cleaning interval is essential to minimize the power losses. Modules are needed to be cleaned more frequently if its location has a high soiling rate. The losses can vary with time, therefore a cleaning interval could also differ. For a tropical region, annual cleaning of the plant at the end of the winter season has resulted in 12% in energy yield [72].

Most of the solar energy operation and maintenance team performs the cleaning procedure based on a fixed time interval or on a visual inspection. A situation of low or intermediate rainfall even within a few days of cleaning might facilitate hard shading, that significantly degrades the total plant output. As discussed in section 1.4, cleaning procedure includes a large amount of water, which might an issue for a dry place. Frequent cleaning leads to the formation of scratches, frame damage, degradation of front glass as well as occurring permanent spots on a module. Too much or too little cleaning undermines the PV performance. Therefore, a device that could quantify the transmission losses and indicate an optimal cleaning time would help to reduce the overall revenue loss by increasing the yield. All the commercially available products listed in table 1.4 are based on a principle of comparing soiled to the clean module and needs a daily cleaning process for a good measurement. They also have moving parts, which needs a timely maintenance. All these features drive the cost of these instruments and a standard installation procedure needs to be followed that might be problematic in some cases.

Therefore, a soiling monitoring system has been developed here in Kipp & Zonen BV, called the "DustIQ". It measures the transmission loss in PV modules due to the accumulation of dust utilizing an optical technology. It can work independently without the use of sunlight and has no moving parts, that reduces the overall O&M cost. The device is factory calibrated with one dust type that gives an output (SR) with respect to that particular dust. Therefore, once it is field calibrated with the local dust, it can independently measure accurate SR throughout its lifetime without any maintenance. In this chapter, the principles involved in the measurement and calibration of the DustIQ will be discussed, followed by a number of tests conducted to select a suitable PV module to integrate on the DustIQ, dust color as well as dust grain-size dependency on its output signal.

3.1. Introduction

The DustIQ is a unique device that measures the irradiance loss due to soiling. The device is mounted next to a PV module to ensure the same soiling rate and cleaning patterns. It consists of two measurement sensors on the sides and an onboard mini-PV module (1.6 W_p). A front view and a side view of

the device is shown in Figures 3.1 and 3.2.

Figure 3.1: Front view of the DustIQ.

Figure 3.2: Side view of the DustIQ with sensors ON.

The transmission loss due to soiling is determined with the help of these sensors, once it is calibrated with the local dust on the site. This loss in the irradiance directly relates to the soiling ratio (SR) as represented in the equation 1.2, which is also a final output from the DustIQ. The SR measured by the DustIQ need not be temperature corrected because the calibration time takes merely a minute and assuming no temperature change. The system communicates via a Modbus® protocol that is also compatible with inverters and data acquisition systems. The device is framed with an anodized aluminum that is lightweight and gives mechanical and thermal stability to the device. The different layers of the DustIQ include a front glass cover, is similar to one in most of the PV modules. The front glass acts as a window for incident irradiance and also protect the device from foreign elements. Next is a white main cover that consists of a mini PV module and protected by ethylene-vinyl acetate (EVA) based encapsulant from both the sides. At last, it is shielded with a back cover that facilitates a space for the junction box and two DustIQ sensors [1].
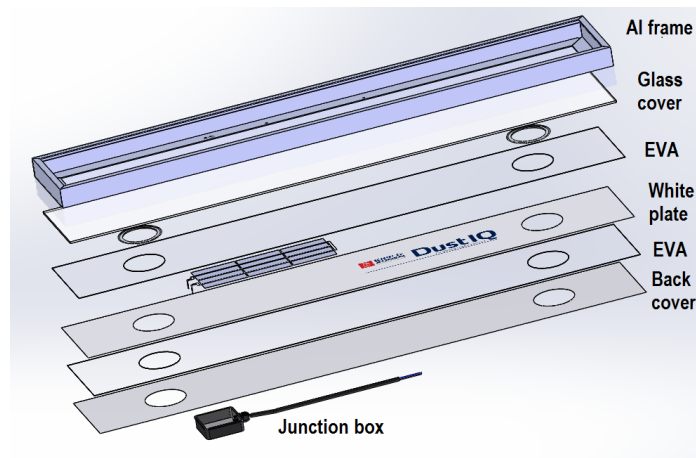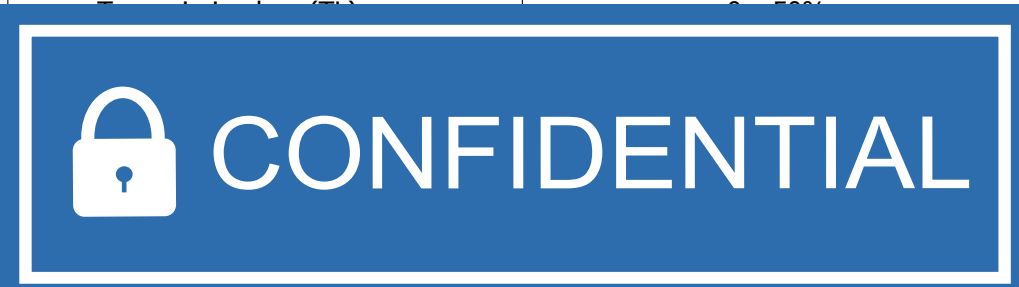
Figure 3.3: Different layers in the DustIQ.

The DustIQ is fully protected from water and harmful dust with IP rating-65, which can be cleaned

---

[1]Personal contact with Rob Van Polanen on 28 February 2018

in the same way as the PV modules. An external power supply of 12–30V and max 300mA is needed for its operation. The electrical and optical specifications of the DustIQ has been given in table 3.1.

Table 3.1: DustIQ specifications [2].

Power	12 to 30 V$_{DC}$, 200 to 700mA (<2 Watts)
Glass type	standard PV glass
DustIQ Dimensions	990 ×160 ×40 mm
PV-cell Dimensions	78 ×40 mm
No. of PV cells	6
Weight	5 kg

The DustIQ should be mounted next to or in between the PV modules with the help of 4 clamps at the same tilt and azimuth to avoid differences in soil accumulation as shown in Figure 3.4[3].
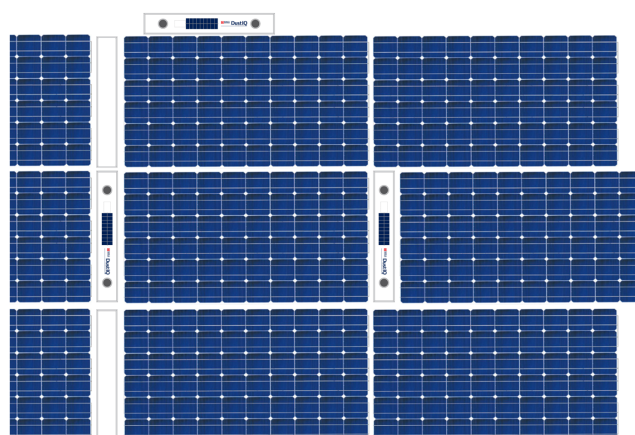
Figure 3.4: The mounting of the DustIQ in a PV park.

For a good approximation of soiling loss across the PV plant, multiple DustIQ's is recommended to be installed on the plant. In future, a user will also have an option to buy the DustIQ-array-fillers in order to install the DustIQ in the middle of an array without any gaps in between.

3.2. Working Principle

The sensor does not use solar irradiance, therefore the whole measurement technique is independent of the Sun's position and Sky conditions. Below the glass plate, there are the measurement sensors that use the principle of optical soiling measurement (OSM) technology to measure the scattered light due to soiling on the glass cover as shown in Figure 3.5. Two sensors are used to make a comparison in case of the spot soiling in only one sensor. Each sensor has one blue LED that lights up against the glass cover. The choice of the blue light was chosen because it has has a stable and UV-resistant narrow spectrum compared to other. The reflected signal from each sensor is received by two photodiodes as shown in figure 3.5[4].

---

[3]Retrieved from https://blog.kippzonen.com/dustiq-position
[4]Personal contact with Marc Korevaar on 20 November 2017

'clean' signal   'soiled' signal

LED   Photodiode   LED   Photodiode

(a)   (b)
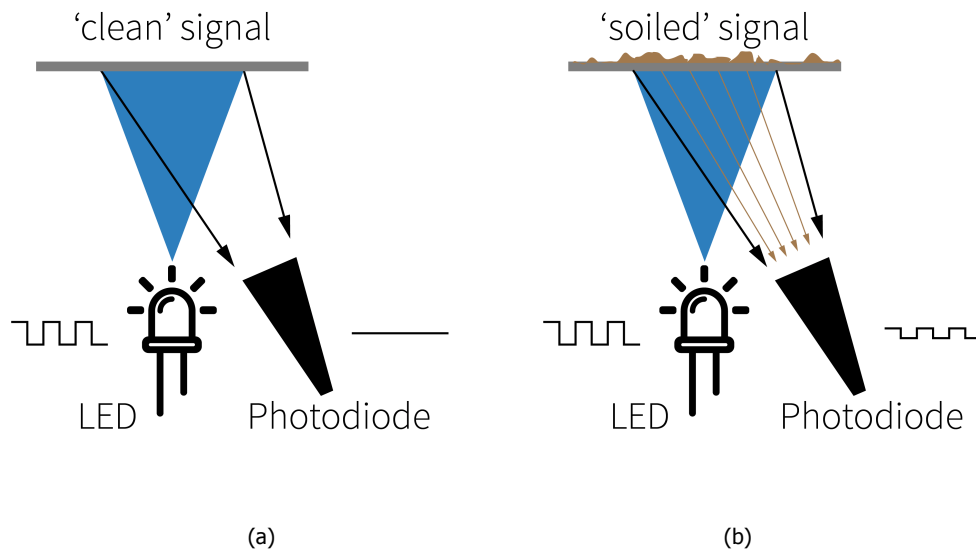
Figure 3.5: Optical Soiling Measurement (OSM) technology involved in the DustIQ.

🔒 CONFIDENTIAL

🔒 CONFIDENTIAL

$_c$),
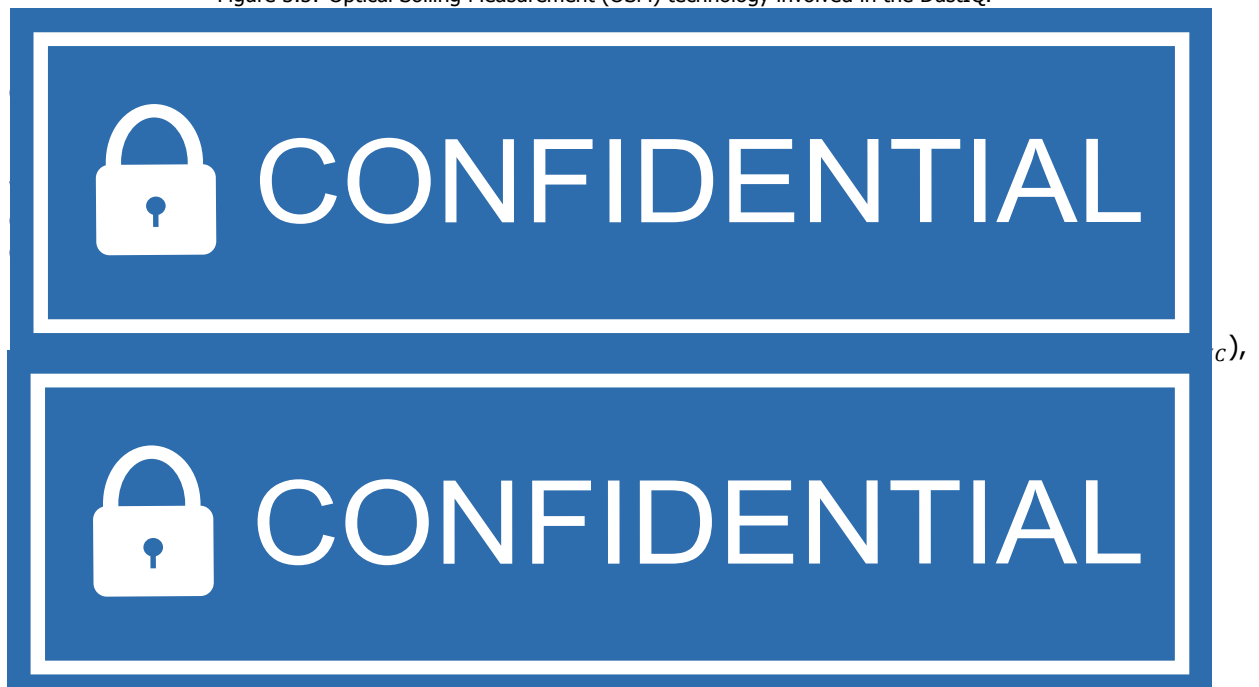
3.3. DustIQ Calibration

The calibration of the DustIQ involves clean and the soiled signal based on the local dust deposited on it. Once the DustIQ has been calibrated, it can measure and report the soiling ratio 24/7. A fine calibration involves ideal outdoor conditions. Calibration done during these conditions result in good soiling measurements. Some of these conditions are listed next;

3.3.1. Assumptions for DustIQ Calibration

1. The DustIQ should lie in the proximity with other modules in a PV plant.
2. The mounting mechanism should be similar with the same module tilt and azimuth in order to avoid angular misalignment.
3. The measurement should be done in the middle of the day on a clear day with enough sunlight (>500 W/m^2) to minimize the uncertainty during the measurement.
4. The calibration time should not result in module's temperature change.

3.3.2. General Protocol for DustIQ Field Calibration

The general steps involved in the DustIQ calibration are:

1. Factory calibrated DustIQ is mounted next to the modules in a PV park.
2. The DustIQ is left for the accumulation of dust (depending on a location from a week to months).
3. The DustIQ signal (raw and reference) is measured along with the short circuit current (I_{sc}) by pressing a provided button for 10 seconds.
5. The left sensor of the DustIQ is cleaned first and the button is pressed again. Next, the entire surface is neatly cleaned and measurements are taken by pushing the button for the third time.
6. A new calibration factor is determined by comparing the transmission loss and DustIQ signal for cleaned and soiled condition.
7. Finally, SCADA or the DustIQ firmware is updated with a new calibration factor with a final press of the button.

As explained above, the Figure 3.6 represents the the result of a calibration process at high amount of soiling (T_{loss}=22%).
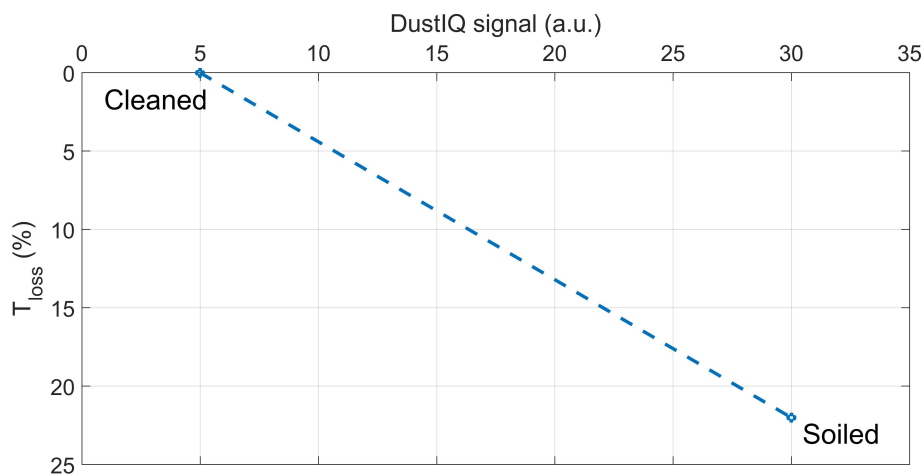
Figure 3.6: Result of DustIQ calibration.

When the glass was completely clean there was no transmission loss only small reflected signal because of the glass itself. After soiling, the DustIQ signal and transmission loss increased linearly. The final transmission loss value is calculated with the help of factory calibration value and field calibration value as given by equation 3.1 and 3.2,

$$\%\text{Transmission loss}(T_{loss}) = \text{reflected signal} \times \text{factory calibration} \times \text{field calibration} \quad (3.1)$$

$$SR = 100\% - T_{loss} \quad (3.2)$$

3.4. Test Results

After determining the linear relationship between a clean and soiled signal, it is interesting to test with the different dust colors and size as used in Figure 2.24. Moreover, a number of tests were performed to choose a suitable PV module to integrate on the DustIQ.

extremely small compared to the area of the module.

in Figure 3.7.

Figure 3.7: P_{loss} estimation of four PV specimens.
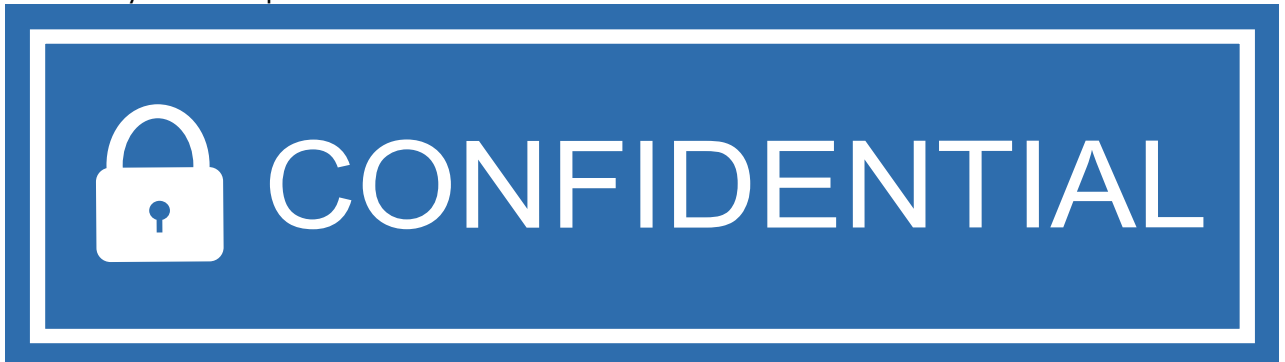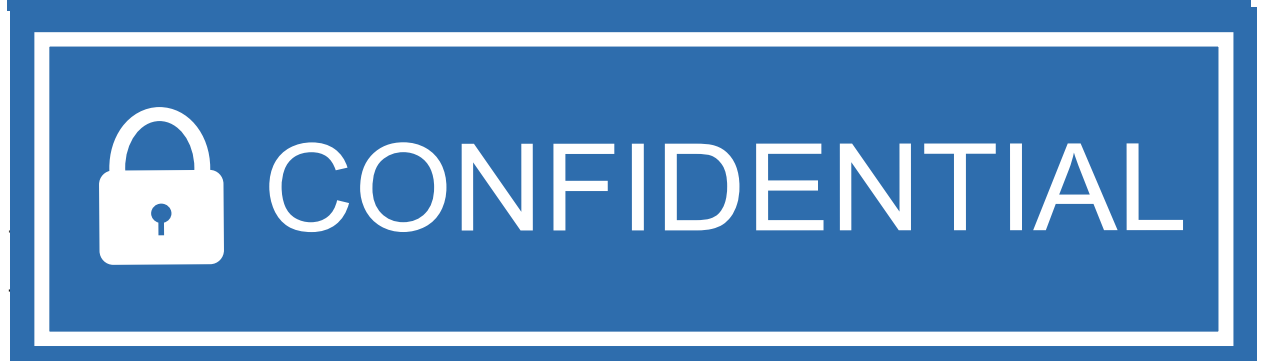
devices.

3.4.2. Color Test

After validating a linear relationship between soiled and a clean signal, dust color response or also called a color slope ratio was next examined. The main idea was to determine how the transmission

loss and sensor output is dependent on dust color. To do so, three different soil solutions were prepared and applied homogeneously on a glass plate of 340 ×170 mm following the same soiling procedure as explained in 2.3.1. Dust solution was repeated for three courses to examine the DustIQ output. A half soiled glass sample with white quartz can be seen in Figure 3.8.
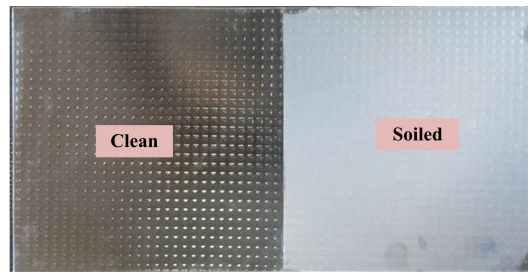
Figure 3.8: A glass sample used for the experiment.

In figure 3.8, left half of the glass represents the clean part, whereas right half represents a uniformly soiled part of the glass. The glass plate soiled with black, brown and white dust was individually kept in front of the PV module and the DustIQ sensors. A constant light source was 2000 W incandescent light shown in 2.23. The reflected signal from the different zones of the plate was taken in order to account for the non-uniformity during soiling. Each second's signal was measured using a Modbus master simulator called the Modbus Poll. The transmission loss and the sensor output were averaged and shown in Figure 3.9.
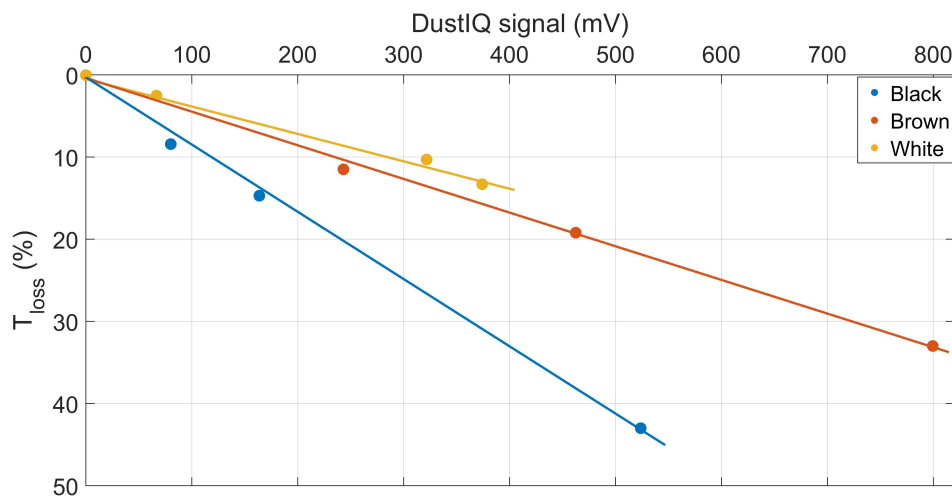
Figure 3.9: Dust color test.

The results showed that the increase in T_{loss} translates to the increased sensor signal. The linearity in each signal was seen for each soil irrespective of its color. The slope of the response increased with the darkness of the soil, i.e. for light color (white), the slope was smaller than for the black color. The reason might be due to the larger scattering of the white dust at glass surface, whereas for a black dust majority of the light is absorbed resulting in a lesser scattered signal received by the photodiode.

3.4.3. Grain-size Dependency

Dust particles size collected from the modules depends on its location. If it is near an urban/semi-urban area, smoke and haze particles in the order of µm are dominant, whereas for an arid/desert location particle sizes ranging from mm to µm are dominant. Therefore, it is crucial to estimate the effects of dust size on the module and accordingly on the DustIQ. To examine this effect, four different dust samples of Arizona-Staub Quartz (SiO_2) with varying grain-sizes were taken i.e. A1-5.5 µm, A2-11 µm, A3- 22 µm and A4-44 µm. An average dust size represents 60% of dust distribution in each

sample. Dust solutions were prepared by mixing 8 grams each dust with 200 ml of de-ionized water. Finally, each course of 8 ml (4.15 g/m^2) was applied for four times on a similar glass plate shown in Figure 3.8. The transmission loss (T$_{loss}$) from a module in the DustIQ after each spraying session was measured and shown in Figure 3.10. Since each spraying session was done at the same airgun height and distance from the plate, the mass loading was calculated considering 75% of the sprayed solution was able to get deposited.
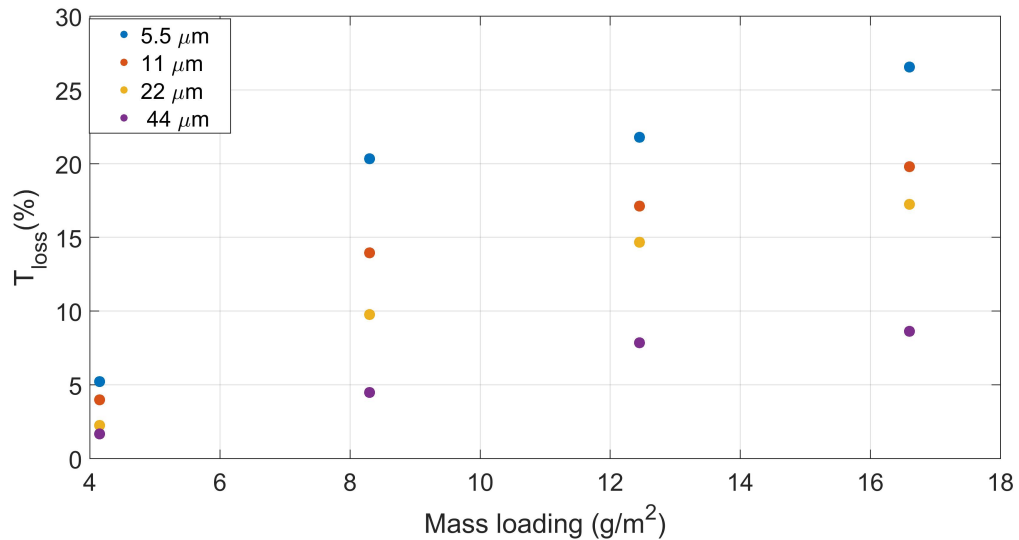
Figure 3.10: Transmission loss at different grain-size.

At the same mass density, finer particles possessed higher transmission loss. Dust particle of 5.5 µm was found to have almost twice the loss compared with 40 µm for the same mass density. As mentioned in section 1.2.3, smaller particles result in larger light scattering and hence, higher transmission loss. At 12.45 g/m^2, more dust layers were deposited in case of smaller particles compared to the larger resulting in higher transmission loss. These results were then compared with the DustIQ signal logged with Modbus Poll. The module transmission loss was plotted against the DustIQ signal to make a swift comparison in Figure 3.11.
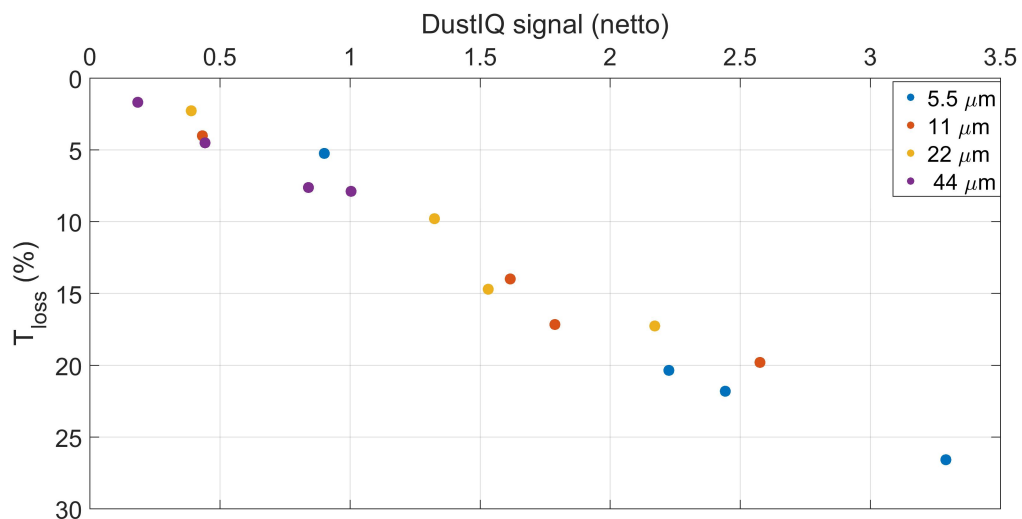
Figure 3.11: Grain-size dependency of the DUstIQ.

Irrespective of the grain-size, increase in dust density was found to the increase in light signal being

reflected towards the photodiode. The majority of the signals were found to be linearly related with some outliers. The transmission loss at each grain-size resulted in similar DustIQ signal therefore, the DustIQ output can be regarded to be independent of dust grain-size. This makes it easier to install it anywhere irrespective of the location and particle size on the module.

4

SR Determination with IAM

Module manufacturers typically mention the electrical parameters at only two operating conditions (STC and NOCT). With diurnal and seasonal fluctuations, module's performance keeps on varying, which makes it difficult for yield prediction just from electrical parameters (V_{oc}, I_{sc}, P_{max}, and module temperature). The energy yield of a PV module should be estimated considering all the possible scenarios that can take place. A glazing surface is normally a glass or smooth surface, which reflects back a certain amount of light incident on it. However, this optical effect with surface coatings becomes more resilient towards the effect of angle of incidence (AOI) [12], a certain fraction of the light beam cannot be utilized by a module even at the clean condition as it suffers from the reflection losses due to changing position of the light source. As discussed in chapter 2.3.3, the optical response of PV module is a surface characteristics, thus the irradiance might be highly attenuated by the presence of soiling. These additional angular losses are extremely necessary to be considered during the yield prediction. The SR was measured for outdoor and indoor experiments were not constant but changed with the position of the light and presence of dust. The angular losses in a soiled module, became very large at larger AOI representing the dusk and dawn time.

Working principle of the soiling sensor (DustIQ) was explained in chapter 3. It accurately measures the soiling ratio (1-$TL_{GENERIC}$) at the middle of the day. Once the sensor is cleaned, no further measurements are possible before it again accumulates enough dust. Due to the inability of the DustIQ to measure the specific transmission loss ($TL_{SPECIFIC}$) at any time instant and to aid in accurate yield prediction, an empirical equation has been introduced based on incident angle modifier (IAM) for soiled and cleaned PV modules. The proposed equation has used to determine SR for an entire day based on instantaneous Sun's AOI and a single mid-day SR value measured with the DustIQ. First, a module was subjected for different soiling levels with an interval of 1% starting from clean (T_{loss}=0) to soiled (T_{loss}=13.1%) to estimate a dimensionless parameter called angular loss coefficient (a_r). Calculated a_r were then used to estimate the angular losses (AL) at different AOI of Sun as defined by Martin and Ruiz [29]. SR of a soiled module was measured over the course of a day for three conditions of high, medium and low daily average irradiance as seen in section 2.2.3. These measured soiling ratio values were taken as a reference to compare the modeled values. An average residual between a measured (SR^{Isc}) and modeled (SR^{model}) values was determined with the help of root mean square deviation (RMSD). Finally, a low pass filter called "Savitzky-Golay smoothing filter" was also employed to filter out noisy SR to check for a better approximation of modeled SR.

SR measurement done for three different days characterized by their daily average irradiances; high irradiance (758.18 W/m^2) on 27th Aug. 2017, medium irradiance (559.12 W/m^2) on 23th Aug. 2017, low irradiance (275.87 W/m^2) on 24th Aug. 2017 has been taken from Figure 2.9.

4.1. PV module Angular Losses

Angular losses (AL) for PV modules are generally calculated referencing a normal incidence of radiation at which the electrical characteristics of PV module are also provided. Incident angle modifier (IAM)

can be determined by four different modelling approaches namely, ASHRAE IAM model, Physical IAM model, Sandia IAM model and Martin and Ruiz IAM model [71]. For this modelling, Martin and Ruiz model was chosen based on its agreeability at all AOI, which lacks in case of other models. The losses at an AOI of θ can be calculated with the following formula [29],

$$AL(\theta) = 1 - \frac{T(\theta)}{T(0)} \tag{4.1}$$

where, T(θ) and T(0) represent the air to solar cell at angles θ and 0° respectively. A complement to the unity of angular losses (AL) is known as angular factor ($f_{I\alpha}$) [29]. It represents the relative optical response of a module at an AOI. The experimental value of angular factor can be obtained as the ratio of cosine corrected short-circuit current at an angle θ ($I_{sc}(\theta)$) to the short circuit current at normal incidence ($I_{sc}(\theta = 0°)$) represented by equation 4.2 [29].

$$f_{I\alpha} = \frac{I_{sc}(\theta)}{I_{sc}(0) \times \cos\theta} \tag{4.2}$$

The optical response any module with or without anti-reflective coatings can be determined with the help of an analytical equation 4.3 [29].

$$AL(\theta) = 1 - \frac{1 - exp(-\cos\theta/a_r)}{1 - exp(-1/a_r)} \tag{4.3}$$

$$IAM(\theta) = 1 - AL(\theta) \tag{4.4}$$

where a_r is the empirical angular loss coefficient, which depends on PV module technology. Equation 4.4 represents incident angle modifier (IAM) the is the complement of angular losses (AL) with a maximum of 1 and minimum 0. It signifies the degree of module performance for any angle of incidence (AOI) with a maximum value at lowest AOI (solar noon).

In the work of [73], equation 4.3 was found to accurately describe the angular losses of all analyzed PV configurations with the high value of determination (R^2) coefficients. For our calculations, the generated short-circuit currents for each module were first scaled up to the same reference irradiance as it was during solar noon by equation 4.5.

$$I_{sc}(t) = \frac{I_{sc,t} \times G_{ref}}{G_t} \tag{4.5}$$

I_{sc}(t) is the scaled short-circuit current with the help of temperature-corrected instantaneous short-circuit current ($I_{sc,t}$) and irradiance (G_t) at time t. (G_{ref}) is the reference irradiance at the mid of that day. The angular factor ($f_{I\alpha}$) in equation 4.2 was determined at each AOI of the Sun on a module and soiling level. The calculated angular factors at each transmission loss interval were then plugged in equation 4.3 to determine the angular loss factor (a_r) at an AOI of 5°, 10°, 15°, 20°, 25°and 30°. Finally, an average a_r at each soiling level was substituted into equation 4.2 and 4.3 to calculate the incidence angle modifier of the module at every AOI from 0°to 90°.

The rooftop PV setup was also used to determine the angular losses on the PV modules. To do so, Sun's altitude and azimuth were calculated over the whole year for the measurement location following the methods and formulas described in [43]. An extensive explanation can be found in Appendix C.1. On 11th of July 2017, the solar zenith angle (SZA) was observed to be exactly perpendicular on at 60° with respect to the modules tilted at an angle of 30° horizontal. Therefore, different AOI of the Sun for 27th of August were calculated with respect to its position on 11th of July. For our range of interest between 10:57 to 16:30, the AOI of Sun was found to impart the only direct component of the irradiance without much influence of the shading by nearby buildings/trees as well as the diffused light. A minute average voltage drop for both modules was translated to the short-circuit current using

equation 2.1.

As mentioned in section 2.2.3, SR at solar noon was found to be 86.9%. The angular factor ($f_{I\alpha}$) and angular loss factor (a_r) were calculated for different soiling ratio (SR) with an interval of around 1% starting from 86.9% to 99.2% with the help of equation 4.2 and 4.3. The graph shown in 4.1 represents of IAM at increasing soiling level (T_{loss}) and corresponding angular loss coefficients (a_r) value for high irradiance day. The IAM for medium and low irradiance for the soiled and clean condition has been presented in the Appendix B.2.
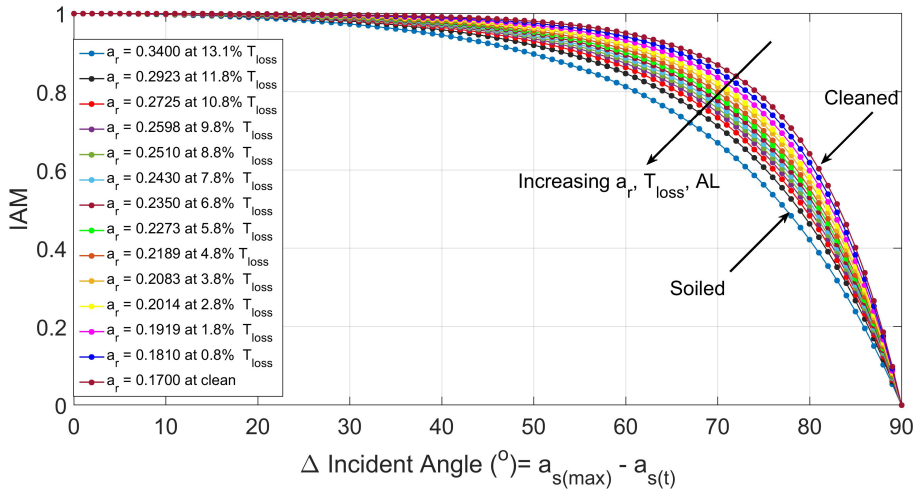
Figure 4.1: IAM at different soiling ratio (SR) from 86.9% to 99.2%.

The x-axis represents the difference between Sun's altitude at the mid of the day (when maximum) and at any time t. The angular loss factor (a_r) was found to be lowest for a clean module at 0.17 represented by the bottom-most blue curve while it increased and reached 0.34 at T_{loss} of 13.1% (SR=86.9%) represented by the top red curve. The increasing pattern of a_r associates with the increase in angular losses with soiling level. Comparing the IAM for cleaned and soiled modules at the same AOI of 30° helps to understand the detrimental effect of soiling on the PV module. The angular loss of a cleaned module was 0.0018 while for the soiled module the losses increased to 0.0164 that is more than 9 times larger. The angular losses were found to decrease with lesser dust spread on a module as represented by the legend box of Figure 4.1. This IAM of soiled and cleaned modules was next used to model SR pattern throughout the day.

4.2. SR Modelling based on Angular Losses

The soiling ratio (SR) over a course of the day as represented in Figure 2.11 will be now modeled with the help of a single mid-day SR value (86.8%) and estimated angular losses in the modules. The angular losses for a clean and soiled module at each AOI from Figure 4.1 was multiplied with mid-day SR value with the help of empirical equation 4.6.

$$SR_{modelling} = \frac{IAM_s(\theta)}{IAM_c(\theta)} \times SR_{mid-day} = IAM_{ratio}(\theta) \times SR_{mid-day} \qquad (4.6)$$

As it was noticed from equation 1.2, the soiling ratio (SR) was the comparison between soiled and the cleaned module thus; the IAM_{ratio} in equation 4.6 has also been presented as the ratio of IAM associated with the soiled module (IAM_s) to that of cleaned (IAM_c). After modeling SR for each solar AOI, the curve shown in 4.2 was generated that compares measured SR^{Isc} from section 2.11 and modeled SR.
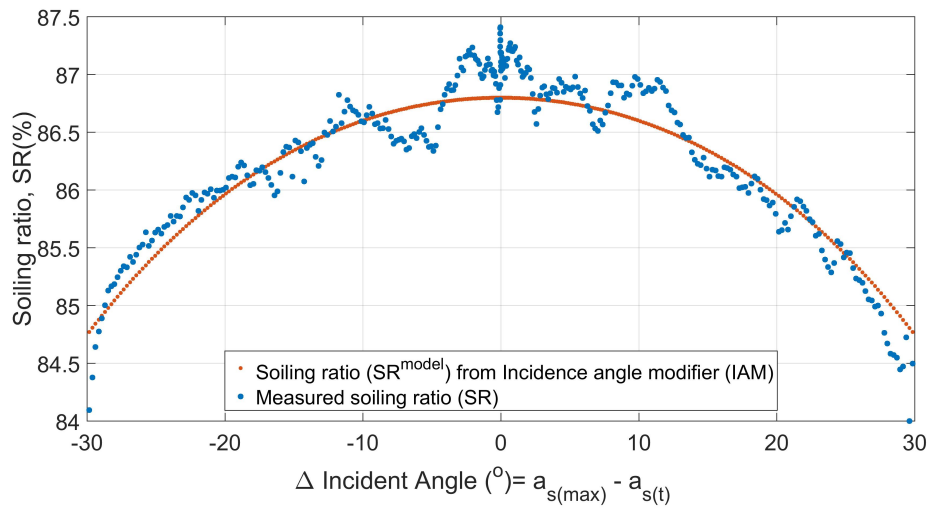
Figure 4.2: Modeled soiling ratio (SR^{model}) vs measured soiling ratio (SR^{Isc}) for 24th August 2017.

The modelled SR represented by a blue curve was seen to be much smoother compared to the measured SR. On the measurement day, the moving of clouds and dynamic shading could be the reason for varying SR even at the middle of the day shown by a red curve. From a visual inspection, the modelled curve seems to quite agree with the measured values. It can be seen that, due to larger solar angle during morning and evening time, the angular losses was high even in case of modeled curve. Similar estimation for medium and low irradiance day has been presented in Figure 4.3 and 4.4 respectively.
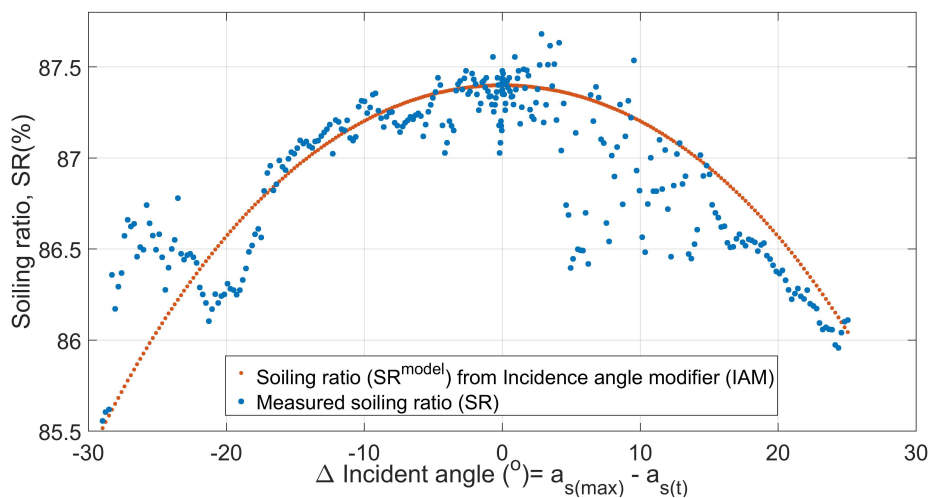
Figure 4.3: Modeled soiling ratio (SR^{model}) vs measured SR (SR^{Isc}) for 23rd August 2017.
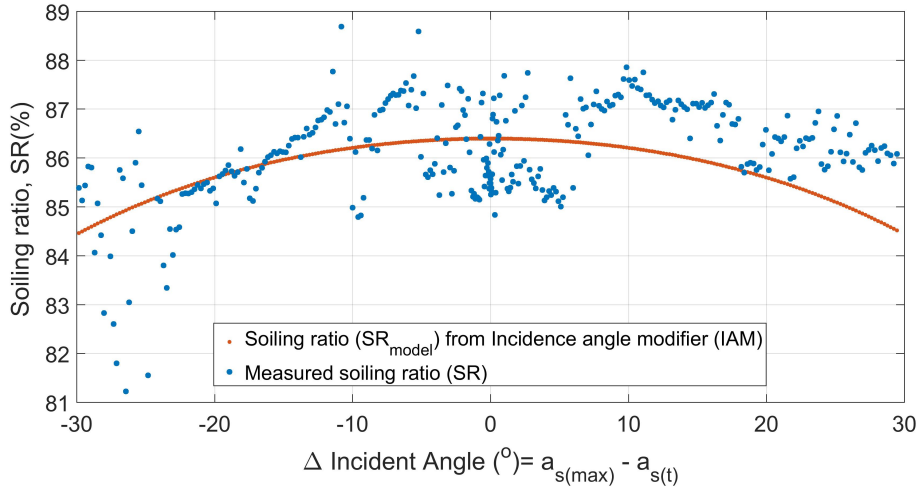
Figure 4.4: Modeled soiling ratio (SR^{model}) vs measured SR (SR^{Isc}) for 24th August 2017.

4.3. Deviation Between Measured and Modeled SR

An error or residuals calculation represents the deviation of modelled value compared to an observed or true value and this deviation facilitates to quantify the error present on the data of interest. To measure the closeness of the proposed model (equation 4.6) and measured SR, root mean square deviation (RMSD) will be calculated for each data point. It represents an average deviation of a modelled value from measured one [74]. RMSD calculation was carried out with the help of equation 4.7. [75],

$$RMSD = \sqrt{\frac{1}{n}\sum_{i=1}^{n}(m_i - p_i)^2} \qquad (4.7)$$

where m_i represents measured values, whereas p_i shows the modeled value at time i of n data events, RMSD has a unit in %. For high irradiance day, there were 334 data events representing each minute resulting in a mean squared error of 0.0458%. Thus, RMSD between measured and modelled data set was then found to be ±0.21%. This signifies that modeled soiling ratio values predicted the measured with a variance of ±0.21%. The error associated with medium and low irradiance situation was also estimated in a similar manner. A comparison for each irradiance condition has been summarized in the table 4.1.

Table 4.1: RMSD for three irradiance conditions of measured and modeled data.

Day	Date	Daily avg. irradiance (W/m^2)	RMSD (%)
High irradiance	27th Aug. 2017	758.18	±0.21
Medium irradiance	23rd Aug. 2017	559.12	±0.28
Low irradiance	24th Aug. 2017	275.87	±1.04

The low light condition was analogous to a high degree of deviation of around ±1% probably due to constant AOI of Sun during cloudy days resulting in the larger amplitude of noise and difficult in the angular loss a prediction. But during the day with an adequate amount of light the residual error was quite low at around ±0.2% and ±0.28%. These results suggest that the model predict the soiling ratio very well during high irradiance condition while it is less accurate on cloudy days.

4.4. RMSD Between Modelled and Filtered SR

As seen from Figures 2.9 and 2.10, large fluctuations in the irradiance was the reason for high degree of RMS deviation. Thus, the measured SR data will now be filtered using a low pass filter known as "Savitzky-Golay smoothing filter" in MATLAB. The "sgolayfilt" function uses n number of neighboring

data points and a polynomial of order p to these data sets. The point at the center of the n points is replaced by the value given by the polynomial fit of neighbouring data points. Therefore, the smoothing is found to have a stronger effect for higher n and smaller p. The MATLAB function has been represented with the help of equation 4.8.

$$\text{sgf} = \text{sgolayfilt}(x, p, n) \tag{4.8}$$

'sgf' in the above function represents the filtered data sets of x matrix for polynomial order p and frame length n. For this analysis, a frame length of one hour has been taken, which means for every hour data sets a polynomial fit will define the center of each interval point. Again, the measured SR represented in Figures 4.2, 4.4 and 4.3 will be used to analyze the role played by this filter. Finally, RMSE was calculated and compared for each irradiance condition similar to table 4.2. For a quick comparison between modelled soiling ratio and filtered soiling ratio for a high irradiance day has been presented in the Figure 4.5. The filtered curve has lesser noise amplitude compared to Figure 4.2. Furthermore, the filtered graphical plot for medium irradiance and low irradiance has been presented in Appendix B.3.
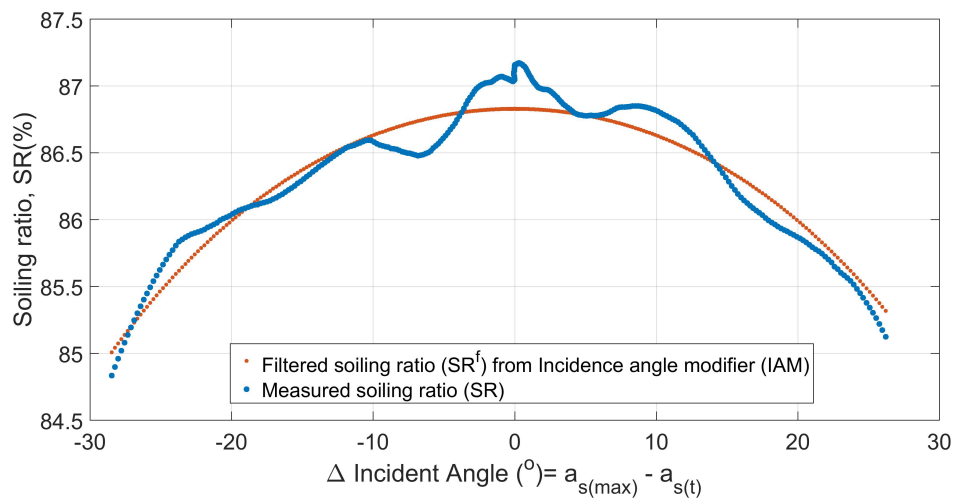
Figure 4.5: Modeled soiling ratio (SR^{model}) vs filtered soiling ratio ($SR^{f,Isc}$).

A modelled value, p_i will be compared with filtered value, m_i using equation 4.7. The shape of SR curve for a perfect condition (high irradiance and no cloud coverage) is parabolic thus, the order of the polynomial p was taken as 2. The mean squared error for high irradiance condition was found to be 0.021%, whereas RMSD after the use of filter found to be $\pm 0.14\%$. Similarly, table 4.2 has been presented to show the results of deviation calculated between filtered and measured SR.

Table 4.2: RMSD for three irradiance conditions for filtered and modeled data.

Day	Date	Avg. irradiance (W/m^2)	RMSD (%)	Error reduction (%)
High irradiance	27th Aug. 2017	758.18	± 0.14	33.33
Medium irradiance	23rd Aug. 2017	559.12	± 0.18	35.7
Low irradiance	24th Aug. 2017	275.87	± 0.72	30.76

In table 4.2, the resulting residuals after using a low pass filter at each irradiance day decreased by approximately 30-35%. Therefore, "Savitzky-Golay filter" can be used to filter out noises without disturbing the data pattern.

4.5. Inference

Soiling ratio (SR) from short circuit current method was chosen to determine SR over the course of the day. However, it should be noted that soiling ratio could be estimated by maximum power point

method as well that might give a slightly different result. Soiling ratio was found to be influenced by the AOI of the Sun with a high degree of module angular losses during morning and evening time. An analytical model developed by Martin and Ruiz was followed to characterize the angular loss coefficient (a_r) at increasing T_{loss} and was found to increase with the soiling level. The soiled and cleaned PV modules had angular loss coefficient values of 0.34 and 0.17 respectively for a high irradiance day (758.18 W/m^2). It was also noticed that the presence of dust on a module attenuated the angular losses (AL), therefore decreasing the transmittance of irradiance at the same AOI compared to the cleaned module. The proposed empirical equation based on the incidence angle modifier (IAM) and a single mid-day SR measurement was found to have a very low deviation of $\pm$±0.21% for a sunny day. The soiling ratio curve was found to be influenced due to movement of the clouds, thus increasing the RMSD. The average RMS deviation was found to decrease by around 35% after using the smoothing filter. Furthermore, if there was less irradiance fluctuation, the RMSD would have been anticipated to decrease resulting into the more accurate estimation.

In section 2.2, dust colors were found to be independent of the angular losses at the same mass density. Thus, this proposed model with the help of the DustIQ can be used to determine the SR^{SPECIFIC} at any instant of time. Therefore, with an aim of a scientific journal publication, a manuscript has been written following IEEE norms attached at the end of this report.

5

Natural Soiling

PV module once deployed on the site, limited or no study is done on different factors that limit its performance. The atmospheric dust intensity gives a good estimate of soiling on the PV modules. The effect is generally higher in case of frequent vehicular movement, nearby industries, sandstorm events, and bird droppings. Dust intensity map 1.1 showed higher atmospheric dust concentration in MENA and Asian Pacific regions while European countries had relatively less. A thorough study of dust effect was done in chapter 1. PV modules installed in Belgium was found to have yearly soiling power loss of 3-4% [76], whereas in Malaga, which is located in southern Europe was reported to have an annual energy loss of 4.4% [7]. Similarly, if a PV park is located near the seashore, it could suffer from frequent bird droppings, which is a most severe form of soiling as it contributes toward partial shading.

Although there are few studies done in Germany, Spain, and Belgium, the soiling transmission and power loss in Delft is another important aspect of this research. This experiment was very crucial because no previous soiling research was done to estimate the effect of natural soiling on the PV modules. In Europe, the dust storm is not an issue but all other factors might contribute to soiling loss. After studying various soiling effects with the artificial soiling procedure, the deposition and influence of natural soiling will be analyzed next. The observed soiling behavior and their effects are employed to realize the annual energy loss due to soiling.

In this chapter, natural accumulation of soiling was measured in the same rooftop PV setup shown in Figure 2.3. Six PV modules were left uncleaned for 7 dry days in the last week of August 2017. On a day before rainfall, transmission and power loss from the modules were measured with the help of curve tracing device. This estimation was then used to estimate an annual energy loss at three different soiling scenarios. Finally, an optimal module cleaning frequency was estimated and recommended to minimize the energy loss.

5.1. Transmission Loss

The transmission loss signifies the percentage of solar irradiance failed to reach the semiconductor materials due to the presence blocking objects (snow or soil). Six polycrystalline PV modules from the first three rows in Figure 2.3 were observed for the natural deposition of dust from the period of 22nd of Aug. to 28th of Aug. 2017. A number of soiled and cleaned readings from each module were taken before the rainfall on 29th of Aug. using MP-11 I-V curve tracer provided by EKO instruments. The PV modules were neatly cleaned with the help of deionized water and a clean fabric. Instantaneous irradiance was measured with the help of CMP-21 pyranometer provided by Kipp & Zonen installed in the plane of the array (POA). Similarly, two temperature sensors were applied to each module for temperature correction. One of the naturally soiled modules can be seen in Figure 5.1.

Figure 5.1: Dust in the PV module due to the natural accumulation for 8 days period.

A uniformly deposited thin layer of dust can be seen from the figure. The transmission was estimated from measured short-circuit current (I_{sc}) from soiled and cleaned PV modules after temperature correction using equation 1.1. The indicated transmission at each point has been presented in the Figure 5.2 and the lines are linear fits between them.
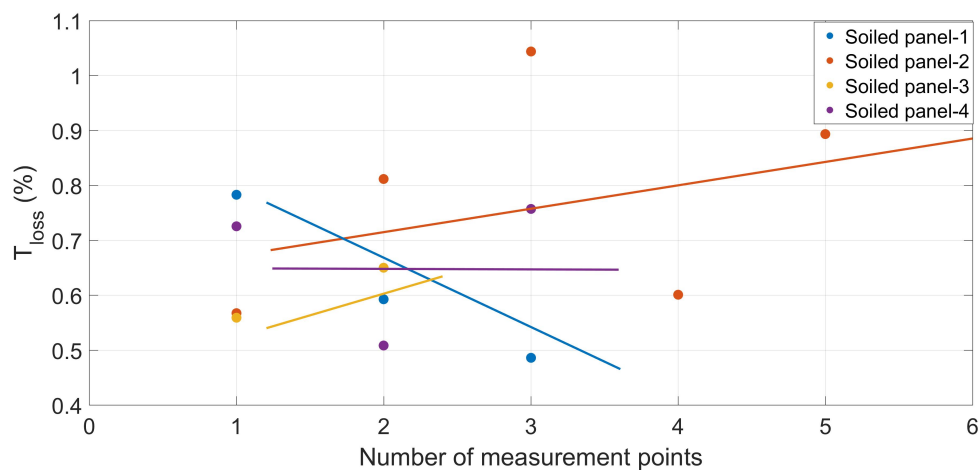
Figure 5.2: Transmission loss in four different soiled modules for 8 days in Delft.

The transmission loss at different measurements was found to vary possibly due to a slight change in irradiance due to cloud movement. Only relative transmission loss has been considered here, however, the manufacturing defect or module aging contributed additional average T_{loss} of 3.5% in each module. This was estimated by comparing the irradiance from a clean module and pyranometer readings. The power loss from the module was also estimated from the measured data. The average transmission and power loss in each module were calculated and represented in the form of the bar graph in Figure 5.3.
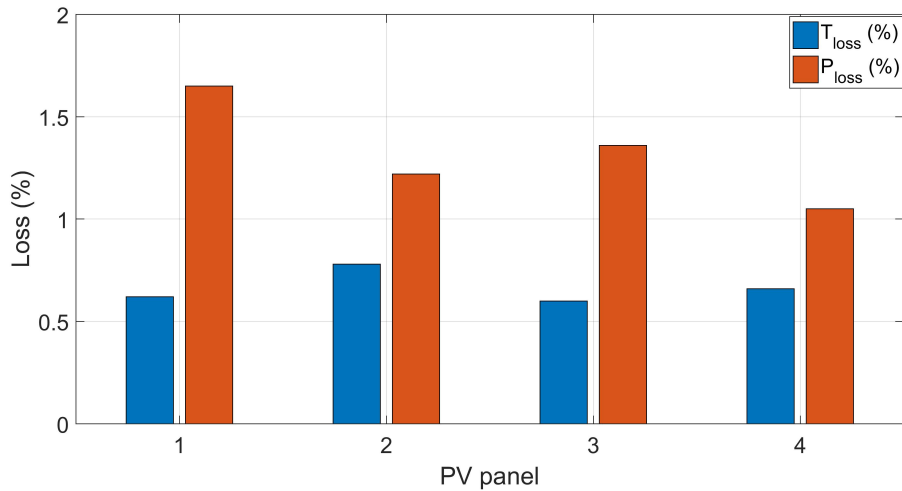
Figure 5.3: Average transmission and power loss in four modules due to the natural soiling for 8 days in Delft.

The average transmission loss from all the modules was calculated to be 0.083% per day, whereas the average power loss was estimated to be 0.165% per day. The corresponding power loss at each module was found to be higher than the transmission loss in Figure 5.3. This soiling rate for Delft, which is located in northern Europe is quite a significant number. Although the system is located 16 meters from the ground, a large number of vehicular movement at the nearby highway could be the major reason for this high loss rate. Combustion of fuel majorly emits carbon compounds (black dust), which results in higher losses also noticed from Figure 2.25.

As discussed in section 1.4, rainfall is the natural source for module cleaning. Soiling loss generally increases linearly with time in the absence of cleaning [7]. Soiling loss represents the average transmission loss seen in 5.1. The above modules were not cleaned manually but only due to rain (excluding a day for the experiment). Based on experience, a total rainfall of 2 mm or more has been considered to be sufficient enough to clean the modules. For a rain-free period (RF_p), daily soiling losses in a module increase linearly but gets completely cleaned (T_{loss} = 0%) after sufficient rain. A rain-free periods for an entire year was calculated with the help of rainfall data retrieved from Royal Netherlands Meteorological Institute's (KNMI) database. Therefore, considering 0.083%/day of transmission loss, the soiling loss as a function of rainfall events for the whole year has been represented in the Figure 5.4.
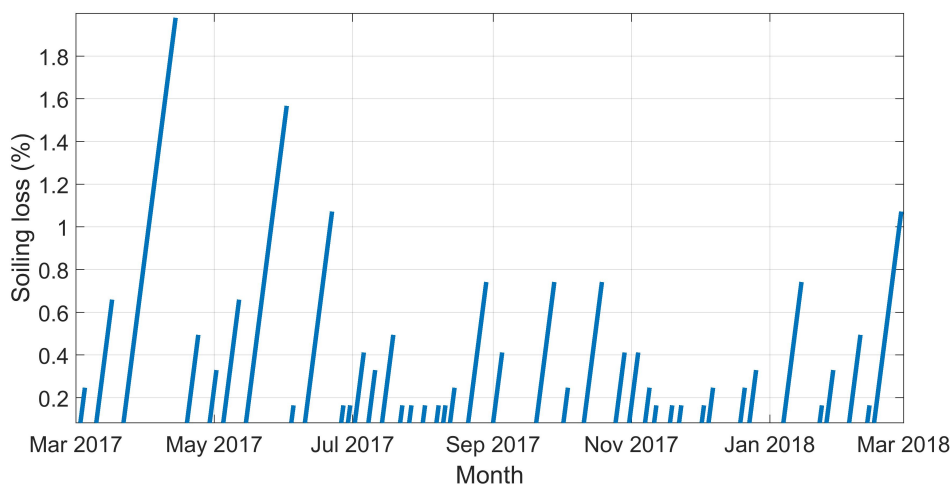
Figure 5.4: Soiling loss from March 2017 to Feb. 2018.

The losses were quite high for the dry months of March, April, May and June. Highest transmission loss of 1.98% was seen on 14th of April 2017. Frequent but lesser intense soiling losses were seen on a winter time. A closer look at the soiling and cleaning action for the month of May has been plotted in Figure 5.5.
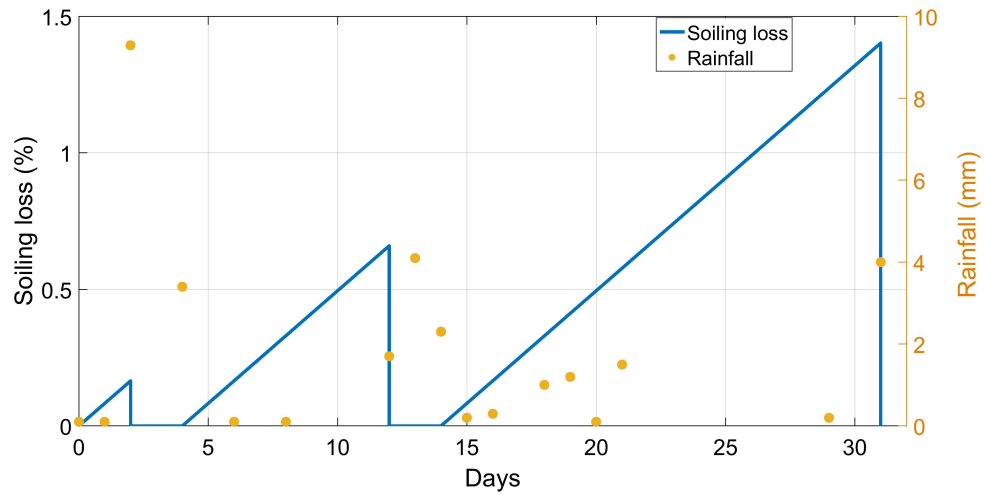
Figure 5.5: Soiling loss vs rainfall for the month of May.

A continuous blue line in Figure 5.5, represents a linear increase in the soiling loss for dry days and red dots is the rainfall event. For a rainfall of 2 mm or more, soiling loss is set to 0%. Last 15 days of the month experienced no-rainfall increasing the loss to 1.4% on a day before rainfall.

5.2. Energy Loss

Dust-induced soiling loss attenuates the total amount of electricity generated from a system. In this section, the results obtained from soiling effects analysis in the experiments above will be finally utilized to estimate the total energy loss in the module. Soiling rate for a rain-free period (RF_p) along with the change in incidence angle modifier (IAM) has been included as the most influencing parameters to reduce the total irradiation on a module. The role played by these parameters was analyzed by calculating the total energy output for an entire year. Soiling loss during each rain-free period (RF_p) was taken from the Figure 5.4. Energy loss analysis was initiated with the calculation of Sun's hourly position for an entire year as the total amount of irradiance incident on a module is a function of a module orientation as well as the position of the Sun over time. The plane of array (POA) irradiance (G_M) is a function of direct, diffused and albedo component, which was calculated using equations 5.1, 5.3 and 5.4. The hourly global horizontal irradiance (GHI), direct normal irradiance (DNI) and diffused horizontal irradiance (DHI) were retrieved from Meteonorm software. An extensive explanation for a solar position calculation can be found in Appendix C.1 or in the book [43] but in brief, the following equations were used to calculate the three components of light reaching the modules.

$$G_M^{dir} = I_e^{dir} \times cos\gamma \tag{5.1}$$

$$SVF = \frac{1 + cos\theta_M}{2} \tag{5.2}$$

$$G_M^{diff} = SVF \times DHI \tag{5.3}$$

$$G_M^{gr} = GHI \times \alpha \times (1 - SVF) \tag{5.4}$$

In equation 5.1, I_e^{dir} is the DNI and γ is the Sun's angle of incidence (AOI). SVF is the sky view factor, which was used to calculate the intensity of the diffused light using the isotropic sky model and the amount of light reflected from the ground towards the module. α is the albedo of the ground considered

to be 0.2 due to the presence of a reflective surface in the background. Finally, the POA irradiance on the module was estimated using equation 5.5

$$G_M = G_M^{dir} + G_M^{diff} + G_M^{gr} \tag{5.5}$$

Calculated hourly POA irradiance on the module has been plotted and presented in Appendix C.2. A module's performance is also dependent on its instantaneous temperature. A module's output as a function of irradiance was seen by equations 1.4, 1.5 and 1.6 respectively. Similarly, the temperature effects were discussed in equation 2.2. Therefore, the hourly module temperature was calculated using Fluid Dynamic Model, which inputs Nominal Operating Cell Temperature (NOCT) of a module, wind speed, ambient temperature (T_a) as well as a module's dimension [43]. A detailed description of this model can be found in Appendix C.3. Thus, the calculated POA irradiance (G_M) and the module temperature (T_M) were used to estimate hourly module efficiency (η) and maximum power produced (P_{mpp}) from the module with an area, A_m using equations 5.6, 5.7 and 5.8.

$$\eta(T_M, G_M) = \eta(25°C, G_M)(1 + \kappa(T_M - 25°C)) \tag{5.6}$$

$$\eta(25°C, G_M) = \frac{P_{mpp}(25°C, G_M)}{G_M \times A_m} \tag{5.7}$$

$$P_{mpp}(25°C, G_M) = I_{sc}(25°C, G_M) \times V_{oc}(25°C, G_M) \times FF \tag{5.8}$$

κ in equation 5.6 is the temperature coefficient for efficiency whose typical value for crystalline silicon module is -0.0035/°C [43]. The calculation of I_{sc} and V_{oc} at 25°C were done as in equation 1.4 and 1.5. A module's power output from above calculations was be used as an input to estimate inverter's efficiency using Sandia National Laboratories (SNL) model. The rooftop PV system has six Enphase215 micro-inverters of which two were replaced with Enphase250 on 10th July 2017 due to power clipping issue. The hourly input and output of the inverter were simulated to calculate its efficiency. The values of used parameters and empirical coefficients were retrieved from System Advisory Model's (SAM) database. A detailed explanation can be followed by Appendix C.4. Now, total energy produced from a module can be finally represented by equation 5.9.

$$P_{out} = G_M \times A_m \times \eta_{PV} \times \eta_{inv} \times \eta_{soil} \times \eta_{IAM} \tag{5.9}$$

After, developing a model to determine a module's output, total annual energy loss at various soiling cases will be determined. Hourly POA irradiance (G_M) of a soiled module was reduced due to the different soiling level for each case.

i. 2% Soiling: Most of the PV design software packages use a default value of 2 or 3% per day of soiling losses irrespective of location [77]. Using this fixed value might under or over-estimate the energy loss. A default condition of 2% soiling for Delft will be assumed to determine an annual energy loss.

$$G_M(t) = \left[G_M^{dir}(t) + G_M^{diff}(t) + G_M^{gr}(t)\right] \times \eta_{2\%} \tag{5.10}$$

ii. 2% Soiling and IAM: Here, the incidence angle modifier (IAM) has also been estimated for the soiled and cleaned modules. The maximum altitude of the Sun was compared with rest of the positions on each day to find the additional angular loss in soiled module. Using equation 4.3 with a_r=0.17 for a clean condition (soiling loss =0%) and a_r=0.1919 for 2% of soiling loss, hourly IAM was calculated for each day. The soiled and cleaned IAM were compared to use it as a derating factor for POA irradiance as shown in equation 5.11.

$$G_M(t) = \left[G_M^{dir}(t) + G_M^{diff}(t) + G_M^{gr}(t)\right] \times \eta_{2\%} \times \eta_{IAM} \tag{5.11}$$

iii. 0.083% Soiling: Average soiling loss per day value determined from section 5.1 as a factor to reduce irradiance incident on the module. Soiling losses for next day will be determined by rain-free period (RF$_p$). If a following day experienced a rainfall of 2 mm or more, the soiling losses will be set to 0%, otherwise increases linearly.

$$G_M(t) = \left[G_M^{dir}(t) + G_M^{diff}(t) + G_M^{gr}(t) \right] \times \eta_{0.083\%} \tag{5.12}$$

iv. 0.083% Soiling and IAM: Similar to point ii, IAM was again estimated for soiled and cleaned modules. Here, a$_r$=0.17 for a clean condition (soiling loss =0%), a$_r$=0.181 for soiling loss of ≤1% and a$_r$=0.1919 for soiling loss of >1% were used and hourly IAM was calculated for each day. The soiled and cleaned IAM were compared to use it as a derating factor for POA irradiance as shown in equation 5.13.

$$G_M(t) = \left[G_M^{dir}(t) + G_M^{diff}(t) + G_M^{gr}(t) \right] \times \eta_{0.083\%} \times \eta_{IAM} \tag{5.13}$$

Results form above four cases have been summarized in the table 5.1.

Table 5.1: Annual energy loss (kWh) in 6 PV modules due to soiling.

Condition	Enphase215 (kWh/year/module)	Enphase250 (kWh/year/module)	Total energy produced(kWh)	kWh loss
No soiling	274.86	262.67	1624.78	-
2% soiling	269.59	257.64	1593.64	31.14
2% soiling +IAM	267.84	256.28	1583.86	40.92
0.083% soiling	273.04	260.88	1613.92	10.86
0.083% soiling + IAM	272.1	260.08	1608.56	16.22

The total energy production from six cleaned PV modules of 1.62 KW$_p$ was found to be 1.62 MWh. When soiling related loss was randomly taken as 2%, this overestimated the soiling losses (31.14 and 40.9 kWh) for this location but it might as well underestimate for a location with high soiling rate. In chapter 4, dust on the module was found to attenuate the irradiance by increasing the angular losses of the module. Therefore, assuming only 0.083% of soiling loss, resulted in total energy loss of 10.86 kWh, whereas after including angular losses, the total energy loss was found to be 16.22 kWh. The differences in energy generation from a soiled module and same module if it was clean on 14th April 2017 can be closely seen from Figure 5.6. The soiling loss on this day was noticed to be the highest of 1.98%.
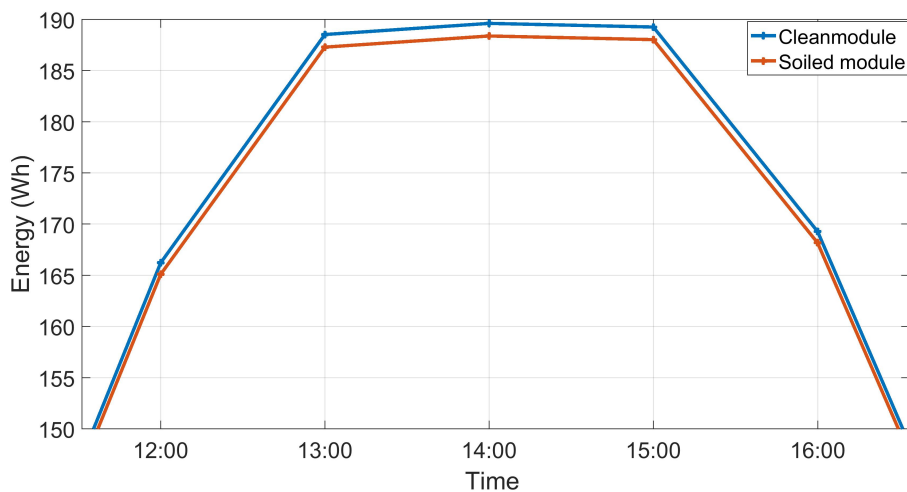
Figure 5.6: Energy produced from a cleaned and soiled module on 14th April 2017.

The area between red and blue curve represents the energy loss due to soiling. The total energy lost on this day was found to be 3.37 kWh. Although annual energy loss was just 1% of the total electricity production, it should be noted that the size of the PV system was small. The losses would have been very significant for a larger system size like a PV park of several MWs.

5.3. Cleaning Frequency

An optimum cleaning frequency eliminates additional cost as well as the energy loss. For the calculated energy loss, now an optimal cleaning frequency will be estimated using equation 1.8. Although 16.22 kWh is not a very significant amount to change the LCOE of the generated energy, a cleaning period will be calculated based on some assumptions. It was considered that the cleaning activity will be performed locally without outsourcing to avoid an additional cost. The cost of water and other cleansing agents has been estimated as €0.02 per module while the feed-in-tariff (FIT) rate was taken to be €0.09/kWh [78]. The energy loss for each rain-free period and its optimum cleaning period has been shown in the Figure 5.7.
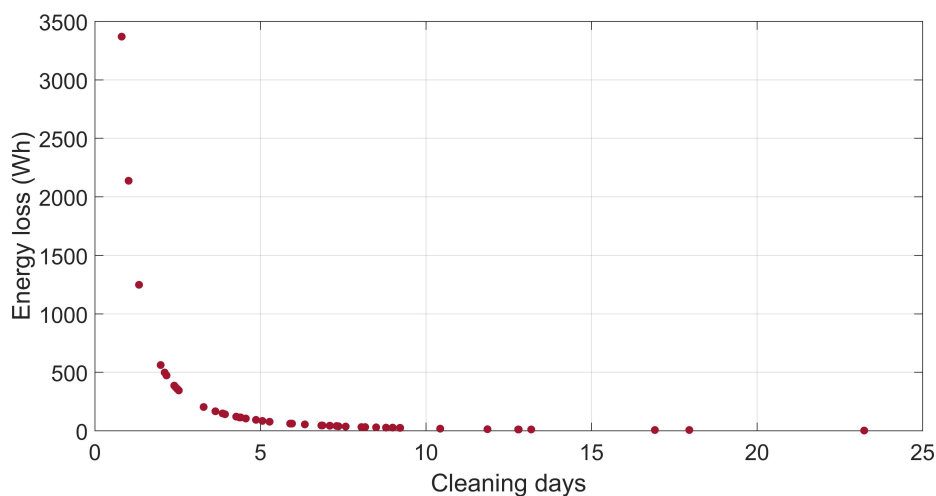
Figure 5.7: Energy loss vs cleaning days from March 2017 to Feb. 2018.

The figure represents higher energy loss resulted in frequent cleaning periods to avoid extra energy loss. When there was a maximum energy loss on 14th April, cleaning period was found to be 1 day, which means the system's energy output is decreasing by 3.37 kWh per day then everyday cleaning is needed. If the energy loss for each rain-free period is taken as the average value of 240Wh, the cleaning frequency was found to be 8 days. Therefore, for Delft, it is beneficial to clean panels locally every eight days. The average cleaning frequency can be an optimum for a location with constant and high soiling rate but here, soiling rate is less significant to carry out cleaning cycle more than twice or thrice in a year.

6

Conclusions and Outlook

6.1. Conclusions

This research work included a number of experiments to study the soiling effect on a PV module. The test results performed during the development of the soiling sensor, The DustIQ were discussed in chapter 3. Consequently, this thesis also focused on developing an empirical equation based on incident angle modifier (IAM) for soiled and cleaned PV modules. The proposed equation was further applied to accurately determine SR. Finally, the results from different experiments were applied to estimate an annual energy loss from a rooftop PV system in Delft. The conclusions derived from each chapter are discussed hereby.

- What are the characteristic differences between soiling measurement methods (Short-circuit current and Power)?

- What are the methods to create good outdoor/indoor soiling conditions for soiling experiments?

- How a soiled module is dependent on the position of a light source?

- How can dust inhomogeneity and grain-size be taken into account?

The composition of dust and its grain-size largely is a result of a module's location. For a coastal region, salts content is more dominant, whereas carbon content in dust is higher for urban/semi-urban locations. A module's tilt, cell connection, its glazing surface, and mounting mechanism directly relates its susceptibility to soiling. Dust particles deposited on the surface gets modified due to rainfall, dew events, and temperature. Therefore, monitoring a soiling behaviour is very crucial for predicting the yield of a system. To do so, different commercial products are available in the market, that compares a soiled module to clean one by calculating the soiling ratio (SR), which is also a main soil monitoring parameter used in this thesis. SR calculated either from current or power has its significance, SR^{Isc} is used to estimate irradiance loss whereas SR^{Pmax} gives the actual module output. A standard outdoor/indoor soiling procedure was explained in the chapter 2. It involved some of the major components like; dust samples and deionized water, an airtight chamber, paint gun, an artificial light source, multimeters, curve tracer, and temperature sensors. The calculated SR ratio was found to change with the position of the light source. When the Sun was at its maximum, the angular losses were found to be minimal due to lesser light scattering, but for larger AOI, losses increased making a parabolic shaped curve measured at an absolute uncertainty of $\pm 1\%$. Furthermore, measuring only short-circuit current during soiling inhomogeneity might largely underestimate or overestimate the losses, whereas power measurement results in accurate loss estimation at all cases. The transmission and power loss of a module was found to depend on dust color. The black color was found to be most severe due to its light absorbing nature. The angular loss of the soiled module was independent of dust color at same mass loading. Dust on a PV module leads to cosine reduction of irradiance due to its spherical shape as the shading of dust particles changes with the altitude of the Sun.

- What are the principle features and first calibration results of the new soiling sensor, the DustIQ?

The existing soiling measurement devices have drawbacks of frequent manual cleaning and moving parts, which increases its O&M cost. Keeping this in mind, a soiling detection sensor (DustIQ) was developed and tested at Kipp & Zonen BV, for accurate and effective soiling measurement. With the help of two measurement sensors after field calibration with the local dust, it provides information about existing SR due to surface dust deposition. The relationship between the DustIQ diode signal and PV transmission loss showed a linear behavior for different types of dust. The device was found to be independent of the dust grain-size influence, which was investigated by depositing Arizona dust (Quartz) with four grain-sizes (5.5 µm, 11 µm, 22 µm and 44 µm). The DustIQ provides information about the relative transmission loss but not the additional angular losses due to the soil. To answer these additional angular losses, an empirical equation has been introduced, which utilizes a single SR measured from the DustIQ and Incidence angle modifier (IAM) to estimate true SR of the soiled module. The RMS deviation for a high irradiance day was found to be $\pm 0.21\%$, whereas for low light conditions the deviation was around $\pm 1\%$. The results suggested that the model predicts the soiling ratio very well during high irradiance condition while it was less accurate on cloudy days.

- By Knowing the irradiance loss due to soiling, how can the energy loss of a module be determined?

The analyzed effects of soiling were used to estimate the annual energy loss from six different modules. In Delft, an average transmission and power loss for 8 dry days was found to be 0.083% and 0.165% per day respectively. Considering rainfall ($\geq$ 2mm) as the only source of cleaning, this soiling rate resulted in an annual energy loss of 16.22 kWh for 1.62kW$_p$ system, which is only 1% of the total energy generated. Although the value seems quite low, it can be very significant for a larger system by lowering its LCOE. The cleaning frequency at this loss rate does not have any trade-off, thus the modules can be left without cleaning. But, cleaning locally in every 8 days was found to minimize the prevailing losses.

6.2. Outlook

Several aspects could be interesting to investigate and study the soiling behaviour in the future. Some suggestions as an outlook in this field include:

- Validate if SR from the maximum power point method has a similar angular dependency of the light source.

- Investigate the attenuation of the light spectrum due to dust color and density.

- Development of a physical model for PV module soiling. Soiling is a function of various environmental parameters and module characteristics, therefore a model which takes soiling rate, weather conditions like; GHI, DNI, DHI, rainfall data, wind speed along with the nature of the dust; its size, amount, and color as an input, to estimate the daily, monthly or early soiling loss for a location.

Bibliography

[1] Fraunhofer Institute for Solar Energy Systems, *Photovoltaics report,* www.ise.fraunhofer.de , 1 (2017).

[2] IEA (International Energy Agency), *Snapshot of Global Photovoltaic Markets - IEA PVPS,* , 1 (2017).

[3] M. Gostein, B. Littmann, J. R. Caron, and L. Dunn, *Comparing PV power plant soiling measurements extracted from PV module irradiance and power measurements,* Conference Record of the IEEE Photovoltaic Specialists Conference , 3004 (2013).

[4] V. Donkelaar, R. V. Martin, and M. Brauer, *Global estimates of ambient ne particulate matter concentrations from satellite-based aerosol optical depth development and application,* Environmental Health Perspectives **118**, 847 (2010).

[5] M. R. Maghami, H. Hizam, C. Gomes, M. A. Radzi, M. I. Rezadad, and S. Hajighorbani, *Power loss due to soiling on solar panel: A review,* Renewable and Sustainable Energy Reviews **59**, 1307 (2016).

[6] M. Mani and R. Pillai, *Impact of dust on solar photovoltaic (PV) performance: Research status, challenges and recommendations,* Renewable and Sustainable Energy Reviews **14**, 3124 (2010).

[7] J. Zorrilla-Casanova, M. Piliougine, J. Carretero, P. Bernaola, P. Carpena, L. Mora-Lopez, and M. Sidrach-de Cardona, *Analysis of dust losses in photovoltaic modules,* World Renewable Energy Congress 2011 – Sweden , 2985 (2011).

[8] R. Appels, B. Lefevre, B. Herteleer, H. Goverde, A. Beerten, R. Paesen, K. D. Medts, J. Driesen, and J. Poortmans, *Effect of Soiling on Photovoltaic Modules,* Solar Energy **96**, 283 (2013).

[9] A. Kimber, L. Mitchell, S. Nogradi, and H. Wenger, *The Effect of Soiling on Large Grid Connected Photovoltaic Systems in California and the Southwest Region of the United States,* IEEE Journal of Photovoltaics , 2391 (2006).

[10] H. K. Elminir, A. E. Ghitas, R. H. Hamid, F. El-Hussainy, M. M. Beheary, and K. M. Abdel-Moneim, *Effect of dust on the transparent cover of solar collectors,* Energy Conversion and Management **47**, 3192 (2006).

[11] R. Hammond, D. Srinivasan, A. Harris, K. Whitfield, and J. Wohlgemuth, *Effects of soiling on PV module and radiometer performance,* Conference Record of the Twenty Sixth IEEE Photovoltaic Specialists Conference - 1997 , 1121 (1997).

[12] J. J. John, *Characterization of Soiling Loss on Photovoltaic Modules , and Development of a Novel Cleaning System,* Indian Institute of Technology Bombay , 146 (2015).

[13] J. Sips-Williem, C. Lee, and R. Ringoir, *6 Key influences that determine PV performance ratios,* www.kippzonen.com , 1 (2017).

[14] T. Sarver, A. Al-Qaraghuli, and L. L. Kazmerski, *A comprehensive review of the impact of dust on the use of solar energy: History, investigations, results, literature, and mitigation approaches,* Renewable and Sustainable Energy Reviews **22**, 698 (2013).

[15] S. Salvador and E. Salvador, *Overview of Particle Air Pollution Air Quality Communication Workshop,* Environmental Protection Agency , 1 (2012).

[16] Environmental Protection Agency (EPA), *Particulate Matter Emissions,* , 1 (2011).

[17] D. Schwela, L. Morawska, and D. Kotzias, *Guidelines for Exposure-Response Measurement of Fine and Ultra Fine Particulate Matter,* World Health , 1 (2000).

[18] NASA, *Tracking dust across the atlantic. NASA Earth Observatory,* NASA'S Earth Observatory (2013).

[19] A. Buekens, G. S. Cholakov, and B. Nath, *Pollution Control Technologies,* Encyclopedia of Life Support Systems (UNESCO-EOLSS) **3** (2009).

[20] H. Qasem, *Efect of accumulated dust on the performance of photovoltaic modules,* PhD, Loughborough University Institutional Repository (2013).

[21] L. Kazmerski, M. A. Jardan, Y. A. Jnoobi, Y. A. Shaya, and J. John, *Ashes to ashes, dust to dust: Averting a potential showstopper for solar photovoltaics,* Photovoltaic Specialist Conference (PVSC) , 0187 (2014).

[22] R. Bagnold, *The physics of Blown Sand and desert dunes,* ISBN 978-94-009- 5684-1 (Print) 978-94-009-5682-7 (Online) **iSBN 978-9** (1954).

[23] A. Sayyah, M. N. Horenstein, and M. K. Mazumder, *Energy yield loss caused by dust deposition on photovoltaic panels,* Solar Energy **107**, 576 (2014).

[24] E. F. Cuddihy, *Theoretical considerations of soil retention,* Solar Energy Materials **3**, 21 (1980).

[25] K. Ilse, M. Khan, V. Naumann, M. Werner, C. Hagendorf, and J. Bagdahn, *Microstructural Investigations of Soiling Processes in Desert Locations,* International PV Soiling Workshop , 1 (2017).

[26] A. Sayyah, M. N. Horenstein, and M. K. Mazumder, *Energy yield loss caused by dust deposition on photovoltaic panels,* Solar Energy **107**, 576 (2014).

[27] J. Cano, *Photovoltaic Modules: Effect of Tilt Angle on Soiling,* System , 2 (2011).

[28] A. Salim, F. Huraib, and N. Eugenio, *PV power-study of system options and optimization,* International Photovoltaic Solar Energy Conference , 688 (1988).

[29] N. Martin and J. M. Ruiz, *Calculation of the PV modules angular losses under field conditions by means of an analytical model,* Solar Energy Materials and Solar Cells **70**, 25 (2001).

[30] W. Nositschka, D. Neumann, M. Prast, and F. Gromball, *Light trapping cover glasses for solar modules tested in outdoor conditions at different sites in Germany and Spain,* European Photovoltaic Solar Energy Conference , 2548 (2007).

[31] T. Sample, J. Lopez-garcia, and A. Pozza, *Long-Term Soiling in a Moderate Subtropical Climate,* Photovoltaic Module Reliability Workshop , 21 (2014).

[32] H. A. McGowan and A. Clark, *A vertical profile of PM10 dust concentrations measured during a regional dust event identified by modis terra, Western Queensland, Australia,* Journal of Geophysical Research: Earth Surface **113** (2008).

[33] C. Sioutas, R. J. Delfino, and M. Singh, *Exposure assessment for atmospheric Ultrafine Particles (UFPs) and implications in epidemiologic research,* Environmental Health Perspectives **113**, 947 (2005).

[34] H. Vuollekoski, M. Vogt, V. A. Sinclair, J. Duplissy, H. Järvinen, E. M. Kyrö, R. Makkonen, T. Petäjä, N. L. Prisle, P. Räisänen, M. Sipilä, J. Ylhäisi, and M. Kulmala, *Estimates of global dew collection potential on artificial surfaces,* Hydrology and Earth System Sciences **19**, 601 (2015).

[35] A. M. El-Nashar, *Seasonal effect of dust deposition on a field of evacuated tube collectors on the performance of a solar desalination plant,* Desalination **238**, 66 (2009).

[36] A. A. Hegazy, *Effect of dust accumulation on solar transmittance through glass covers of plate-type collectors,* Renewable energy **22**, 525 (2001).

[37] A. Ibrahim, *Effect of shadow and dust on the performance of silicon solar cell,* Journal of Basic and Applied Scientific Research (JBASR) **1**, 222 (2011).

[38] B. Aïssa, R. J. Isaifan, V. E. Madhavan, and A. A. Abdallah, *Structural and physical properties of the dust particles in Qatar and their influence on the PV panel performance,* Scientific Reports **6**, 1 (2016).

[39] M. Gostein, J. R. Caron, and B. Littmann, *Measuring soiling losses at utility-scale PV power plants,* 2014 IEEE 40th Photovoltaic Specialist Conference, PVSC 2014 , 885 (2014).

[40] International Electrotechnical comission (IEC):61724-1, *Photovoltaic system performace: Part 1-Monitoring,* (2017).

[41] A. Y. Al-Hasan and A. A. Ghoneim, *A new correlation between photovoltaic panel's efficiency and amount of sand dust accumulated on their surface,* International Journal of Solar Energy **24**, 187 (2005).

[42] B. Figgis, A. Ennaoui, S. Ahzi, and Y. Remond, *Review of PV soiling measurement methods,* Proceedings of 2016 International Renewable and Sustainable Energy Conference, IRSEC 2016 , 176 (2017).

[43] K. Jager, O. Isabella, A. H. M. Smets, R. A. C. M. M. van Swaaij, and M. Zeman, *Solar Energy: The Physics and Engineering of Photovoltaic Conversion, Technologies and Systems,* UIT Cambridge , 1 (2016).

[44] Canadian Solar, *CS6K-260|265|270|275P datasheet,* (2017).

[45] B. Guo, W. Javed, B. W. Figgis, and T. Mirza, *Effect of Dust and Weather Conditions on Effect of Dust and Weather Conditions on Photovoltaic Performance in Doha , Qatar,* Smart Grid and renewable Energy (SGRE) (2015), 10.13140/RG.2.1.1109.1681.

[46] W. K. Yap, R. Galet, and K. C. Yeo, *Quantitative Analysis of Dust and Soiling on Solar PV Panels in the Tropics Utilizing Image-Processing Methods,* Asia Pacific Solar Research Conference , 10 (2015).

[47] Intelligence Sobolt energy, *DirtDetect,* https://www.sobolt.com/products/ (2017).

[48] M. Korevaar, J. Mes, and X. V. Mechelen, *Novel soiling detection system for solar panels,* , 61724 (2016).

[49] Campbell Scientific Inc., *In-Field Soiling Measurement for Operational and Site Assessments,* Solar-module-performance Monitoring (2017).

[50] Campbell Scientific Inc., *Soiling Index Measurement Solution,* Solar-module-performance Monitoring , 1 (2017).

[51] Groundwork, *PVSOIL : PV Soiling Measurement System PVSOIL : PV Soiling Measurement System WHY GROUNDWORK ?* (2017).

[52] Ammonit, *Efficiency losses due to soiling ? Ammonit Soiling Measurement Systems,* (2017).

[53] B. Stueve, *Techniques and equipment for accurately measuring PV soiling losses,* International PV Soiling Workshop (2017).

[54] F. Chen, *Soiling Monitoring Solution & Field Test Results in MENA Area,* Soiling Effect on PV Modules Workshop 2016 (2016).

[55] NRGSystems, *Soiling Measurement Kit,* (2017).

[56] D. Young, *To Wash or Not to Wash? Framework for Making an Informed Decision,* Solar O&M: North America , 1 (2014).

[57] G. Patil, *An Overview of Robotic Mechanical Systems,* International PV Soiling Workshop , 1 (2014).

[58] M. Corsetto, *Introducing the next generation SunPower® Oasis robotic cleaning system,* International PV soiling workshop (2017).

[59] K. A. Moharram, M. S. Abd-Elhady, H. A. Kandil, and H. El-Sherif, *Influence of cleaning using water and surfactants on the performance of photovoltaic panels,* Energy Conversion and Management **68**, 266 (2013).

[60] SUNPOWER, *The SunPower Oasis Solar Power Plant Anatomy of a SunPower Oasis Power Plant Technical Specifi cations,* , 5 (2017).

[61] Wylton Group, *Solarrobots,* http://www.wylton.com/en/page/Solarrobots/index.php (2015).

[62] A. D. Pettersen, *Simulation and experimental study of power losses due to shading and soiling on photovoltaic (PV) module,* Norwegian University of Life Sciences , 119 (2015).

[63] P. Tummers, *Outdoor Modelling of Anti-Soiling Coatings Performance for PV Applications,* International PV Soiling Workshop (2017).

[64] MORESUN, *CSD nano coating development,* International PV Soiling Workshop , 3 (2009).

[65] Transcat, *Fluke 80 Series V Multimeters Users Manual,* (2017).

[66] N. Hyett, *BSRN Uncertainty Report,* Bureau of Meteorology, Australia (2000).

[67] L. Dunn, M. Gostein, and K. Emery, *Comparison of pyranometers vs. pv reference cells for evaluation of pv array performance, Conference Record of the IEEE Photovoltaic Specialists Conference,* (2012).

[68] M. Leilaeioun and Z. C. Holman, *Accuracy of expressions for the fill factor of a solar cell in terms of open-circuit voltage and ideality factor,* Journal of Applied Physics **120** (2016), 10.1063/1.4962511.

[69] H. Zhang, Y. Sun, L. Wu, X. Zhang, and Y. Xiang, *Tracking mechanism and cosine effect study of Module-Heliostat Solar Collector,* Proceedings of the 2016 4th International Conference on Machinery, Materials and Information Technology Applications **71**, 469 (2016).

[70] D. L. King, W. E. Boyson, and J. A. Kratochvil, *Photovoltaic array performance model,* Sandia Report No. 2004-3535 **8**, 1 (2004).

[71] National Technology and Engineering Solutions of Sandia, *Shading, Soiling, and Reflection Losses,* PV Performance Modelling Collaborative (2018).

[72] Googleblog, *Should you Spring Clean your Solar,* (2009).

[73] N. Martín, F. Chenlo, E. Mejuto, F. Soriano, S. Temprano, and M. C. Alonso-García, *Validating an angular of incidence losses model with different pv technologies and soiling conditions,* 27th European Photovoltaic Solar Energy Conference and Exhibition , 3436 (2012).

[74] Universidade Federal de Alagoas, *Model evaluation methods,* (2010).

[75] G. Piñeiro, S. Perelman, J. P. Guerschman, and J. M. Paruelo, *How to evaluate models: Observed vs. predicted or predicted vs. observed?* Ecological Modelling **216**, 316 (2008), arXiv:arXiv:1011.1669v3 .

[76] R. Appels, B. Lefevre, B. Herteleer, H. Goverde, A. Beerten, R. Paesen, K. De Medts, J. Driesen, and J. Poortmans, *Effect of soiling on photovoltaic modules,* Solar Energy **96**, 283 (2013).

[77] Folsom labs, *User Manual HelioScope,* (2014).

[78] EEA, *Energy Support 2005-2012. Country profile – Netherlands,* , 5 (2011).

[79] International Electrotechnical comission (IEC):60891, *Photovoltaic Devices—Procedure for Temperature and Irradiance Corrections to Measured I-V Characteristics,* (2009).

[80] Campbell Scientific, *CR6 measurement and control system - Campbell Scientific operator's manual,* (2015).

[81] Omega Engineering Inc., *RTD-Introduction to Resistance Temperature Detectors,* (2015).

[82] A. R. . ACCREDIA: L'Ente Italiano Di Accreditamento, *Joint Research Center European Solar Test Installation Accreditation Certificate,* (2011).

[83] C. R. Osterwald, *Translation of device performance measurements to reference conditions,* Solar Cells,18,3-4,Pages 269-279 **80401**, 269 (1986).

[84] I. Reda, *Method to Calculate Uncertainties in Measuring Shortwave Solar Irradiance Using Thermopile and Semiconductor Solar Radiometers,* (2011).

A

Appendix-A

A.1. Module specifications

Table A.1: Datasheet of Canadian Solar CS6K-270P [44].

Electrical data (STC)	
Nominal Max. Power (P_{max})	270 W
Opt. Operating Voltage (V_{mp})	30.8 V
Opt. Operating Current (I_{mp})	8.75 A
Open Circuit Voltage (V_{oc})	37.9 V
Short Circuit Current (I_{sc})	9.32 A
Module Efficiency	16.50%
Operating Temperature	-40°C to +85°C
Max. System Voltage	1000 V (IEC)
Power Tolerance	0 to +5 W
Electrical data (NOCT)	
Nominal Max. Power (P_{max})	196 W
Opt. Operating Voltage (V_{mp})	28.1 V
Opt. Operating Current (I_{mp})	6.97 A
Open Circuit Voltage (V_{oc})	34.8 V
Short Circuit Current (I_{sc})	7.55 A
Mechanical data	
Cell Type	Poly-crystalline, 6 inch
Cell Arrangement	60 (6 ×10)
Dimensions	1650 ×992 ×40 mm
Weight	18.2 kg
Front Cover	3.2 mm tempered glass
Frame Material	Anodized aluminium alloy
J-Box	IP67, 3 diodes
Connector	T4
Temperature characteristics	
Temperature Coefficient (P_{max})	-0.41 %/°C
Temperature Coefficient (V_{oc})	-0.31 %/°C
Temperature Coefficient (I_{sc})	0.053 %/°C
Nominal Operating Cell Temperature	45±2 °C

Table A.2: Datasheet of mini-monocrystalline module

Electrical data (STC)	
Nominal Max. Power (P_{max})	2 W
Opt. Operating Voltage (V_{mp})	6 V
Opt. Operating Current (I_{mp})	0.34 A
Open Circuit Voltage (V_{oc})	7.5 V
Short Circuit Current (I_{sc})	0.36 A
Module Efficiency	19%
No. of cells	12
Temperature Coefficient (P_{max})	-0.7 %/°C
Temperature Coefficient (V_{oc})	-0.64 %/°C
Temperature Coefficient (I_{sc})	0.05 %/°C

A.2. SR measurement uncertainty

Here, a detailed procedure to determine the measurement uncertainty of SR has been discussed. Modeling of the equations and curve fitting was done with the help of *cftool* in MATLAB software.

A.2.1. General method for uncertainty calculation

Here, the general methods followed to evaluate the uncertainty in the SR measurement has been listed. The process can be fragmented into following steps [66]:

1. Formulation of mathematical model in the form of variables contributing towards it.

$$A = f(B_1, B_2, B_3, ...) \tag{A.1}$$

where, B_1, B_2, B_3 are the variables contributing towards uncertainty and A is the resulting output.

2. Make a list of all the variables contributing towards the uncertainty in the measurement.

3. Estimate the sensitivity coefficient and degrees of freedom (DoF) in the measurement for different variables. The sensitivity coefficient calculation can be represented as,

$$c_i = \frac{\partial y}{\partial x_i} \tag{A.2}$$

where, c_i is the sensitivity coefficient and $\partial y / \partial x_i$ is the first order differentiation of y with respect to x_i.

4.Calculation of combined standard uncertainty with root-sum-squares method of all variables.

$$u_c^2 = [c_1 u_1]^2 + [c_2 u_2]^2 + [c_3 u_3]^3 + ... = \sum_i^N [c_i u_i]^2 \tag{A.3}$$

5.Calculate the expanded uncertainty with the help of coverage factor and combined DoF.

$$U_a = k_a u_c \tag{A.4}$$

where, U_a is the expanded uncertainty for a, k_a is the coverage factor determined from the student's t distribution and u_c is the combined standard uncertainty from 4.

A.2.2. Model equation

Soiling ratio based on short circuit current method was presented in equation 1.2. Subjecting equation 1.2 with calibration values and considering the translation method for temperature correction, the expanded SR model equation presented by equation A.5 [3] [79].

$$SR = \frac{I_{sc,s}(1 - \alpha(T_{m,s} - T_{ref}))}{I_{sc,c}(1 - \alpha(T_{m,c} - T_{ref}))} \times \frac{I_{sc,cc}(1 - \alpha(T_{m,cc} - T_{ref}))}{I_{sc,sc}(1 - \alpha(T_{m,sc} - T_{ref}))} \tag{A.5}$$

The value of α was taken from the manufacturer's datasheet A.1. In equation 1.2 and A.5, $I_{sc,sc}$ and $I_{sc,cc}$ represents the measured short circuit current of soiled and clean module at calibration level. On the other hand, $T_{m,s}, T_{m,c}, T_{m,sc}$ and $T_{m,cc}$ are measured module temperature of soiled, clean, soiled at calibration and clean at calibration respectively.

A.2.3. SR uncertainty

Following the ISO GUM model general method, I_{sc} and T_m of each module at experimental and calibration level were considered as error contributing variables. The temperature coefficient (α) of module at only experimental level has been considered as the calibration of the modules were already temperature corrected.

A.2.4. Sensitivity coefficient

The sensitivity coefficient related to each variables were defined as the first order differentiation as in equation A.6 with respect to each variable.

$$\frac{\partial SR}{\partial v_i} = \frac{\partial\left(\frac{I_{sc,s}(1-\alpha(T_{m,s}-T_{ref}))}{I_{sc,c}(1-\alpha(T_{m,c}-T_{ref}))} \times \frac{I_{sc,cc}(1-\alpha(T_{m,cc}-T_{ref}))}{I_{sc,sc}(1-\alpha(T_{m,sc}-T_{ref}))}\right)}{\partial v_i} \tag{A.6}$$

In equation A.6, v_i represents the different variables assessing towards error. The detailed partial differentiation of SR equation with respect to each error contributing variables has been presented next.

Sensitivity coefficient of soiled module I_{sc} at experimental condition:

$$\frac{\partial SR}{\partial I_{sc,s}} = \frac{\partial\left(\frac{I_{sc,s}(1-\alpha(T_{m,s}-T_{ref}))}{I_{sc,c}(1-\alpha(T_{m,c}-T_{ref}))} \times \frac{I_{sc,cc}(1-\alpha(T_{m,cc}-T_{ref}))}{I_{sc,sc}(1-\alpha(T_{m,sc}-T_{ref}))}\right)}{\partial I_{sc,s}} \tag{A.7}$$

$$c_{Isc,s} = \frac{(I_{sc,cc}(\alpha(T_{m,cc} - T_{ref}) - 1)(\alpha(T_{m,s} - T_{ref}) - 1))}{(I_{sc,c}I_{sc,sc}(\alpha(T_{m,c} - T_{ref}) - 1)(\alpha(T_{m,sc} - T_{ref}) - 1))} \tag{A.8}$$

Sensitivity coefficient of cleaned module I_{sc} at experimental condition:

$$\frac{\partial SR}{\partial I_{sc,c}} = \frac{\partial\left(\frac{I_{sc,s}(1-\alpha(T_{m,s}-T_{ref}))}{I_{sc,c}(1-\alpha(T_{m,c}-T_{ref}))} \times \frac{I_{sc,cc}(1-\alpha(T_{m,cc}-T_{ref}))}{I_{sc,sc}(1-\alpha(T_{m,sc}-T_{ref}))}\right)}{\partial I_{sc,c}} \tag{A.9}$$

$$c_{Isc,c} = \frac{-(I_{scs}I_{sc,cc}(\alpha(T_{m,cc} - T_{ref}) - 1)(\alpha(T_{m,s} - T_{ref}) - 1))}{(I_{sc,c}^2 I_{sc,sc}(\alpha(T_{m,c} - T_{ref}) - 1)(\alpha(T_{m,sc} - T_{ref}) - 1))} \tag{A.10}$$

Sensitivity coefficient of soiled module I_{sc} at calibration level:

$$\frac{\partial SR}{\partial I_{sc,sc}} = \frac{\partial\left(\frac{I_{sc,s}(-\alpha(T_{m,s}-T_{ref}))}{I_{sc,c}(1-\alpha(T_{m,c}-T_{ref}))} \times \frac{I_{sc,cc}(1-\alpha(T_{m,cc}-T_{ref}))}{I_{sc,sc}(1-\alpha(T_{m,sc}-T_{ref}))}\right)}{\partial I_{sc,sc}} \tag{A.11}$$

$$c_{Isc,sc} = \frac{(-I_{sc,s}I_{sc,cc}(\alpha(T_{m,cc} - T_{ref}) - 1)(\alpha(T_{m,s} - T_{ref}) - 1))}{(I_{sc,c}I_{sc,sc}^2(\alpha(T_{m,c} - T_{ref}) - 1)(\alpha(T_{m,sc} - T_{ref}) - 1))} \tag{A.12}$$

Sensitivity coefficient of cleaned module I$_{sc}$ at calibration level:

$$\frac{\partial SR}{\partial I_{sc,cc}} = \frac{\partial\left(\frac{I_{sc,s}(1-\alpha(T_{m,s}-T_{ref}))}{I_{sc,c}(1-\alpha(T_{m,c}-T_{ref}))} \times \frac{I_{sc,cc}(1-\alpha(T_{m,cc}-T_{ref}))}{I_{sc,sc}(1-\alpha(T_{m,sc}-T_{ref}))}\right)}{\partial I_{sc,cc}} \tag{A.13}$$

$$c_{Isc,cc} = \frac{(I_{scs}(\alpha(T_{m,cc}-T_{ref})-1)(\alpha(T_{m,s}-T_{ref})-1))}{(I_{sc,c}I_{sc,sc}(\alpha(T_{m,c}-T_{ref})-1)(\alpha(T_{m,sc}-T_{ref})-1))} \tag{A.14}$$

Sensitivity coefficient of soiled module temperature at experimental condition:

$$\frac{\partial SR}{\partial T_{m,s}} = \frac{\partial\left(\frac{I_{sc,s}(1-\alpha(T_{m,s}-T_{ref}))}{I_{sc,c}(1-\alpha(T_{m,c}-T_{ref}))} \times \frac{I_{sc,cc}(1-\alpha(T_{m,cc}-T_{ref}))}{I_{sc,sc}(1-\alpha(T_{m,sc}-T_{ref}))}\right)}{\partial T_{m,s}} \tag{A.15}$$

$$c_{Tm,s} = \frac{(I_{sc,s}I_{sc,cc}((\alpha)\alpha(T_{m,cc}-T_{ref})-1))}{(I_{sc,c}I_{sc,sc}(\alpha(T_{m,c}-T_{ref})-1)(\alpha(T_{m,sc}-T_{ref})-1))} \tag{A.16}$$

Sensitivity coefficient for cleaned module temperature at experimental condition:

$$\frac{\partial SR}{\partial T_{m,c}} = \frac{\partial\left(\frac{I_{sc,s}(1-\alpha(T_{m,s}-T_{ref}))}{I_{sc,c}(1-\alpha(T_{m,c}-T_{ref}))} \times \frac{I_{sc,cc}(1-\alpha(T_{m,cc}-T_{ref}))}{I_{sc,sc}(1-\alpha(T_{m,sc}-T_{ref}))}\right)}{\partial T_{m,c}} \tag{A.17}$$

$$c_{Tm,c} = \frac{(-I_{sc,s}I_{sc,cc}((\alpha)\alpha(T_{m,cc}-T_{ref})-1)(\alpha(T_{m,s}-T_{ref})-1)}{(I_{sc,c}I_{sc,sc}(\alpha(T_{m,c}-T_{ref})-1)^2(\alpha(T_{m,sc}-T_{ref})-1))} \tag{A.18}$$

Sensitivity coefficient for soiled module temperature at calibration level:

$$\frac{\partial SR}{\partial T_{m,sc}} = \frac{\partial\left(\frac{I_{sc,s}(1-\alpha(T_{m,s}-T_{ref}))}{I_{sc,c}(1-\alpha(T_{m,c}-T_{ref}))} \times \frac{I_{sc,cc}(1-\alpha(T_{m,cc}-T_{ref}))}{I_{sc,sc}(1-\alpha(T_{m,sc}-T_{ref}))}\right)}{\partial T_{m,sc}} \tag{A.19}$$

$$c_{Tm,cs} = \frac{-(I_{scs}I_{sc,cc}(\alpha)(\alpha(T_{m,cc}-T_{ref})))(\alpha(T_{m,s}-T_{ref})-1)}{(I_{sc,c}I_{sc,sc}(\alpha(T_{m,c}-T_{ref})-1)(\alpha(T_{m,sc}-T_{ref})-1)^2)} \tag{A.20}$$

Sensitivity coefficient for cleaned module temperature at calibration level:

$$\frac{\partial SR}{\partial T_{m,cc}} = \frac{\partial\left(\frac{I_{sc,s}(1-\alpha(T_{m,s}-T_{ref}))}{I_{sc,c}(1-\alpha(T_{m,c}-T_{ref}))} \times \frac{I_{sc,cc}(1-\alpha(T_{m,cc}-T_{ref}))}{I_{sc,sc}(1-\alpha(T_{m,sc}-T_{ref}))}\right)}{\partial T_{m,cc}} \tag{A.21}$$

$$c_{Tm,cc} = \frac{(I_{scs}I_{sc,cc}(\alpha)(\alpha(T_{m,s}-T_{ref})-1)}{(I_{sc,c}I_{sc,sc}(\alpha(T_{m,c}-T_{ref})-1)(\alpha(T_{m,sc}-T_{ref})-1))} \tag{A.22}$$

Sensitivity coefficient for the temperature coefficient:

$$\frac{\partial SR}{\partial \alpha} = \frac{\partial\left(\frac{I_{sc,s}(1-\alpha(T_{m,s}-T_{ref}))}{I_{sc,c}(1-\alpha(T_{m,c}-T_{ref}))} \times \frac{I_{sc,cc}(1-\alpha(T_{m,cc}-T_{ref}))}{I_{sc,sc}(1-\alpha(T_{m,sc}-T_{ref}))}\right)}{\partial \alpha} \tag{A.23}$$

$$c_{\alpha} = \frac{(I_{scs}I_{sc,cc}((T_{m,cc}-T_{ref}))(\alpha(T_{m,s}-T_{ref})-1))}{(I_{sc,c}I_{sc,sc}(\alpha(T_{m,c}-T_{ref})-1)(\alpha(T_{m,sc}-T_{ref})-1))} +$$
$$\frac{(I_{sc,s}I_{sc,cc}(T_{m,s}-T_{ref}(\alpha(T_{m,sc}-T_{ref})-1)}{(I_{sc,c}I_{sc,sc}(\alpha(T_{m,c}-T_{ref})-1)(\alpha(T_{m,sc}-T_{ref})-1))} -$$
$$\frac{(I_{sc,s}I_{sc,cc}(T_{m,c}-T_{ref}(\alpha(T_{m,cc}-T_{ref})-1)(\alpha(T_{m,s}-T_{ref})-1)}{(I_{sc,c}I_{sc,sc}(\alpha(T_{m,c}-T_{ref})-1)^2(\alpha(T_{m,sc}-T_{ref})-1))} -$$
$$\frac{(I_{sc,s}I_{sc,cc}(T_{m,sc}-T_{ref}(\alpha(T_{m,cc}-T_{ref})-1)(\alpha(T_{m,s}-T_{ref})-1)}{(I_{sc,c}I_{sc,sc}(\alpha(T_{m,c}-T_{ref})-1)(\alpha(T_{m,sc}-T_{ref})-1)^2)} \tag{A.24}$$

A.2.5. Standard uncertainty calculation for different variables

Standard uncertainty of measured I_{sc}

The standard uncertainty in short circuit current measurement is $\pm$(0.2% of the instantaneous short circuit current and 0.06% of the measurement scale) at 95% confidence interval [67]. This assumption takes both types (A and B) of uncertainties into account as defined in ISO GUM. The absolute measurement of the current is given by the first term is type A (statistical) uncertainty and measurement repeatability is type B (non-statistical) uncertainty. Here, an additional 0.1% uncertainty contribution in the measured I_{sc} was considered due to the offset experienced at the V_{oc} condition. The 2% offset of open circuit voltage have been experienced during the true I_{sc} condition(V_{oc}=0)[67].

For a measured short-circuit current of 6 A from a soiled module, the measurement scale is 15.87 A (the measurement scale of datalogger is 1000 mV [80] and the resistance in the short circuit cable was found to be 63 mΩ). The above consideration can be shown by the following calculation.

$$a_{Isc,s} = (0.002 \times 6 + 0.0006 \times 15.87 + 0.001 \times 6) = 0.0278A. \tag{A.25}$$

where a is defined as semi-range of the limits between the quantity under investigation lies. Again, assuming the short-circuit current to be rectangular probability distribution with an infinite number of degrees of freedom at 95% confidence interval results into coverage factor, $k = \sqrt{3}$ [66].

Figure A.1: Representation of a typical rectangular probability distribution.

Therefore, the standard uncertainty for instantaneous short circuit current measurement of a soiled module is found to be

$$u_{Isc} = a_{Isc,s}/\sqrt{3} = \pm 0.016A. \tag{A.26}$$

Similarly, an instantaneous standard uncertainty of measured current of a clean module was also calculated with similar assumptions. The standard uncertainty associated with modules at their calibration level was found considering $\pm$(0.1% of the instantaneous short circuit current and 0.03% of the measurement scale) at 95% confidence interval[67].

A.2.6. Standard uncertainty of measured module temperature (T_m)

An instantaneous T_m of soiled and cleaned module were measured by two different temperature measuring sensor (Negative temperature coefficient (NTC), 10kΩ), which was applied at the back side of the module. The temperature sensors were applied to the same cell in both modules to avoid discrepancies if in case of hotspot formation. The NTC temperature sensor was assumed to have same uncertainty as Pt100 RTD, which was $\pm$0.3 Ω at 0°C and $\pm$0.8 Ω at 100°C [81]. A linear interpolation was done for each measured temperature to account the exactly associated uncertainty in the measurement. The linear equation can be expressed as,

$$y = \frac{30 + 0.5 \times x}{100} \tag{A.27}$$

where x is the measured instantaneous temperature and y is the calculated uncertainty of RTD. An additional uncertainty of 0.1% of a full scale (150°C) associated with electronics configuration of RTD measurement has been also assumed [81]. It is well known that the actual front cell temperature cannot exactly be approximated by measuring back cell temperature. So, an additional 2°C uncertainty

was considered based on the previous work [70]. The above considerations can be well represented by the following equation with an example at 50°C of module temperature,

$$a_{Tm,s} = y + 0.001 \times 150 + 2 = 2.7^o C \tag{A.28}$$

In the above equation, $a_{Tm,s}$ again represents a semi-range of the limits between which the temperature lies. Again, assuming the measured temperature to be rectangular probability distribution with an infinite number of degrees of freedom at 95% confi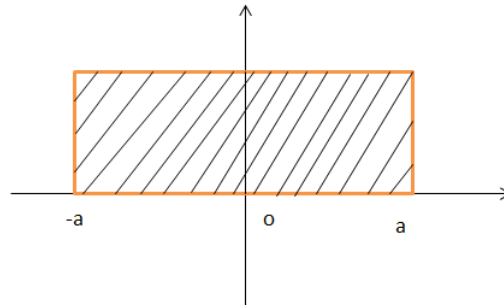dence interval results into coverage factor, $k = \sqrt{3}$. Therefore, the standard uncertainty for instantaneous temperature measurement of a soiled module was found to be

$$u_{Tm,s} = a_{Tm,s}/\sqrt{3} = \pm 1.558^o C. \tag{A.29}$$

The standard uncertainty of clean module and modules under calibration were also estimated with the same criteria.

A.2.7. Standard uncertainty in temperature coefficient due to T_m

The assumption of uncertainty in α due to increasing or decreasing module temperature was done based on the previous work done by [67]. The uncertainty in α measurement can be 0.016%/°C [82]. Considering this value with the reference module taken for experiment having a temperature coefficient of 0.053%/°C. The expanded uncertainty results to $\pm$ 30.2%. A work done as a part of PEP 1987 reference cell and module at six different international laboratories found an uncertainty of around $\pm$42% [83]. Based on these findings, 50% of the uncertainty associated with the temperature coefficient was taken conservatively resulting into uncertainty of $\pm$0.0265%/°C. Again, assuming the temperature coefficient to be rectangular probability distribution with infinite number of degrees of freedom at 95% confidence interval results into coverage factor, $k = \sqrt{3}$.

A.2.8. Combined standard uncertainty

Now, the sensitivity coefficients of different variables were multiplied with the standard uncertainty with the help of equation A.30 to find the combined standard uncertainty (u_{SR}). It can be defined by the root-sum-squares method.

$$
\begin{aligned}
[u_{SR}]^2 = & [u_{Isc,s} \cdot c_{Isc,s}]^2 + [u_{Tm,s} \cdot c_{Tm,s}]^2 + [u_\alpha \cdot c_\alpha]^2 + [u_{Isc,c} \cdot c_{Isc,c}]^2 + \\
& [u_{Tm,c} \cdot c_{Tm,c}]^2 + [u_\alpha \cdot c_\alpha]^2 + [u_{Isc,sc} \cdot c_{Isc,sc}]^2 + [u_{Tm,sc} \cdot c_{Tm,sc}]^2 + \\
& [u_{Isc,cc} \cdot c_{Isc,cc}]^2 + [u_{Tm,cc} \cdot c_{Tm,cc}]^2
\end{aligned}
\tag{A.30}
$$

The combined standard uncertainty is then multiplied by a coverage factor, k=1.96 assuming the combined DoF is infinite at 95% confidence interval and it is related to the expanded uncertainty as explained above.

A.2.9. Results and discussion

The results showed that the expanded uncertainty in soiling ratio (SR) measurement varied between 0.649% to 0.926% at an irradiance level of >400W/m^2. Figure 2.8 was plotted to represent the expanded uncertainty during the course of the day at different insolation level. It can be clearly seen that the expanded uncertainty was minimum value during the noon (1089.4 W/m^2) and drastically scaled up for low irradiance. The irradiance represented by cyan curve was measured with the help of CMP 21 pyranometer by Kipp and Zonen installed on a plane of array (POA). The expanded uncertainty in SR measurement has been represented by a green curve. The blue and red color curve represented uncertainty contribution by measured short circuit current at experimental and calibration level respectively. Finally, error contribution by module temperature and temperature coefficient are represented by yellow and purple curve respectively.

It is also important to know the relative contribution of each variable towards the expanded uncertainty of SR measurement. The relative uncertainty was calculated with the help of equation A.31 [84].

$$U_{rel,i} = U_{SR} \frac{u_i \times c_i}{\sum_i^N u_i \times c_i} \tag{A.31}$$

Using equation A.31, a bar chart has been plotted for a clear representation of the uncertainty contribution from each variable as represented in Figure A.2. The major uncertainty was due to I_{sc} at experimental followed by the calibration levels. The least contribution was from the α of the module.
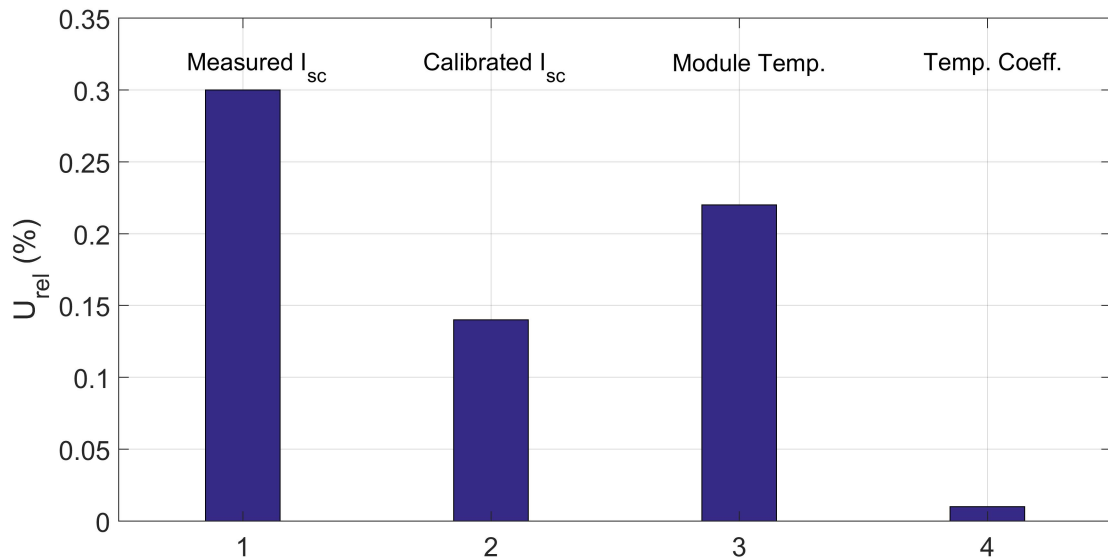

Figure A.2: Relative contribution of each variable towards calculated expanded uncertainty in SR at a time, t=107 mins.

A.2.10. Effect of angular misalignment

Angular misalignment between two PV modules (clean and dirty) under observation becomes very significant if the misalignment is >0.5°. A module's altitude and azimuth discrepancy could result in the bias of SR measurement during the course of the day. If a module is more tilted than other than one might get a larger amount of direct normal irradiance (DNI), which could significantly affect the SR calculation. The effect becomes more prominent for a soiled module as different altitude and azimuth might result in larger/smaller scattering of incident rays. Considering the work of Gostein et al. in Phoenix, Arizona, the effect of <0.5°angular misalignment resulted <0.25% reduced uncertainty in 2 hours[67]. Thus, if we consider the angular misalignment uncertainty then the total expanded uncertainty was found almost to be $\pm$ 1%.

A.2.11. Inference

It has been found that the soiling ratio (SR) can be measured with an accuracy of $< \pm$ 1% during mid of the day. The uncertainty measurement should be done at the middle of the day at constant irradiation to avoid large uncertainties. It was seen in Figure 2.8, the irradiance below 400 W/m^2 associated with high expanded uncertainty. The measured I_{sc} was found to have larger contribution towards the expanded uncertainty. The angular misalignment also contributes towards increasing the uncertainty in measurement. For larger PV parks, spatial variability for different measurement stations could result in different SR and uncertainties [67].

B

Appendix-B

B.1. Soiling ratio (SR) calculation

B.1.1. Medium irradiance

SR (SR^{Isc}) on 23rd 2017 at the rooftop PV setup of Kipp & Zonen BV, Delft, The Netherlands as mentioned in section 2.2.3.
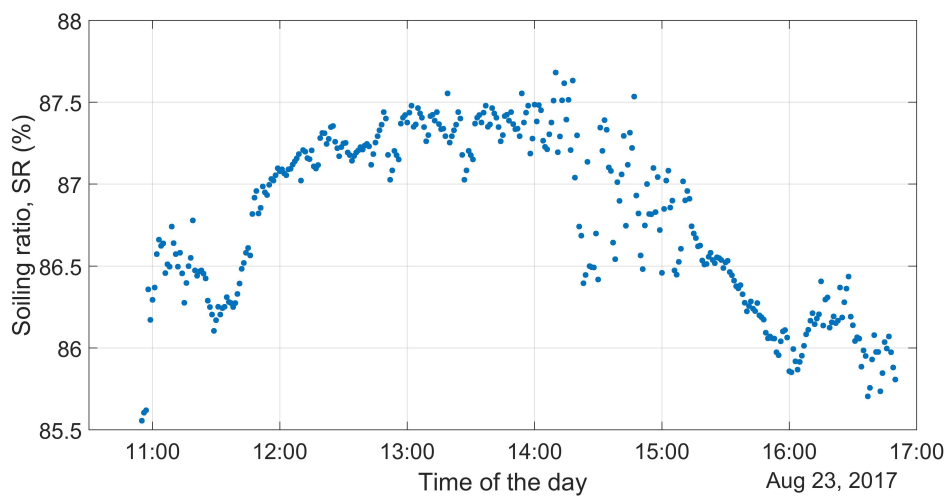
B.1.2. Low irradiance

SR (SR^{Isc}) on 24th 2017 at the rooftop PV setup of Kipp & Zonen BV, Delft, The Netherlands as mentioned in section 2.2.3.
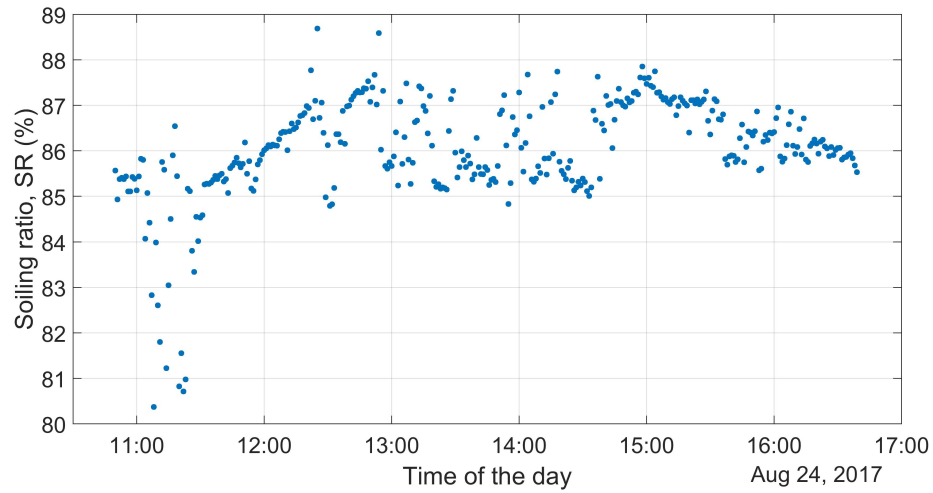
B.2. Incidence angle modifier (IAM)

B.2.1. Medium irradiance

IAM at clean and soiled condition for 23rd August 2017 as mentioned in section 4.1.
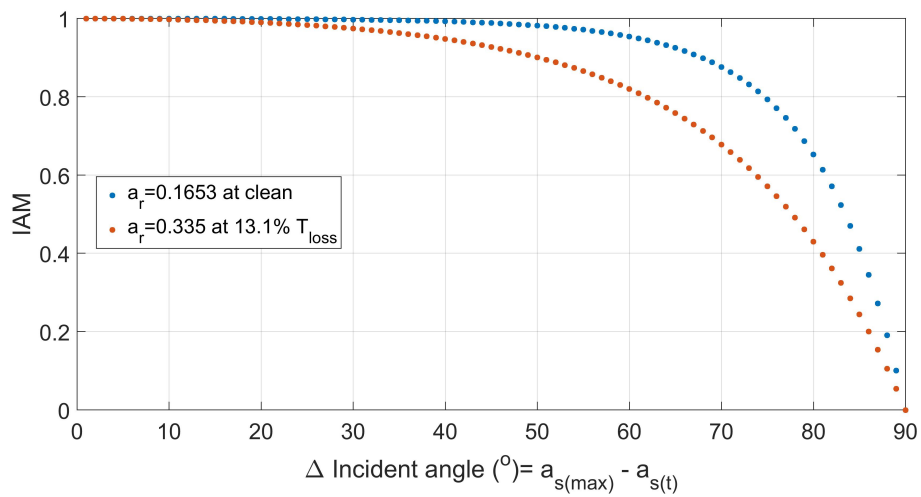
B.2.2. Low irradiance

IAM at clean and soiled condition for 24th August 2017 as mentioned in section 4.1.
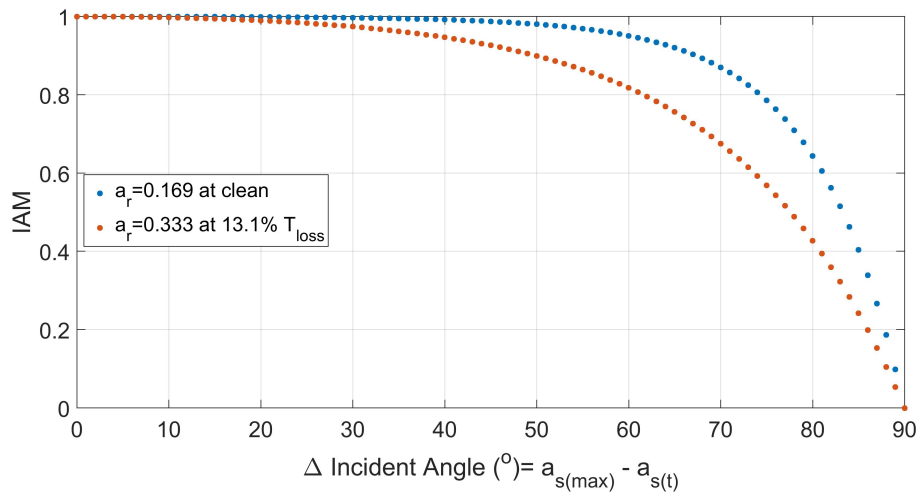
B.3. Modeled and filtered SR

B.3.1. Medium irradiance

Modeled soiling ratio (SR^{model}) vs filtered SR ($SR^{f,Isc}$) for 23th August 2017 as mentioned in section 4.4.
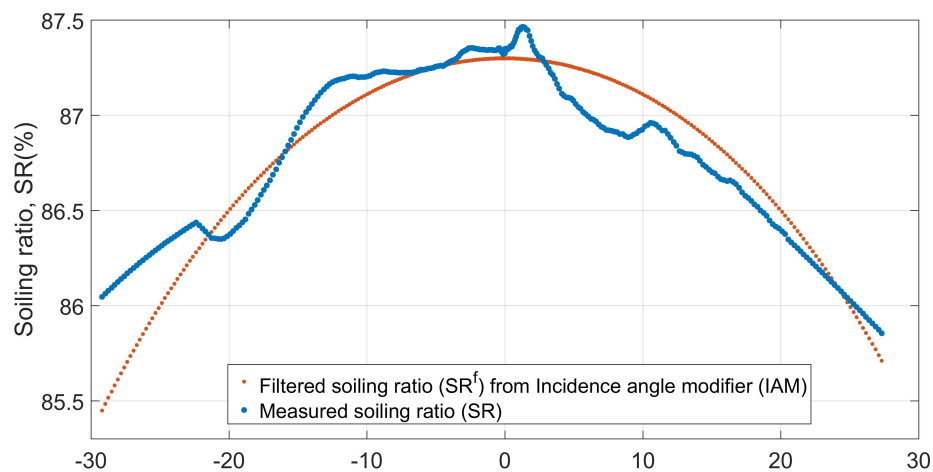
B.3.2. Low irradiance

Modeled soiling ratio (SR^{model}) vs filtered SR ($SR^{f,Isc}$) for 24th August 2017 as mentioned in section 4.4.
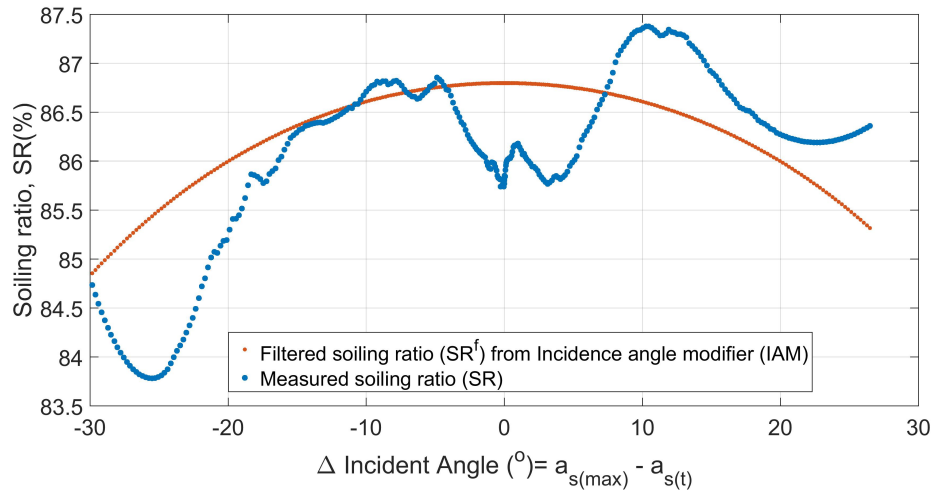
C

Appendix-C

C.1. Sun position

The position of the Sun was first expressed as the time D elapsed since Greenwich noon, terrestrial time on 1 January 2000 in a number of days. D was then related to the Julian Date JD, the number of days since 1 January 4713 BC in a proleptic Julian Calendar using equation C.1.

$$D = JD - 2451545.0 \tag{C.1}$$

The mean longitude and the mean anomaly of the Sun can be calculated by correcting for the aberration of the light and the elliptic orbit of the Earth as shown in equation C.2 and C.3

$$q = 280.459° + 0.98564736°D \tag{C.2}$$

$$g = 357.529° + 0.98560028°D \tag{C.3}$$

The values obtained for q and g were normalized from 0-360°to estimate the ecliptic longitude of the Sun by equation C.4

$$\lambda_S = q + 1.915°sing + 0.020°sin2g \tag{C.4}$$

It is necessary to convert from ecliptic to horizon coordinates as well as the angle ε with which the fundamental plane of these coordinates is tilted to the ecliptic is given by equation C.5

$$\varepsilon = 23.429° - 0.00000036°D \tag{C.5}$$

Now, the local mean sidereal time, θ_L, which is defined as the angle between the vernal equinox and the meridian was found by determining the Greenwich mean sidereal time (GMST).

$$GMST = 18.697374558h + 24.06570982441908h \times D + 0.000026h \times T^2 \tag{C.6}$$

Here, T is the number of centuries since Greenwich noon, Terrestrial time, on 1 January 2000 expressed as

$$T = \frac{D}{36525} \tag{C.7}$$

The unit of GMST is hours, which needs to be normalized to 0-24 h. Now the local mean sidereal time in degrees can be estimated as,

$$\theta_L = GMST\frac{15°}{\lambda_o} \tag{C.8}$$

where λ_o is the observer's longitude. The final expression to determine the exact position of the Sun is given by equations C.9 and C.10,

$$tanA_s = \frac{-sin\theta_L \times cos\lambda_s + cos\theta_L \times cos\varepsilon \times sin\lambda_s}{-sin\phi_o \times cos\theta_L \times cos\lambda_s - (sin\phi_o \times sin\theta_L \times cos\varepsilon - cos\phi_o \times sin\varepsilon)sin\lambda_s} \tag{C.9}$$

$$sina_s = cos\phi_o \times cos\theta_L \times cos\lambda_s + (cos\phi_o \times sin\theta_L \times cos\varepsilon + sin\phi_o \times sin\varepsilon)sin\lambda_s \tag{C.10}$$

A_s and a_s are the azimuth and altitude of the Sun respectively. Now, hourly orientation and altitude of the Sun were calculated throughout the year by simulating the above equations in MATLAB software.

C.2. POA irradiance

Hourly POA irradiance incident on the module was calculated for an entire year (March 2017 - Feb 2018) with equation 5.5 and plotted in the Figure C.1.
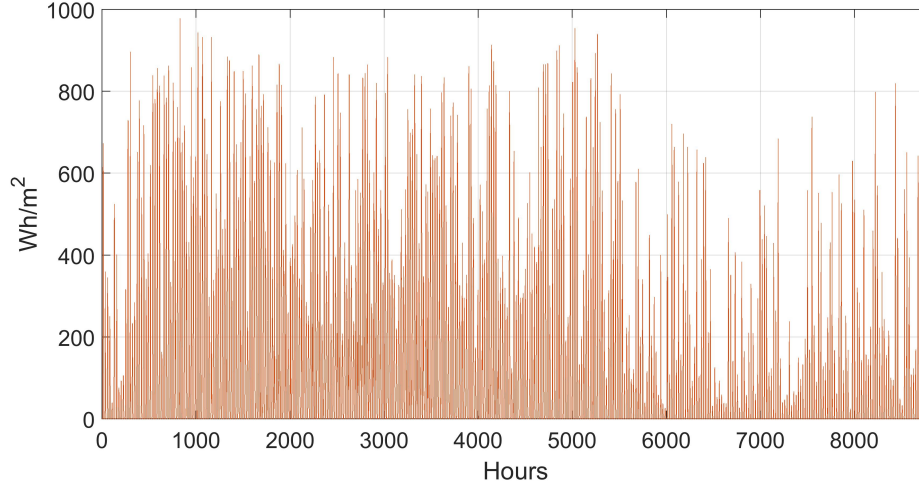
Figure C.1: Hourly POA irradiance on the module at a tilt angle of 30°in Delft, The Netherlands.

C.3. Fluid dynamic model

In this model, a module is considered to have a uniform temperature of T_M. This model was utilized to accurately estimate a module's working temperature as a function of meteorological parameters retrieved from Meteonorm software. This model estimates the temperature based on a detailed energy balance between a module and the environment conditions. The constants used for the calculation has been mentioned in the table C.1:

Table C.1: Constants used in Fluid dynamic model.

Constants	
Module reflectivity (R)	0.1
Module efficiency (η)	16.5%
Back surface emmisivity (ε_{back})	0.89
Front surface emmisivity (ε_{front})	0.84
Density of air (ρ_{air})	1.249 Kg/m^3
Specific heat capacity of air (c_{air})	1005 J/Kg.K
Kinematic viscosity of air (v_{air})	$14.205{\times}10^{-6} m^2/s$
Prandtl number (Pr)	0.71
Heat conductivity of air (k)	0.025 W/m.K
Thermal expansion coefficient of air (β)	$3.55{\times}10^{-3} 1/K$
Acceleration due to gravity (g)	9.81 m/s^2
Stefan-Boltzmann constant (σ)	$5.67{\times}10^{-8} W/m^2K^4$

The NOCT of the module was taken from A.1 to calculate the Installed Nominal Operating Condition Temperature (INOCT) as given by equation C.11. The sky temperature (T_{sky}) was expressed in as a function of ambient temperature (T_a), humidity, cloud cover and cloud elevation. For a clear day, (T_{sky}) is given as in equation C.12.

$$T_{INOCT} = T_{NOCT} - 3°C \qquad (C.11)$$

$$T_{sky} = 0.0552 \times T_a^{3/2} \qquad (C.12)$$

The absorptivity (α) of a module is defined as the fraction of the incident radiation converted into thermal energy.

$$\alpha = (1 - R) \times (1 - \eta) \qquad (C.13)$$

The convective heat transfer is divided as a free and forced component. The latter one is again distinguished between laminar and turbulent flow. The heat transfer coefficient for both the flows was calculated by equation C.14 and C.15.

$$h_{forced}^{lam} = \frac{0.86 \times Re^{-0.5}}{Pr^{0.4}} \times \rho_{air} \times C_{air} \times w \tag{C.14}$$

$$h_{forced}^{tur} = \frac{0.028 \times Re^{-0.2}}{Pr^{0.4}} \times \rho_{air} \times c_{air} \times w \tag{C.15}$$

Re is the Reynolds number, which is the ratio of the inertial forces to viscous forces C.16, whereas Pr is the Prandtl number defined as the ratio between the momentum and the thermal diffusivity.

$$Re = \frac{w \times D_h}{v_{air}} \tag{C.16}$$

Here, w is the wind speed (m/s) at the height of the module and the hydraulic diameter (D_h) of the module is used as a relevant length scale as defined by C.17. L and W are the dimensions module.

$$D_h = \frac{2 \times L \times W}{L + W} \tag{C.17}$$

Finally, the forced convective heat transfer is given by,

$$h_{forced} = h_{forced}^{lam} + h_{forced}^{tur} \tag{C.18}$$

Next, the free heat transfer coefficient was determined by measuring the Nusselt's number, Nu. It is the ratio between convective and conductive heat transfer.

$$Nu = \frac{h_{free} \times D_h}{k} = 0.21(Gr \times Pr)^{0.32} \tag{C.19}$$

The ratio of buoyancy to viscous forces is given by a Grashof number (Gr) calculated with equation C.20.

$$Gr = \frac{g \times \beta \times (T_m - T_a) \times D_h^3}{v_{air}^2} \tag{C.20}$$

β is the volumetric thermal expansion coefficient of air and can be expressed as β = 1/T. The total mixed heat convective mass transfer coefficient using equation can finally be calculated by equation C.21.

$$h_{mixed} = h_c^T = \sqrt[3]{h_{forced}^3 + h_{free}^3} \tag{C.21}$$

The convective heat transfer on the rear will be lower compared to the top surface. The exact heat transfer at the rear side can be calculated by estimating the ratio of actual to the ideal heat loss from the back-side given by the equation C.22.

$$R = \frac{\alpha \times G_m - h_c^T \times (T_{INOCT} - T_a) - \varepsilon_{front} \times \sigma \times (T_{NOCT}^4 - T_{sky}^4)}{h_c^T \times (T_{INOCT} - T_a) + \varepsilon_{top} \times \sigma \times (T_{NOCT}^4 - T_{sky}^4)} \tag{C.22}$$

The convection at the back side of a module is therefore given by,

$$h_c^B = R \times h_c^T \tag{C.23}$$

Finally, the overall heat transfer coefficient can be written as,

$$h_c = h_c^T + h_c^B \tag{C.24}$$

The heat exchange coefficients of the sky and ground as function of the module's temperature are given by equation C.25 and C.26.

$$h_{r,sky} = \varepsilon_{top} \times \sigma \times (T_m^2 + T_{sky}^2) \times (T_m + T_{sky}) \tag{C.25}$$

$$h_{r,gr} = \varepsilon_{back} \times \sigma \times (T_m^2 + T_{sky}^2) \times (T_m + T_{gr}) \tag{C.26}$$

Rearranging these equations to represent in terms of module temperature (T_m).

$$T_m = \frac{(\alpha \times G_m) + (T_a \times h_c) + (h_{r,sky} \times T_{sky}) + (h_{r,gr} \times T_{gr})}{h_c + h_{r,sky} + h_{r,gr}} \tag{C.27}$$

$h_{r,sky}$ and $h_{r,gr}$ being also a function of T_m the above equation were be solved by iterations. An initial reference module temperature was given to estimate $h_{r,sky}$ and $h_{r,gr}$, which were updated till it varied by <0.1°C. This method was used to determine the hourly T_m for the period of one year (March 2017 - Feb 2018) using MATLAB software and plotted in Figure C.2.
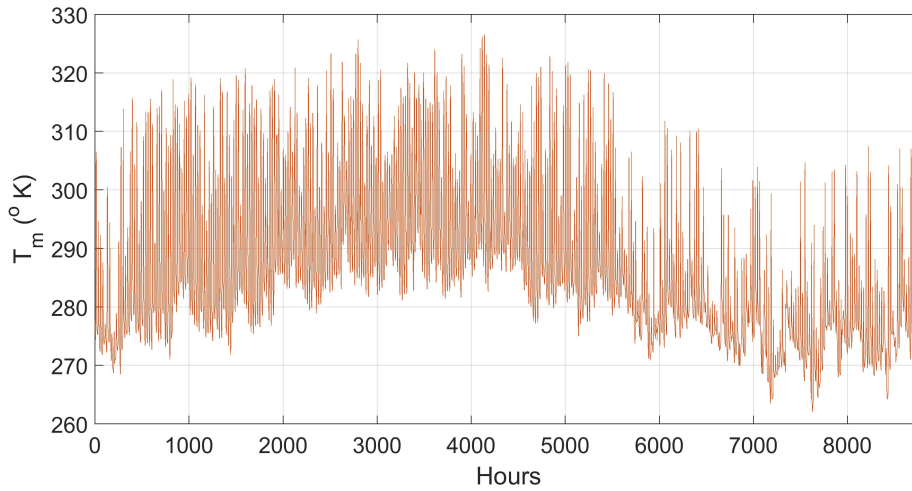
Figure C.2: PV module temperature (T_m) for every hour for an entire year.

C.4. Inverter efficiency

Inverter's performance was calculated by referring to the sandia national laboratories model (SNL), which compares efficiency at each input from the module. The output AC power from an inverter was given by equation C.28 [43].

$$P_{ac} = [\frac{P_{aco}}{A - B} - C(A - B)] \times (P_{dc} - B) - C(P_{dc} - B)^2 \tag{C.28}$$

The coefficients A, B and C are represented as,

$$A = P_{dco}[1 + C_1(V_{dc} - V_{dco})] \tag{C.29}$$

$$B = P_o[1 + C_2(V_{dc} - V_{dco})] \tag{C.30}$$

$$C = C_o[1 + C_3(V_{dc} - V_{dco})] \tag{C.31}$$

The values empirical coefficients C_1, C_2 and C_3 and other variable was taken from the System Advisory Model (SAM). SNL model considers of all the losses due to self-consumption, switching and ohmic losses to give less than 0.1% of output error between modeled and measures inverter efficiency [70]. The parameters used for both the inverters (Enphase215 and Enphase250) are defined in table C.2 following table [1],

---

[1]Retrieved from https://sam.nrel.gov/

Table C.2: Inverter parameters for efficiency calculation.

Parameter	Definition	Enplase215	Enphase250
V_{dc} (w)	DC input voltage	37.9	37.9
P_{aco} (W)	Max. AC power rating at nominal operating condition	215	250
P_{dco} (W)	DC power level at nominal operating condition	224.362	249.557
V_{dco} (V)	DC voltage level at nominal operating condition	28.94	37
P_{so} (W)	DC power required to start the inversion process	0.707	0.5966
C_o (1/W)	Parameter defining the curvature between AC output and DC input power	-6.24×10^{-5}	-5.26343×10^{-5}
C_1 (1/V)	Empirical coefficient allowing P_{dco} to vary linearly with DC input voltage	-0.000791	-0.000291388
C_2 (1/V)	Empirical coefficient allowing P_{dco} to vary linearly with DC input voltage	-0.0251161	-0.00932316
C_3 (1/V)	Empirical coefficient allowing P_{dco} to vary linearly with DC input voltage	-0.102907	-0.0552982

The inverter's efficiency is calculated as a ratio of AC output to the DC input given as,

$$\eta_{inv} = \frac{P_{ac}}{P_{dc}} \times 100\% \tag{C.32}$$

Using the above parameters and equation C.32, an hourly inverter's efficiency for Enphase215 has been plotted (March 2017 - Feb 2018) and presented in the Figure C.3.
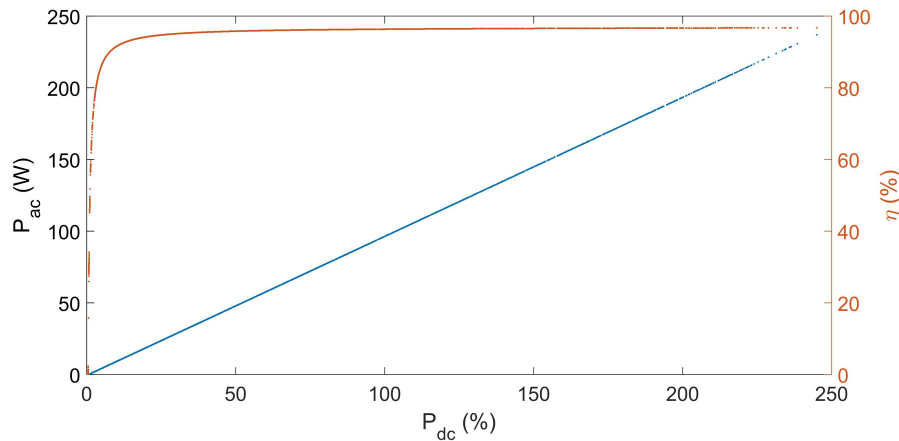

Figure C.3: AC power output and inverter efficiency for Enphase215.
.

The maximum inverter efficiency was 96.76%, while the average efficiency was 91.7%.

D

Appendix-D

D.1. List of Acronyms

PV	Photovoltaic	**OSM**	Optical Soiling Measurement
GW$_p$	Gigawatt Peak	**SCADA**	Supervisory Control and Data Acquisition
PPA	Power Purchase Agreement	**DDS**	Dust Detection System
PR	Performance Ratio	**EDS**	Electrodynamic Screen
MENA	Middle East and North Africa	**NTC**	Negative Temperature Coefficient
PM10	Particulate Matter $\leq 10\mu$m	**BSRN**	Baseline Surface Radiation Network
PM2.5	Particulate Matter $\leq 2.5\mu$m	**ISO**	International Standards Organization
BOS	Balance of Systems	**LT**	Linear Technology
LCOE	Levelized Cost of Electricity	**MPP**	Maximum Power Point
kWh	Kilowatt Hour	**K$_B$**	Boltzmann's Constant
RH	Relative Humidity	**FF**	Fill Factor
NASA	National Aeronautics and Space Administration	**ATD**	Arizona Test Dust
XRD	X-Ray Diffraction Analysis	**EVA**	Ethylene-vinyl Acetate
nN	Nanonewton	**UV**	Ultraviolet
AOI	Angle of Incidence	**LED**	Light Emitting Diode
a-Si	Amorphous Silicon	**RMSD**	Root Mean Square Deviation
CdTe	Cadmium Telluride	**IAM**	Incidence Angle Modifier
CIGS	Copper Indium Gallium Selenide	**SZA**	Solar Zenith Angle
DNI	Direct Normal Irradiance	**KNMI**	Royal Netherlands Meteorological Institute
GHI	Global Horizontal Irradiance	**SAM**	System Advisory Model
DHI	Diffused Horizontal Irradiance	**FIT**	Feed-in-Tariff
TL	Transmission loss	**GUM**	Guide to the Expression of Uncertainty in Measurement
AL	Angular loss	**SPICE**	Simulation Program with Integrated Circuit Emphasis
SR	Soiling Ratio		
RF$_p$	Rain-free period		
POA	Plane of Array		
IEC	International Electrotechnical Commission		
STC	Standard test Condition		
NOCT	Nominal Operating Cell Temperature		
IR	Infrared		

Accurate Soiling Ratio Determination with Incidence Angle Modifier for PV Modules

Pramod Nepal, Marc Korevaar, Hesan Ziar, Olindo Isabella, and Miro Zeman

Abstract— **The deposition of dust, soil, and microfibers resulting from the surroundings as well as the growth of minute pollens like moss and fungi contributes toward photovoltaic (PV) module soiling. Soiling is a lesser acknowledged factor that significantly reduces the power production by acting as a barrier for effective light absorption by the module. The estimated loss in the irradiance and power can be determined with the help of soiling ratio (SR) parameter which is the ratio of short-circuit current (I_{sc}) or maximum power produced (P_{max}) by a soiled panel to the clean one. The measured SR is normally not constant throughout a day but changed with the position of the Sun and amount of dust on the module. This paper proposes an empirical equation to determine SR at any time instant of the day based on instantaneous Sun's angle of incidence (AOI) on the module and a single SR value measured at the mid of the day. First, the SR of an artificially soiled panel was measured over the course of the day for three conditions of high, medium, and low daily average irradiance. Then, an empirical equation is introduced based on incident angle modifier (IAM) for soiled and cleaned PV modules. The proposed equation was further used to determine SR. Finally, the average residuals between the measured and the modeled soiling ratios were determined with the help of root mean square deviation (RMSD). The results showed that the modeled SR was determined with a deviation of ±0.21% and ±0.28% respectively for a high and medium irradiance day, whereas the deviation increased to 1.04% in case of a cloudy condition.**

Index Terms— **Photovoltaic (PV) module, soiling ratio (SR), incidence angle modifier (IAM), angle of incidence (AOI), angular loss (AL), transmission loss (TL), root mean square deviation (RMSD).**

I. INTRODUCTION

Solar energy in the form of photons can be converted to electricity with the help of semiconductor materials using Photovoltaic (PV) technology [1]. In the recent past, the technological advancement in this field has provided PV technology as one of the leading renewable energy source currently available. The annual growth of PV installations was reported to be 40% from 2010 to 2016 [2]. This means the global cumulative installed PV was at least 303.1 GW$_p$ which accounted for annual electricity production of 375 TWh during the year 2016 [3]. Despite this outstanding growth, the performance ratio (PR) of PV systems has been greatly compromised due to various environmental factors like

P. Nepal is an M.Sc. student studying Sustainable Energy Technology (SET) at Delft University of Technology, 2628CD Delft, The Netherlands (e-mail: nepalpramod91@gmail.com).

M. Korevaar is with the Kipp & Zonen, Delftechpark 36, 2628 XH, Delft, The Netherlands (email: marc.korevaar@kippzonen.com).

H. Ziar, O. Isabella, and M. Zeman are with the Photovoltaic Materials and Devices Group, Delft University of Technology, 2628CD Delft, The

Netherlands (e-mail: h.ziar@tudelft.nl; o.isabella@tudelft.nl; m.zeman@tudelft.nl).

non-uniform irradiance, wind, rain, module temperature, and soiling. The accumulation of dust, sand, and biological deposits like the growth of algae, moss or bird droppings, and air pollution are categorized as PV module soiling [4]. It directly obstructs the irradiation falling on the module by forming a thin layer of dust usually lesser than 10 μm which depends on the environmental conditions including wind intensity, a probability of volcanic eruptions or vehicular movement [5]. The module soiling is considered to be the third major environmental factor after irradiation and temperature which directly accounts for lower performance statistics of a PV system [6]. The irradiance and module temperature are well understood but for soiling, there is still limited understanding and only basic measurements are carried out.

The soiling of PV modules majorly depends on two factors: (i) Location of the PV plant (ii) Local environmental conditions like relative humidity (RH), wind, and rainfall [7]. Therefore, dust accumulation is a result of the rate of deposition and rate of removal by the wind and rain event [8]. Six major types of dust to have significant influence are identified as ash, calcium, limestone, soil, sand, and silica [5]. Thus based on the location and dust types the soiling losses might vary. The average daily energy loss due to soiling was found to be around 4.5% in Malaga, Spain whereas, during long dry periods, the daily energy loss was much higher than 20% [9]. In another experiment carried out on a module tilted at an optimum angle of 35° resulted in an annual power loss of 3-4% in northern part of Belgium [10]. Similarly, an average soiling loss in rural and suburban locations of USA was measured to be 0.1%/day but for desert regions, the losses were as high as 0.3%/day [11]. Several experiments suggested that the average soiling loss in the Middle East regions were more severe compared to other parts of the world [5]. In Egypt, an experiment was performed on 100 different glass samples installed at different tilt angles and azimuth orientations for 8 months, the cell at an angle of 45° facing south resulted in a reduction of output power by 17.4% per month [12]. Rainfall event acts as a natural cleaning for the soiled modules. Around 5 mm of rainfall was noticed to completely clean the panel in Arizona region [13]. However, for a location like Northern California rainfall of 5 mm was not sufficient, therefore more than 20 mm of rain event was required to fully clean the system in order to regain its normal efficiency [11].

A PV module is subjected to two types of the angle of incidence (AOI) influences, namely mechanical and optical [14]. The mechanical response is associated with its tilt and

orientation and the light source [14]. Based on the angle of incidence, solar radiation is derated by a cosine angle between zenith and Sun's altitude and azimuth commonly known as "cosine effect" [15]. On the other hand, the optical effect is due to the surface properties of the module. For a module with surface coatings; anti-reflective coating (ARC) was found to be more resilient towards the effect of AOI than without [14]. Higher AOI increases reflectance losses and thus reducing the amount of solar beam that can be utilized by the panel. As discussed, the optical response of PV module is a surface characteristic, therefore solar irradiance is highly influenced due to the presence of the soiling. In this paper, a module was subjected to various soiling condition from low to high amount to estimate the dimensionless parameter called angular loss coefficient (a_r) and then angular losses (AL) as defined by Martin and Ruiz [16]. Then, the soiling ratio curves were constructed with the help of calculated angular losses (AL) and a single SR measurement done at solar noon for three different scenarios of high, medium, low irradiances condition. Finally, the measured soiling ratio (SR) curve was compared with modeled soiling ratio (SR^{model}) by calculating the root mean square deviation (RMSD).

II. METHODOLOGY

A. Measurement setup

The experiment was carried out at the rooftop PV setup for the height of around 16 meters from the ground at Kipp & Zonen BV, Delft, The Netherlands. Two polycrystalline modules have been chosen, CS6K-270P produced by Canadian solar installed at a tilt angle of 30° facing south with an identical mounting mechanism to avoid the angular misalignment. One of the modules was uniformly soiled while the other one was kept clean to make a comparison. An instantaneous short circuit current (I_{sc}) from both the modules was recorded by measuring its voltage drop (V_{drop}) over a 10-meter long TUV solar cable with a resistance (R_{cable}) of 63mΩ ± 0.126mΩ (1 reading ± 0.2%) [17]. The minute average voltage drop from both modules was logged into a CR6 data logger from Campbell Scientific with an average sample time of 5 seconds. Panels short-circuiting were done with the help of low shunt resistor, which is schematically represented in Figure 1.
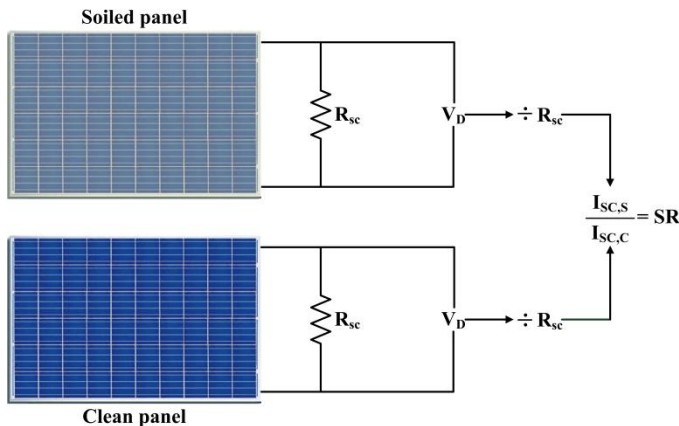

Fig. 1. Circuit diagram representing short-circuiting of clean and soiled panels. In Figure 1, R_{sc} is a low shunt resistor identical for both modules. The voltage drop (V_D) over the resistor was converted into the current by diving it with the value of the shunt resistor (63 mΩ) to calculate the soiling ratio (SR).

Instantaneous irradiance was recorded every minute with the help of CMP-21 pyranometer by Kipp & Zonen installed at the plane of array (POA). The minutely average temperature of soiled and cleaned modules was also measured using two temperature measuring sensors (negative temperature coefficient (NTC) Thermistor of 10kΩ) applied at the backside of each panel. A soiling mixture was prepared by dissolving the Grand Canyon test dust (Eisenoxid-Fe$_2$O$_3$, KSL-312) produced by KSL staubtechnik gmbh with deionized water in 1:10 ratio. To facilitate the homogeneous soiling process by reducing the wind effects, a wooden-aluminium chamber was also built which can be seen in Figure 2. The chamber was placed carefully on top of the PV module to be soiled. Finally, module soiling was carried out with the help of a paint gun at 1.5 bars of air pressure from a 1-meter distance (pointed vertically).
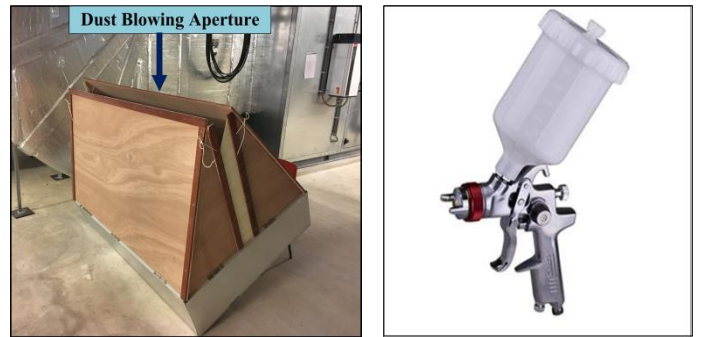

Fig. 2. A wooden-aluminium chamber (1660×1000×900 mm) (left) and the paint gun (600 cc) used for soiling (right). The chamber has a small opening at the top (pointed by an arrow on the left) that provides a space for the gun loaded with the soiling mixture in its container (shown above on right). A pipe at 1.5 bars was connected at the bottom of the gun to provide enough pressure during soiling process.

The experimental setup consisting of cleaned and artificially soiled panel has been presented in Figure 3.
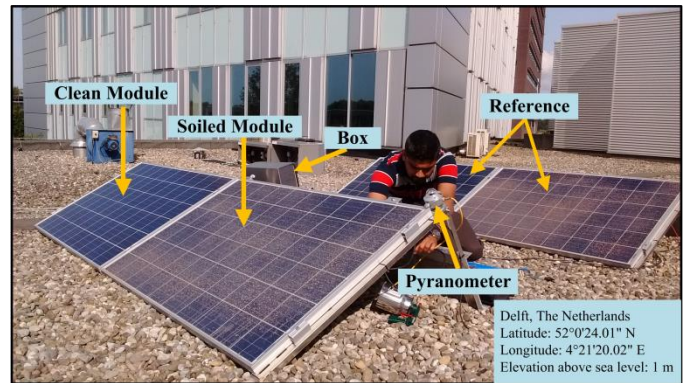

Fig. 3. Experimental setup for soiling ratio (SR) measurement represented by the first row of the modules, whereas the last row represents reference co-planer module to validate the measured data. The experiment was conducted in the month of August 2017 from 10:57 to 17:07. The voltage drop from the panels was recorded with the help of a data logger kept inside a metal box shown above.

B. Soiling ratio (SR) calculation

Soiling ratio (SR) is defined as the ratio of irradiance utilized by a soiled (G_2) to cleaned module (G_1) to produce corresponding short-circuit current ($I_{sc,s}$ and $I_{sc,c}$) or power [18]. Using the translation method explained in IEC-60891, the measured short-circuit currents ($I_{sc,s'}$ and $I_{sc,c'}$) were subjected to temperature correction to account for net irradiance loss only due to soiling (equation (1)). A temperature coefficient (0.053 %/^{o}C) mentioned in the datasheet of the module was considered for temperature correction [19]. Two co-planar modules were normalized with a help of calibration factors when both the modules were clean and at reference temperature (25°C) condition. The panels were subjected for calibration to account for manufacturing defects, differences in cable resistance or any other abnormal behavior that might lead to varying current and power production for an identical condition. The expanded SR equation with calibration values and the translation method for temperature correction can be written as [18] [20]

$$SR = \frac{G_2}{G_1} = \frac{I_{sc,s}}{I_{sc,c}} \tag{1}$$

$$= \frac{I_{sc,s'}(1-\alpha(T_{m,s}-T_{ref}))}{I_{sc,c'}(1-\alpha(T_{m,c}-T_{ref}))} \times \frac{C_c}{C_s} \times 100\%$$

$$T_{loss}(\%) = 1 - SR \tag{2}$$

In (1), $I_{sc,s}$ and $I_{sc,c}$ are temperature corrected short-circuit currents for soiled and cleaned module, respectively. Similarly, α is the temperature coefficient, while C_c and C_s are calibration constants for cleaned and soiled module respectively which were computed by comparing the short-circuit currents of both the modules. Similarly, $T_{m,s}$ and $T_{m,c}$ are the measured temperature of soiled and cleaned PV modules respectively, whereas T_{ref} is the temperature for the module when the ambient temperature is 25°C. T_{loss} in (2) is the transmission loss due to the presence of soiling. The following SR calculation was applied for three days characterized by their average irradiances throughout that day; high irradiance (758.18 W/m^2), medium irradiance (559.12 W/m^2), and low irradiance (275.87 W/m^2). However, it should be noted that soiling ratio could also be estimated by maximum power point method, which might give a slightly different result.

C. PV module angular losses

The angular losses (AL) for PV modules are generally calculated referencing a normal incidence of radiation at either cleaned or soiled condition [21]. The complement to the unity of angular losses (AL) is known as angular factor ($f_{I\alpha}$) [16]. Angular factor represents the relative optical response of a module at an angle of incidence (AOI). The experimental value of angular factor can be obtained as the ratio of cosine corrected short-circuit current at an angle θ (I_{sc} (θ)) to the short-circuit current at normal incidence (I_{sc} ($\theta=0^o$)) represented as [16]

$$f_{I\alpha} = \frac{I_{sc}(\theta)}{I_{sc}(0) \times cos\theta} \tag{3}$$

The optical response of any module with or without anti-reflective coatings can be determined with the help of an analytical equation presented in below [16]

$$AL(\theta) = 1 - \frac{1 - \exp(-cos\theta/a_r)}{1 - \exp(-1/a_r)} \tag{4}$$

$$IAM(\theta) = 1 - AL(\theta) \tag{5}$$

Where a_r is the empirical angular loss coefficient, which depends on PV module technology. For every AOI of the Sun (θ) and a fixed a_r, angular loss (AL) in a PV module is determined from equation (4) and (5). In [21], the analytical model (equation (5)) was found to accurately describe the angular losses of all analysed PV configurations with the high value of determination coefficients (R^2). Equation (5) represents incident angle modifier (IAM) which is the complement for angular losses (AL) with a maximum of 1 and minimum of 0. It signifies the degree of module performance for any angle of incidence (AOI) of light having a maximum value at lowest AOI (solar noon). For our calculations, the generated short-circuit currents from each module were first scaled up to the same reference irradiance as it was during solar noon. The angular factor ($f_{I\alpha}$) in (3) was determined at the different angle of incidence of the Sun and soiling level. The calculated angular factors at each soiling level were then plugged into (4) to determine the angular loss factor (a_r) at an AOI of 5°, 10°, 15°, 20°, 25° and 30°. Finally, an average a_r value of was again substituted in equation (4) and (5) to calculate the incidence angle modifier of the module at every angle of incidence (AOI) from 0° to 90°.

III. RESULTS AND DISCUSSION

In this section, the results of the experiments have been discussed. First, the measured soiling ratio (SR) was plotted for a course of a day. Then, the angular losses (AL) as a function of various transmission loss condition and AOI were calculated. Finally, using an empirical equation, soiling ratio over the day has been determined and compared.

A. Soiling ratio (SR)

The soiling ratios were measured for a shade free window of 6 hours from 10:57 to 17:07 on 27th of Aug. 2017 to avoid partial shading on the PV modules caused by nearby objects. The graph below represents a high irradiance day which showed that soiling ratio (SR) was not constant throughout the day but changed with AOI of the Sun. Soiling ratio was seen to be highest during mid of the day ($\pm$ 1 hour from 13:45) fluctuating between 86.5% and 87%. Therefore, the overall transmission loss in the soiled panel was estimated to be around 13-13.5%. During morning and the evening time, it reached the lowest value due to larger AOI of the Sun. SR was also seen to be varying by around $\pm$ 1% even during the mid-day. This was probably because of the dynamic shading on the module due to the passing of the clouds. Figure 4 shows the result of SR measurements on a high irradiance day.
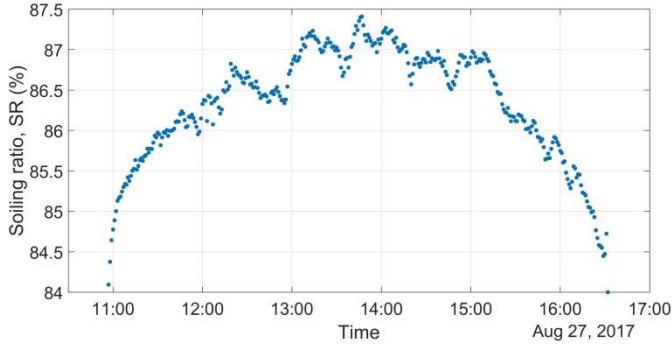
Fig. 4. The measured soiling ratio on 27th August 2017 (high irradiance day) by artificial soiling of a module. SR during morning and evening period is larger signifying to larger losses compared to the middle of the day. The solar noon on this day was noticed at 13:45, which represents one of the largest SR value.

B. Angular losses (AL) on the module

The rooftop PV setup was also used to determine the angular losses on the PV modules. To do so, the Sun's altitude and azimuth were calculated over the whole year for the measurement location. On 11th of July, the solar zenith angle (SZA) was observed to have 60° and Sun became exactly perpendicular with respect to the modules. Therefore, the angles of incidence (AOI) of the Sun for 27th of August were calculated with respect to its position on 11th of July. For our range of interest between 10:57 to 16:30, the AOI of Sun was found to impart the mostly direct component of the irradiance without much influence of the shading nearby and diffused light. The angular factor ($f_{I\alpha}$) was calculated for different soiling levels with an interval of 1% starting from clean (T_{loss}=0) to soiled (T_{loss}=13.1%). It was then used to calculate angular loss factor (a_r) as mentioned by equation (4) and (5). The graph shown in Figure 5 represents incidence angle modifier (IAM) for increasing soiling level (T_{loss}).
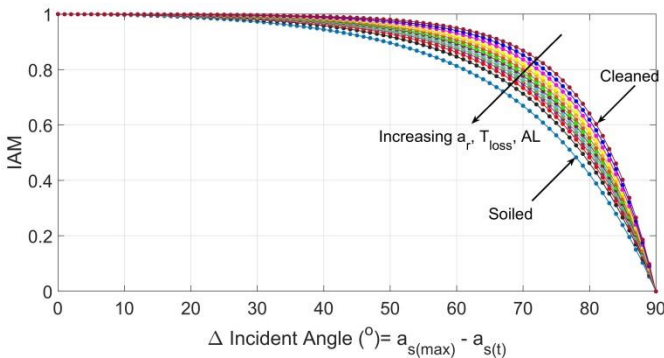

Fig. 5. Incidence angle modifier (IAM) calculated at increasing transmission loss from clean to 13.1%. The red curve at the top represents IAM of the cleaned module, whereas the blue curve at the bottom represents IAM for the soiled module. The in-between twelve curves are at increasing transmission and angular loss from top to the bottom.

The x-axis represents the difference between Sun's altitude at the mid of the day (when maximum) and at any time t. The angular loss factor (a_r) was lowest for the cleaned panel at 0.17 represented by the bottom-most blue curve while it increased

and reached 0.34 at T_{loss} of 13.1%. The pattern of increasing a_r associates with the increase in angular losses with soiling level. Comparing the IAM for cleaned and soiled modules at the same AOI of 30° helps to understand the detrimental effect of soiling on PV modules. The angular loss of a cleaned module was 0.0018 while for the soiled module the losses increased to 0.0164 by 9.12 times. This IAM of soiled and cleaned modules was next used to model SR pattern throughout the day.

C. Soiling ratio modeling based on angular losses

The soiling ratio (SR) over a course of the day as represented in section III.A will be now modeled with the help of calculated angular losses and single mid-day SR value ($SR_{mid-day}$) of 86.9%. The angular losses for cleaned and soiled modules at each AOI from Figure 5 was multiplied with mid-day SR value with an empirical equation presented below

$$SR_{model} = \frac{IAM_s(\theta)}{IAM_c(\theta)} \times SR_{mid-day} \qquad (8)$$
$$= IAM_{ratio}(\theta) \times SR_{mid-day}$$

where $IAM_s(\theta)$ and $IAM_c(\theta)$ are the Incidence angle modifier of soiled (at T_{loss} of 13.1%) and cleaned modules. As it was noticed from equation (1), the soiling ratio (SR) was the comparison between soiled and the cleaned panel thus; the IAM_{ratio} in equation (8) has been presented as the ratio of IAM associated with the soiled module (IAM_s) to that of cleaned (IAM_c). After modeling the SR (SR_{model}) for each angle of incidence for 27th of August, the curve shown in Figure 6 was resulted and plotted with the measured SR values for comparison.
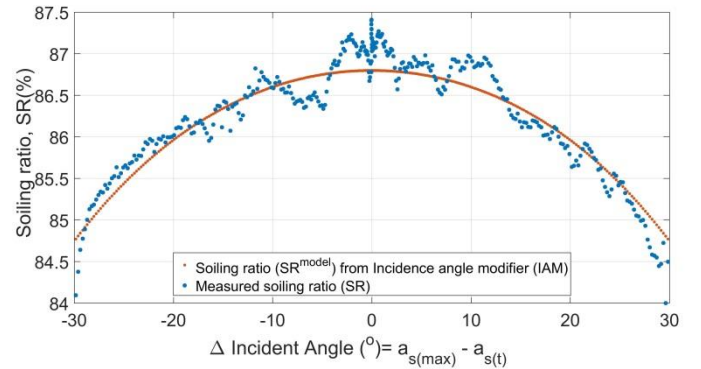

Fig. 6. A comparison of between measured SR values with the modeled values calculated using equation (8). The blue dots represent measured SR values as seen in Figure 5, whereas red dots are modelled SR values using incidence angle modifier (IAM). The modelled values result in a much smoother curve due to the absence of irradiance fluctuations. The two extreme points represented by -30° and $+30^o$, signifies morning and evening time. The calculated SR values were also noticed to increase with time of the day until it reached solar noon. The above curves further confirm the AOI dependency of a soiled module.

From a visual inspection, the modelled curve (blue) much closely seems to follow the pattern of the measured curve (red). The modeled soiling ratio represented in the blue curve can be seen to be much smoother compared to the measured SR. It can be seen that due to larger solar angle during

morning and evening time, the module angular losses was also high for modeled curve.

The characteristics nature of a soiled module's dependency on AOI of the light was also performed indoor with the help of an incandescent light source of 1000 W/m^2 and an artificially soiled mini PV module on a rotatable support. The module was rotated carefully from -90° to +90° with an interval of 10° with respect to the light source and the short-circuit current at each instance was noted. The result showed the similar pattern of soiling ratio at different AOI of the light source as seen in Figure 6.

D. Deviation between measured and modeled SR

An error or residual calculation represents the average deviation of modeled value compared to an actual or observed value [22]. This estimation facilitates the quantification of the deviation for the data of interest. To measure the closeness of the proposed model (equation (8)) modeled and measured SR data, root mean square deviation (RMSD) will be calculated for each point. RMSD calculation was carried out with the help of equation (9) below [23]

$$RMSD = \sqrt{\frac{1}{n}\sum_{i=1}^{n}(o_i - p_i)^2} \tag{9}$$

where o_i represents measured values, whereas p_i shows the modelled values at time i of n data events. For high irradiance day, there were 334 data events representing each minute resulting in a mean squared error of 0.0458%. Thus, RMSD between measured and modelled data set was then found to be ±0.21%. This signifies the proposed model predicted the measured with a variance of ±0.21%. The error associated with medium and low irradiance situation were estimated in the same way. A comparison for each irradiance condition has been summarized in Table I.

TABLE I
RMSD DEVIATION AT THREE IRRADIANCES CONDITION

Date	Day	Daily Avg. Irradiance (W/m^2)	RMSD (%)
27th of August 2017	High irradiance	758.18	±0.21
23rd of August 2017	Medium irradiance	559.12	±0.28
24th of August 2017	Low irradiance	275.87	±1.04

The low light condition was analogous to a high degree of deviation at around ±1% probably due to constant AOI of Sun during cloudy days resulting in a larger amplitude of noise. However, during the day with an adequate amount of light the residual error was quite low at around ±0.2% and ±0.28%. These results suggest that the model predict the soiling ratio very well during high irradiance condition while it is less accurate on cloudy days.

IV. CONCLUSION

Soiling ratio (SR) from short circuit current method was chosen to determine SR over the course of a day. Soiling ratio was found to be influenced by the AOI of the Sun with a high degree of module angular losses during morning and evening time. An analytical model developed by Martin & Ruiz was followed to characterize the angular loss coefficient (a$_r$) at increasing T$_{loss}$ and was found to increase with the soiling level. The soiled and cleaned PV modules had angular loss coefficient values of 0.34 and 0.17 respectively for a high irradiance day (average irradiance of 758.18 W/m^2). It was also noticed that the presence of the dust on the module attenuated the angular losses (AL) and therefore decreasing the transmittance of irradiance at the same AOI compared with the cleaned PV module. The proposed empirical equation based on the incidence angle modifier (IAM) and a single mid-day SR measurement was found to have a low deviation of ±0.21% for a sunny day. The soiling ratio curve was found to be influenced due to movement of the clouds, thus increasing the RMSD.

DISCLAIMER

Results presented in this work strictly concern the type of dust used and the testing condition. The results might differ based on the system's location and local environmental conditions.

REFERENCES

[1] G. Knier, "How do Photovoltaics Work?," *Edge Sunshine*, 2008.

[2] Fraunhofer Institute for Solar Energy Systems, "Photovoltaics report," *www.ise.fraunhofer.de*, pp. 1–44, 2018.

[3] IEA (International Energy Agency), "Snapshot of Global Photovoltaic Markets - IEA PVPS," pp. 1–16, 2017.

[4] J. Sips-Williem, C. Lee, and R. Ringoir, "6 Key influences that determine PV performance ratios," *www.kippzonen.com*, pp. 1–11, 2017.

[5] M. R. Maghami, H. Hizam, C. Gomes, M. A. Radzi, M. I. Rezadad, and S. Hajighorbani, "Power loss due to soiling on solar panel: A review," *Renew. Sustain. Energy Rev.*, vol. 59, pp. 1307–1316, 2016.

[6] M. Gostein, J. R. Caron, and B. Littmann, "Measuring soiling losses at utility-scale PV power plants," *2014 IEEE 40th Photovolt. Spec. Conf. PVSC 2014*, no. November, pp. 885–890, 2014.

[7] M. Mani and R. Pillai, "Impact of dust on solar photovoltaic (PV) performance: Research status, challenges and recommendations," *Renew. Sustain. Energy Rev.*, vol. 14, no. 9, pp. 3124–3131, 2010.

[8] A. Sayyah, M. N. Horenstein, and M. K. Mazumder, "Energy yield loss caused by dust deposition on photovoltaic panels," *Sol. Energy*, vol. 107, no. March, pp. 576–604, 2014.

[9] J. Zorrilla-Casanova *et al.*, "Analysis of dust losses in photovoltaic modules," *World Renew. Energy Congr. 2011 -- Sweden*, pp. 2985–2992, 2011.

[10] R. Appels *et al.*, "Effect of soiling on photovoltaic modules," *Sol. Energy*, vol. 96, pp. 283–291, 2013.

[11] A. Kimber, L. Mitchell, S. Nogradi, and H. Wenger, "The Effect of Soiling on Large Grid - Connected Photovoltaic Systems in California and the Southwest Region of the United States," *IEEE J.*

Photovoltaics, pp. 2391–2395, 2006.

[12]   H. K. Elminir, A. E. Ghitas, R. H. Hamid, F. El-Hussainy, M. M. Beheary, and K. M. Abdel-Moneim, "Effect of dust on the transparent cover of solar collectors," *Energy Convers. Manag.*, vol. 47, no. 18–19, pp. 3192–3203, 2006.

[13]   R. Hammond, D. Srinivasan, A. Harris, K. Whitfield, and J. Wohlgemuth, "Effects of soiling on PV module and radiometer performance," *Conf. Rec. Twenty Sixth IEEE Photovolt. Spec. Conf. - 1997*, pp. 1121–1124, 1997.

[14]   J. J. John, "Characterization of Soiling Loss on Photovoltaic Modules , and Development of a Novel Cleaning System," *Indian Inst. Technol. Bombay*, p. 146, 2015.

[15]   H. Zhang, Y. Sun, L. Wu, X. Zhang, and Y. Xiang, "Tracking mechanism and cosine effect study of Module-Heliostat Solar Collector," *Proc. 2016 4th Int. Conf. Mach. Mater. Inf. Technol. Appl.*, vol. 71, no. January, pp. 469–474, 2016.

[16]   N. Martin and J. M. Ruiz, "Calculation of the PV modules angular losses under field conditions by means of an analytical model," *Sol. Energy Mater. Sol. Cells*, vol. 70, no. 1, pp. 25–38, 2001.

[17]   Transcat, "Fluke 80 Series V Multimeters Users Manual," 2017.

[18]   International Electrotechnical comission (IEC):61724-1, "Photovoltaic system performace: Part 1- Monitoring," 2017.

[19]   Canadian Solar, "CS6K-260|265|270|275P datasheet," 2017.

[20]   M. Gostein, B. Littmann, J. R. Caron, and L. Dunn, "Comparing PV power plant soiling measurements extracted from PV module irradiance and power measurements," *Conf. Rec. IEEE Photovolt. Spec. Conf.*, no. November, pp. 3004–3009, 2013.

[21]   N. Martín and J. M. Ruiz, "Annual angular reflection losses in PV modules," *Prog. Photovoltaics Res. Appl.*, vol. 13, no. 1, pp. 75–84, 2005.

[22]   Universidade Federal de Alagoas, "Model evaluation methods." 2010.

[23]   G. Piñeiro, S. Perelman, J. P. Guerschman, and J. M. Paruelo, "How to evaluate models: Observed vs. predicted or predicted vs. observed?," *Ecol. Modell.*, vol. 216, no. 3–4, pp. 316–322, 2008.